Determinants of flaviviral neuropathology

Kathryn McGuckin Wuertz

A dissertation

submitted in partial fulfillment of the

requirements for the degree of

Doctor of Philosophy

University of Washington

2019

Reading Committee:

Michael Gale Jr., Chair

Piper M. Treuting

Jennifer Lund

Program Authorized to Offer Degree:

Pathobiology

University of Washington

Abstract

Determinants of flaviviral neuropathology

Kathryn McGuckin Wuertz

Chair of the Supervisory Committee:
Professor Michael Gale Jr.
Department of Immunology

In recent years, outbreaks of emerging and re-emerging neuroinvasive West Nile virus (WNV) infection has brought about a critical need to understand host factors that restrict neuropathology and disease. WNV infection in humans typically is either asymptomatic or results in a mild febrile illness, but in some cases virus spreads to the central nervous (CNS) causing a more severe form of neuropathological disease. Previous studies established that both innate and adaptive immune response are essential for controlling WNV disease and restricting the virus from the CNS. In this study, we examined the role of *St*imulator of *In*terferon *G*enes (STING) and upstream sensor cGAS (cyclic GMP-AMP synthase) in conferring host defense during WNV infection in a murine model. Our studies revealed that STING is essential for restricting pathology in the CNS during WNV infection. Further, STING and cGAS both have roles in programming effective immune responses to WNV. In the absence of STING, aberrant immune development leads to ineffective viral clearance and immunopathology in the CNS. These studies uncover a critical and previously unidentified role for cGAS and STING in the restriction of WNV that may have broader implications for a role in conferring host defense against RNA viruses.

TABLE OF CONTENTS

LIST OF FIGURES

LIST OF TABLES

LIST OF ACRONYMS

BW%: percent of original body weight loss

BMDM: bone marrow derived macrophage

CDC: Center for Disease Control

cGAMP: cyclic guanasine-adenosine monophosphate

cGAS: cyclic GMP-AMP synthase

CNS: central nervous system

CS: clinical score

DAMPs: danger associated molecular patterns

DNA: deoxyribonucleic acid

ENS: enteric nervous system

IACUC: Institutional Animal Care and Use Committee

RNA: ribonucleic acid

IFN: interferon

IFNb: interferon beta

IRF3: interferon regulatory factor 3

ISG: interferon stimulated gene

JEV: Japanese encephalitis virus

MAVS: mitochondrial antiviral-signaling protein

mtDNA: mitochondrial DNA

PAMPs: pathogen associated molecular patterns

RIG-I: retinoic acid-inducible gene I

RLR: RIG-I-like receptor

(S): survivor cohort

STING: stimulator of interferon genes

(T): terminal cohort

WNF: West Nile fever

WNND: West Nile neurological disease

WNV: West Nile virus

WNV-TX: West Nile virus; Texas isolate

ZIKV: Zika virus

ACKNOWLEDGEMENTS

This work would not have been possible without the collaborative and supportive team efforts of multiple people, programs and departments at the University of Washington (UW), Madigan Army Medical Center, Department of Defense Army Microbiologists (71A) and LTHET Fellowship.

At the University of Washington, the Departments of Global Health and Immunology along with the staff, faculty and students provided extraordinary support and intellectual input throughout my project. In the Gale Laboratory where I performed my dissertation studies, all members past and present gave invaluable advice, training and assistance to complete my project. Additional essential assistance was provided by members of the Andrew Oberst, Daniel Stetson and Jenny Lund Laboratories at UW, Vanderbilt and Madigan Army Medical Center. In particular, I would like to acknowledge the following persons for their direct assistance on my project:

- *Mouse studies:* Aimee Sekine, Kathleen Voss, Sunil Thomas and Megan De La Riva
- *STING Activation*: Lauren Aarreberg and Katharina Esser-Nobis
- *Flow Analysis:* Emily A. Hemann, Annelise G. Snyder (Oberst Lab) and Jessica B. Graham (Lund Lab)
- *Histopathology/Pathological analysis:* Piper M. Treuting, Jessica M. Snyder, Brian Johnson (UW) and Kelli Boyd (Vanderbilt)
- *Virology and CNS Analysis:* Brian P. Daniels (Gale and Oberst Labs)
- *Bioinformatics analysis of clinical symptoms:* Courtney Wilkins
- *ZIKA placental project:* Nicholas Ieronimakis (MAMC), Jennifer Stencil-Baerenwald and Jennifer Go

Especial thanks go to my program director, Lee Ann Campbell and committee members, Piper M. Treuting (GSR, reading committee), Jennifer Lund (reading committee), Daniel B. Stetson and Keith R. Jerome. From the beginning they provided me with the support, encouragement and guidance that made all the difference.

Most of all, I would like to acknowledge and thank my PI, Michael Gale Jr. He provides mentorship, support, intellectual freedom, technical and theoretical expertise and so much more. It has been an honor and a privilege to work for and with him over these last years. Learning from him and having this opportunity has been a defining experience that will forever enhance and influence me as a person, scientist and leader.

DEDICATION

Family comes in many forms. I am blessed by having a truly global family, and I wouldn't be here without them. This is to all my family.

Friends are the people who carry you through the hard times, laugh with you through the good times and who bring spice to life. This is to all my friends, old and new.

My world is made of my husband Normen, our son Michael, and husky Akeisha. Together we form a team that can accomplish anything. It is with them that this work was completed. Without them, it would not have been possible.

Chapter 1. INTRODUCTION

1.1 EMERGING AND RE-EMERGING ENCEPHALITIC VIRUSES

Recent years have seen a marked increase in the threat presented to global health by emerging and re-emerging encephalitic viruses [1]. In part, this is due to technological advances allowing for increased detection of neurotropic viruses, previously thought to be restricted to the periphery. Examples of newly identified neurotropic viruses include human immunodeficiency virus, influenza A virus, Ebola virus, dengue virus and coronaviruses virus [1-10]. Identification of previously unreported neurovirulence brings to light concerns for unattributed neurovirulence and potential cellular reservoirs for the virus. In addition to increased detection and identification of neurotropic viruses, the expanding distribution of viruses transmitted through arthropod vectors (arboviruses) are of critical import, as global climates and populations change, altering the distribution of vectors world-wide [1, 11]. Growth in human populations, increased urban centers, changes in agricultural practice and a rise in international travel has given rise to unprecedented spread into previously nonendemic regions [1]. Critical among these arboviruses are the mosquito-borne neurotropic *Flaviviruses*. *Flaviviruses* are positive stranded RNA viruses of global import, including the recently emerged Zika virus (ZIKV), and continually re-emerging Dengue virus, Yellow Fever virus, Japanese Encephalitis virus and West Nile virus (WNV) [1, 11-13].

1.2 WEST NILE VIRUS

West Nile virus has become of critical import in the Western Hemisphere, following its emergence in the United States in 1999 [14, 15]. WNV has at least five lineages, although only Lineage 1 and Lineage 2 have been described in human infections [16-20]. Most human cases have been attributed to Lineage 1, where Lineage 2 is predominantly restricted to an enzoonotic

infection in Africa [21-23]. After its introduction in New York, WNV has become endemic throughout the 48 contiguous states, and is now the leading cause of arboviral encephalitic disease in the United States [11, 23-25]. In nature, WNV is maintained through a *Culex* mosquito-bird cycle, with humans and horses as incidental dead-end hosts [21, 26-29]. The risk of WNV has increased as populations have shifted, and global climate change impacts the vector range, predominantly driven by the *Culex* mosquito population [11, 26-30]. Warmer temperatures correlate with increased human incidence, with the majority of infections occurring in the mid-west, and 94% of infections and disease occurring seasonally between July and September [11]. This is thought to be due to decreasing the incubation time from infection to infectiousness in mosquitos, increasing viral transmission efficiency between mosquitos and birds and increasing the geographic vector distribution [30].

1.3 West Nile virus pathology

WNV usually manifests in an asymptomatic or mild febrile illness commonly referred to as West Nile Fever (WNF), but in some cases can progress to form West Nile Neuroinvasive Disease (WNND) [11, 24, 30]. In both forms of disease, symptom onset is abrupt, and treatment is limited to supportive therapy due to the lack of antiviral therapeutics [11]. WNF occurs in approximately 25% of those infected by mosquito bite [1, 11, 31]. Common symptoms include headache, generalized weakness, rash, fever or myalgia, and in some cases vomiting, diarrhea, joint or eye pain [11, 30]. After bypassing the protective barriers between the periphery and CNS, WNV can cause WNND, with symptoms including meningitis (inflammation of the tissues lining the brain) encephalitis (brain inflammation), myelitis (inflammation of the spinal cord) and acute flaccid paralysis, or any combination of the above [30, 32, 33]. Individuals who display severe WNND are less than 1% of the infected population, although ~45% of cases are defined as

neuroinvasive [[11, 34] [CDC]. Individuals over the age of 50, or those who are immunocompromised have an increased risk of acquiring WNND. Diagnosis for both WNF and WNND is made by IgM detection in the serum or cerebral spinal fluid (CSF) of infected patients [1, 10, 11, 14, 30]. Patients with WNV generally display symptoms for days to weeks, most commonly with complete recovery. Those with WNND however, generally maintain symptoms for weeks to months, and often maintain long-term cognitive or functional deficiencies, with the most severe cases leading to death [11, 30].

1.4 West Nile virus neurovirulence

Since it emerged in 1999, WNV has seasonally re-emerged with changes in neurovirulence, and with it associated morbidity and mortality with the most neurovirulent strains occurred in 2002, 2003 and 2012 [11, 24] [CDC]. During these years, WNV was responsible for the three largest recorded outbreaks of neuroinvasive disease in the United States since its introduction in 1999 [11]. Between 1999-2014, 41,762 cases were reported to the CDC, where 18,810 (45%) were described as neuroinvasive, and 22,952 as non-neuroinvasive (55%) [CDC]. Actual rates of infection are difficult to analyze, as many cases are asymptomatic or are misdiagnosed. Incidence trends for neurovirulent WNV are the most complete, however even during well-established outbreaks only 40% of patients with clinically compatible meningitis or encephalitis were tested for WNV [31, 35]. Retrospective studies extrapolate that an estimated 3 million people have been infected in the US, with 780,000 (~26%) developing WNF and 16,196 WNND (<1%), resulting in 1549 deaths between 1999-2012 [36]. This data is particularly concerning in the light of the recent 2012 outbreak, where after years of decline, WNV re-emerged causing a total of 5,674 reported cases, with 2,873 (51%) neurovirulent cases, and 286 (5%) mortality [24]. During the 2012 outbreak, the incidence of neuroinvasive disease increased sharply to 0.92 per 100,000

population, from the preceding years median at 0.18 per 100,000 (2008-2011), nearing the levels of the 2002 and 2003 outbreaks. Factors involved in the annual variation in neurovirulence are essential to understand, because 93% of all deaths are attributed to neurovirulent cases. Analysis of the total cases reported between 1999-2014 shows that 9% of all neurovirulent cases result in death, while only 0.5% of non-neurovirulent cases result in death [CDC]. This brings about a critical need to understand the underlying cause for neurovirulence, and the viral and host factors that restrict neurovirulence.

1.5 IMMUNE CONTROL OF WNV

Upon infection, mosquito salivary components suppress the immune response at the site of infection, allowing infection of target cells including keratinocytes, macrophages and skin-resident dendritic cells [37-39]. Infected macrophages and dendritic cells migrate to draining lymph nodes, generating serum viremia that goes on to infect visceral organs and potentially lead to infection of the central nervous system (CNS) [11, 23, 30]. In cases where neuroinvasion occurs, the mechanism of how WNV accesses the CNS is unclear, but multiple mechanisms have been proposed, including: 1) cytokine-induced vascular permeability and degradation of tight junctions in the blood brain barrier, allowing for direct viral passage to the CNS [40-42], 2) breakdown of the blood-brain barrier allowing for passage to the CNS [43], 3) trafficking of infected immune cells such as macrophages across the blood-brain barrier in a Trojan horse model [44, 45], or through 4) axonal retrograde transport of WNV through olfactory or peripheral neurons to the CNS [44, 46]. To prevent progression to neuroinvasion, both the innate and adaptive immune response are critical to control WNV viremia and prevent viral induced pathogenesis [43, 47-49]. The type I IFN response is essential for host defense against WNV [49-53]. The role of type I IFN in conferring host defense to WNV was first described in 1957, and since have expanded to show its

role in restricting viral replication, limiting tropism and activation of the innate and adaptive antiviral response [50, 52, 54-59]. Following WNV infection, the Type I IFN response is initiated through activation of pattern recognition receptors (PRRs) in the cytoplasm, known as RIG-I like receptors, or RLRs [53, 60-62]. These receptors including RIG-I, MDA5 and LGP2 bind to viral RNA in the cytoplasm, and activate downstream adaptor protein, MAVS [63, 64]. Formation of a MAVS signaling synapse initiates interferon-3 (IRF3), followed by nuclear translocation and upregulation of target genes including interferon stimulated genes (ISG) such as interferon-β (IFNβ). Secretion of IFNβ and other ISGs from the cell initiates an autocrine and paracrine signaling cascade through interferon receptors located on cell surfaces, that activates the downstream Jak/Stat signaling cascade [48]. This RLR-dependent signaling cascade is essential for host survival during WNV infection, and depends on both RIG-I and MDA5 dependent activation of MAVS [65]. IRF3 signaling through MAVS initiates early control of WNV but is also required for development of the adaptive immune response [51, 53]. The innate-adaptive immune interface is mediated through dendritic cells and macrophages, both targets during WNV infection, and are pivotal in programming the humoral, cytotoxic and regulatory T cell responses [48, 51, 53, 56, 65-67]. In particular, $WNV^{+}CD8^{+}$ cytotoxic T cells are essential for clearance of WNV from the CNS [53, 56, 66, 68]. To prevent excessive damage from the $CD8^{+}$ population however, regulatory T cells are required to limit immune-mediated pathology [69, 70].

1.6 A NOVEL PATHWAY IN HOST DEFENSE AGAINST WNV: STIMULATOR OF INTERFERON GENES (STING)

In addition to RLR-dependent type I IFN signaling, host defense against WNV has also been attributed to the recently discovered adaptor protein, *ST*imulator of *IN*terferon *G*enes (STING) [71]. STING was first described in 2008 as an essential defense mechanism against both

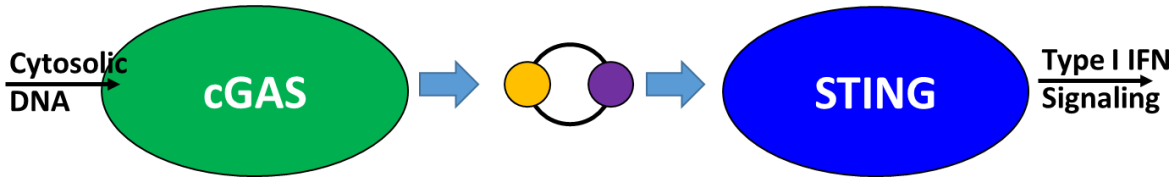

Figure 1-1: cGAS-STING signaling cascade
Cytosolic DNA is detected by cGAS, which produces the cyclic di-nucleotide cGAMP. cGAMP binds to and activates STING, which is phosphorylated and translocated to perinuclear puncta. This initiates a signaling cascade that results in induction of type I IFN signaling.

RNA and DNA viruses [72, 73]. Since then, the signaling pathways to DNA pathogens have been well characterized, however the role of STING in host defense to RNA pathogens is poorly understood [74, 75]. Several DNA sensors have been implicated to signal through STING, however the most ubiquitously functional pathway is mediated through cyclic GMP-AMP synthase (cGAS) (**Figure 1-1**) [76-82]. In the cGAS-STING pathway, cGAS detects and binds cytoplasmic DNA and generates a cyclic-dinucleotide comprised of 2'-3' GMP-AMP (cGAMP) [77, 83-86]. cGAMP then binds to STING and activates it, initiating relocation from the cytoplasm to distinct perinuclear puncta [72, 73, 87]. STING acts as an adaptor molecule, facilitating an IRF3-dependent antiviral response similar to that initiated downstream of MAVS [88]. In recent studies, the role of cGAS and STING signaling has been expanded to include a role in host defense against retroviruses, RNA viruses, tumors, cellular stress, autoimmunity and immune disorders, indicating that this pathway can be utilized both in the detection of pathogen associated molecular patterns (PAMPs) and host danger associated molecular patterns (DAMPs) [74, 89-97]. In the context of RNA viruses, it is unclear whether a viral PAMP is directly recognized, or host DAMP is detected due to cellular stress initiated during infection. Prior studies using bioinformatics analysis have demonstrated that cGAS is a broad inhibitor against multiple RNA viruses, and *in vivo* is essential for host survival against WNV [96, 97]. Intriguingly, studies have also indicated the role of cGAS-independent, STING-dependent signaling in mounting an innate immune response against RNA

viruses [91]. Supporting the role of DAMPs during viral infection, studies have shown that mitochondrial DNA (mtDNA) released during cellular stress initiates STING activation and generation of a type I IFN antiviral response [93]. These studies suggest that both PAMP and DAMP components are capable of mounting a Type I IFN response and may be required for the host defense against WNV.

1.7 THE ROLE OF STING IN HOST DEFENSE OF THE CENTRAL NERVOUS SYSTEM

To date, the role of STING in WNV neuropathogenesis is unknown. However, studies have shown that STING has a neuroprotective role *in vivo* and *in vitro* during JEV and ZIKV infections, suggesting a critical role for STING in the neuronal defense against RNA viruses [98, 99]. Following invasion of the CNS, the innate immune responses generated to WNV is not well understood, however it is possible that a STING-dependent type I IFN response is required for restricting neurotropism in the brain. Historically, the CNS has been considered immune-privileged and without a lymphatic drainage system. These views have been challenged with seminal publications identifying the brain lymphatic system, and studies demonstrating that the CNS mounts robust immune responses to both infectious and sterile injuries [32, 100-102]. Further, free DNA released from dying or damaged cells has been found in serum and cerebral spinal fluid of patients suffering from epilepsy, stroke and traumatic brain injury, suggesting immunostimulatory function [103-106]. In support of this, increased evidence suggests there is a type I IFN response initiated during chronic neurodegenerative diseases such as prion disease and amyotrophic lateral sclerosis [107, 108]. Due to the role of cellular damage and sterile immunity in mounting this response, the cGAS-STING pathway has been implicated as modulating type I IFN signaling during neurodegenerative diseases. Recent reports have provided further evidence of this, demonstrating that cGAS is an essential modulator host

defense against Aicardi-Goutières syndrome, and that key sensors for cGAS signaling are upregulated in brain tissues in a murine chronic neurodegeneration model [109, 110]. Both cGAS and STING, as well as other DNA sensors have been detected in the CNS and cellular subsets, including astrocytes, monocytes, and microglia [109]. Within the brain, STING expression is detected within the olfactory/orbital bulbs, thalamus/midbrain, brainstem and cerebellum, as well as low levels throughout the cortex, overlapping areas affected most severely by WNV infection [32]. STING localization within the spine is unknown, however WNV infection has been detected within the dorsal root ganglion, motor neurons and the anterior horn of the spinal cord [32]. Because of the involvement of STING in multiple neuronal degenerative diseases, it is possible that STING confers neurological host defense through DAMP or PAMP recognition during WNV infection.

1.8 THE ROLE OF STING IN WNV INFECTIONS

Understanding the role of STING in host defense against RNA viruses has been restricted by the lack of mechanistic evidence [75, 111]. Previously, it was demonstrated that STING is essential for host survival from WNV infection using $STING^{gt/gt}$ mice, which are ENU generated STING functionally defective mice, as opposed to the full genetic knock-out $STING^{-/-}$ [71]. This work examines the hypothesis that STING has an essential role in host defense against WNV, specifically in preventing neuropathology in the CNS during WNV infection. To do so, a combination of methodologies including clinical analysis, histopathology, immunology, virology were used to determine the outcome of WNV infection in $STING^{-/-}$ mice, with further work done in $cGAS^{-/-}$ mice to see if both are essential for host defense from WNV infection.

Chapter 2. MATERIALS AND METHODS

2.1 ETHICS STATEMENT

All animal experiments were approved by the University of Washington Institutional Animal Care and Use Committee (IACUC) guidelines as per protocol #4158-05 and follow the recommendations in the Guide for the Care and Use of Laboratory Animals of the National Institutes of Health. Invasive infections and manipulations were performed in ABSL-2 with ABSL-3 practices conditions, under anesthesia with every effort was made to limit suffering.

2.2 ANIMAL SOURCES

C57BL/6J (WT), *Tmem173*$^{-/-}$ (STING$^{-/-}$), cGAS$^{-/-}$, STING$^{gt/gt}$ x cGAS$^{-/-}$ and MAVS$^{-/-}$ mice were genotyped and bred under specific pathogen-free conditions in the animal facility at the University of Washington. STING$^{-/-}$ mice were gifted by the Stetson lab, who generated them as previously described [112] followed by speed congenics to bring them to a 99.4% C57BL/6J background. cGAS$^{-/-}$ and STING$^{gt/gt}$ x cGAS$^{-/-}$ mice were gifted from the Diamond lab. MAVS $^{-/-}$ (*STI*$^{-/-}$) were generated in the Gale lab as previously described [66]. Additional C57BL/6J (WT) mice were purchased from Jackson Laboratories, Bar Harbor, ME. Both male and female mice, ages 8-11 weeks were represented in both the control and infected groups. Mice for primary cortical neurons (WT and STING$^{-/-}$) were set up as timed breeders and embryos were harvested.

2.3 CLINICAL SCORING

Mice were monitored daily and assigned a clinical score to describe overall well-being and signs of hind-limb dysfunction (paresis). Clinical scores (CS) of (0) are asymptomatic, or (1-6) if symptomatic. CS=1: ruffled fur, lethargic; no paresis; CS=2: very mild to mild paresis (in 1 or

more hind limbs with minimal gait disturbance or limb-dysfunction); CS=3: (either) frank paresis involving at least one hind limb (and/or) eye conjunctivitis; CS=4: severe paresis and/or paresis in both hind-limbs; CS=5: true paralysis; CS=6: moribund. Additionally, mice were observed daily for the presence or absence of symptoms including: lethargy (L), ruffled fur/lack of grooming (R), hunched (H), paresis/paralysis (P; any degree of severity), tremors (T), abdominal bloat/gastro-intestinal (GI) distress (G), loss of balance (B), increased reflex/tone in limbs (fore and/or hind) and tail (Stiff; S), decreased reflex/tone in limbs and tail (Floppy; F), eye disorder/disease (E). Each mouse was scored as either exhibiting the symptom (YES = 1) or not, (NO = 0). Each symptom was monitored through the duration of the experiment and the results were graphed as the average daily score/mouse. This clinical scoring system is designed to predict gross anatomical defects within the CNS and to implicate any GI involvement during infection. Clinical scores were selected using modifications of various previously described scoring systems for experimental autoimmune encephalomyelitis [113-116]. Similar neuroanatomic regions were examined pathologically to correlate clinical and neurological phenotype of disease.

2.4 SURVIVAL ANALYSIS

Subcutaneously-infected mice were monitored for 18 days post infection (dpi). Euthanasia criteria was determined as a clinical score >= 5 for 2 or more consecutive days, or 20% loss in body weight. A clinical score of 6 (moribund) or respiratory distress resulted in immediate euthanasia. Mice meeting euthanasia criteria were identified as Terminal (T) and were euthanized by CO2 asphyxiation followed by cervical dislocation. Mice who did not meet euthanasia criteria were monitored until end point (18 dpi) were identified as Survivors (S). All remaining S mice were euthanized at the end of study (18 dpi) as described above.

2.5 PATHOLOGY AND HISTOPATHOLOGIC SCORING

Mice used for morbidity and mortality analysis were necropsied when meeting euthanasia (T) criteria, or study end (S). After euthanasia by CO2, a complete necropsy was performed and tissues were collected and immersion fixed in 10% neutral buffered formalin [117]. The head was removed, and skull cap lifted, leaving the brain within the skull cavity during fixation. The spine was fixed *in situ* to preserve the mesenteric ganglia. Histological preparation hematoxylin and eosin (H&E) and immunohistochemical (IHC) staining was performed by the UW Histology and Imaging Core (HIC) and the Vanderbilt University Medical Center Translational Pathology Shared Resource (TPSR). Primary histopathologic analysis and scoring was performed on the CNS (brain and spine) and gastrointestinal (GI) tract by a board-certified veterinary pathologist (PMT)

Table 1). In the brain, the following changes were scored on a subjective 0-4 scale of increasing severity: perivascular inflammation, parenchymal inflammation, hemorrhage, neuronal necrosis, and meningitis. In the spinal cord the presence (1) or absence (0) of mononuclear inflammation was documented. For the enteric nervous system (ENS), the degree of mononuclear cells present in the myenteric ganglia, extent of the changes and any secondary GI lesions such as dilation or mucosal change were scored on a on a subjective 0-4 scale of increasing severity. IHC staining of TUNEL was kindly performed by Dr. Kelli Boyd at Vanderbuilt. IHC staining of WNV (VRL W1015) and CD3+ T cells (MCA1477 AbD Serotec) were performed by the UW Histology Core.

Table 1. Histological Scoring for Pathology

	Brain					ENS			Spine
Score	**Perivascular inflammation: accumulation of inflammatory cells around vessels within Virchow-Robin's space**	**Parenchymal inflammation: inflammatory cells or gliosis with neuropil**	**Hemorrhage**	**Neuronal necrosis: including neurophagia**	**Meningitis**	**Mononuclear cells within the myenteric ganglia**	**Extent**	**Secondary lesions to GI**	**Mononuclear cells within the cord**
0	None	None	None	None	None	None	None	None	None
1	Few cells <10	Few cells <10	Minimal	Minimal	Minimal thickening	Few cells <5	<25% affected	Minimal dilation, inflammation	Yes
2	Mild cells 11-20, slight expansion of space	Mild cells 11-20	Mild	Few necrotic bodies	Mild thickening, or minimal in multiple regions	Mild cells 6-20 with minimal neuronal damage	25-50% affected	Mild dilation, inflammation, or mucosal atrophy	
3	Moderate cells 21-30 and expansion up to 2X normal	Mild or moderate cells with parenchymal damage	Mild and multifocal	Multiple necrotic bodies or satellitosis	Mild or moderate expansion with superficial parenchymal damage	Mild cells 6-20 with evidence of necrosis or apoptosis	51-75% affected	Moderate dilation, inflammation, or mucosal atrophy, with necrosis or cell sloughing	
4	Perivascular cuffs up to 3X normal space	Marked cells and damage	Moderate	Marked numerous neuronophagic nodules	Marked expansion focally or moderate in multiple regions	Moderate cells >20 or no observable neurons	76-100% affected	Severe dilation, inflammation, or mucosal atrophy, with necrosis or cell sloughing, bacterial overgrowth	

2.6 CELLS

VeroWHO (European Collection of Authenticated Cell Cultures; ECACC) cells were cultured in Dulbecco's modified Eagle medium (DMEM) supplemented with 10% FBS, 1mM sodium pyruvate, 2mM L-glutamine, antibiotic/antimycotic solution and non-essential amino acids (complete DMEM; cDMEM) and split using 0.25% Trypsin following PBS wash. HFF cells were kindly gifted from Stetson Lab and were grown in cDMEM. Cells were split using 0.05% trypsin following PBS wash. Bone marrow was collected from STING$^{-/-}$, MAVS$^{-/-}$ and WT mice and frozen in 10% DMSO/90% FBS. To generate bone marrow derived macrophages (BMDM), bone marrow stocks were thawed, washed and resuspended in cDMEM containing [50 µM] BME and [40ng/mL] mouse MCSF (mMCSF). Cells were cultured for 7 days in non-TC coated plates,

then scraped, washed with PBS and seeded at 1E6 cells/well in 12-well TC coated plates with cDMEM+BME+mMCSF. Cells were infected or transfected the next day.

2.7 VIRUS

WNV-TX biological isolates (2002) were utilized for *in vivo* work, while WNV-TX ic (infectious clone) stocks were utilized for studies. Working stocks were propagated in Vero-E6 (American Type Culture Collection; ATCC) and titered by standard plaque assay on VeroWHO and BHK21 (American Type Culture Collection; ATCC) cells as previously described [53]. Single-use aliquots from the same viral stock lot were prepared and utilized for all experiments described here.

2.8 SUBCUTANEOUS VIRAL INOCULATIONS

Age and sex-matched 8-11-week-old mice were anesthetized by isofluorane and inoculated subcutaneously (s.c.) in the left rear footpad with 100 PFU WNV-TX 2002 (WNV-TX) diluted in 40 uL PBS, administered via 1mL insulin needle. Mice were monitored as described.

2.9 INTRACRANIAL INOCULATIONS (VIRAL)

Mice were anesthetized with ketamine/xylazine, the top of the head was cleaned with EtOH, and the mouse was then restrained manually on a solid surface. The site of injection was approximately halfway between the eye and ear, and just off the midline, in the medial posterior region of the top of the skull. The injection was done with a 29G needle using a Hamilton syringe into the cerebral cortex. Following infection, mice were monitored for revival from anesthesia and then monitored as described. Viral quantification from tissue

To determine the viral load from *in vivo* tissue samples, mice were terminally anesthetized using ketamine/xylazine mixture followed by cardiac perfusion with 30-40 mL PBS. Kidney(s) and spleen were collected whole; brains were harvested and macrodissected into four anatomical regions, including the cerebellum, cortex, sub-cortex, and brainstem [118]; spinal cords were collected by perfusion with PBS. Tissues were harvested into 1 mL PBS on ice in Percelly's tubes with ceramic beads. Following harvest, tissues were homogenized (Percellys 24) 5500/1x 20s/5 min (005) (Setting #1) and centrifuged at 4^{o}C/5 min/10k rpm. Supernatant was collected and analyzed by Plaque Assay on Vero-WHO cells (0.5% agarose overlay, 3% Neutral red counter stain after five days post inoculation; plaques counted >10h post staining).

2.10 WNV INFECTIONS IN TISSUE CULTURE

Cells were inoculated with WNV in serum-free media and the inoculum left for 1hr rocking at 37^{o}C. Inoculum was removed, cells washed 1x and media replaced with cDMEM. At the indicated time-points, supernatant was collected for virologic and cytokine analysis; cells were treated with RIPA buffer for WB analysis (or) with RLT for total cellular RNA isolation.

2.11 PRIMARY CORTICAL NEURON CULTURE AND INFECTIONS

Primary cerebral cortical neuron cultures were generated from E15 WT and STING$^{-/-}$ embryos as previously described [119] and maintained in serum free Neurobasal-A medium (Life Technologies 21103-049) with B27 supplement (Gibco 17504-044). Neuron cultures were used for virologic experiments after 7 days *in vitro*. Cortical neuron cultures were infected at MOI 0.001 with WNV-TX [55]. Multistep growth curve experiments were performed as described [120] and quantified via plaque assay using BHK21-15 cells.

2.12 HARVESTING TISSUES FOR RT-QPCR ANALYSIS

Mice were euthanized in an isoflurane chamber followed by cardiac perfusion with 30-40 mL PBS. Tissues were harvested, and kidney(s) and spleen were collected whole; spinal cords perfused and collected; brains were harvested and macrodissected as previously described [118]. Tissues were harvested into 1 mL RNALater and stored at 4^{o}C for a minimum of 1 week to stabilize the RNA. Tissues were removed from RNALater solution and transferred to 1 mL TRI reagent in Percelly's tubes with ceramic beads at RT. Following harvest, tissues were homogenized in a Percelly's homogenizer (5500/1x20/005) followed by centrifugation (4^{o}C/10k rpm/5min). RNA isolated with the Ribopure kit from TRI reagent using per manufacturer's instructions. cDNA was generated from 350 ng RNA using iSCRIPT kits with random primers per manufacturer's instructions. Cellular and viral gene (Table 2) analysis was assessed by SYBR Green RT-qPCR using an ABI Viia7 and analyzed as the linear fold change (2^-dCT) over a housekeeping gene (GAPDH) from WT mock infected sample or mouse.

Table 2. RT-qPCR Primers

RT-qPCR Primers	**Sequence**	
mGAPDH	5': CAACTACATGGTCTACATGTTC	3': CTCGCTCCTGGAAGATG
WNV	F: TCA GCG ATC TCT CCA CCA AAG	R: GGG TCA GCA CGT TTG TCA TTG
mIFNb	F: GGAGATGACGGAGAAGATGC	R: CCCAGTGCTGGAGAAATTGT
mIFNa2a	Qiagen SABiosciences (PPM03543A)	
mIRF7	F: CCCATCTTCGACTTCAGCAC	R: TGTAGTGTGGTGACCCTTGC
mTNFa	TCCCAGGTTCTCTTCAAGGGA	R: GGTGAGGAGCACGTAGTCGG
mIL6	F: GTTCTCTGGGAAATCGTGGA	R: TGTACTCCAGGTAGCTATGG
mCXCL10	Qiagen SABiosciences (PPM02978E)	
mISG54 (IFIT2)	F: CTGGGGAAACTATGCTTGGGT	R: ACTCTCTCGTTTTGGTTCTTGG
mMX1	F: GACCATAGGGGTCTTGACCAA	R: AGACTTGCTCTTTCTGAAAAGCC

2.13 RNA ANALYSIS FROM TISSUE CULTURE

Cells were harvested in RLT and total cellular RNA isolated for RT-qPCR analysis using Qishredders and the Quiagen RNeasy kit per the manufacturer instructions. cDNA was generated from 100 ng total RNA using the iSCRIPT kit per manufacturer instructions using their provided oligo(dT) and random primers. Cellular and viral genes were analyzed by SYBR Green RT-qPCR using an ABI ViiA7. Primers for BMDM experiments described above (Table 2).

2.14 PROTEIN ANALYSIS FROM TISSUE CULTURE

Protein extracts from cells were prepared in RIPA+ buffer. 7-15 ng protein lysate was analyzed by 4-20% gradient SDS-polyacrylamide gel electrophoresis by immunoblotting, using 5% BSA blocking buffer and nitrocellulose membranes. The following antibodies were utilized: WNV NS3 (R&D BAF2907), Actin (C4; EMD MAB1501), STAT1 (CST 9172P), STING (CST D2PZF), pSTAT1 (Y701; CST 58D6), pSTING (CST D7C3S).

2.15 IMMUNOFLUORESCENCE

8x10^4 HFF cells were seeded onto glass coverslips in a 24-well plate. The following day, cells were infected with WNV-TX at MOIs of 1 and 10 or transfected with calf-thymus DNA (ctDNA) (Thermo Fisher, Waltham, MA, USA) at 3ug/ml final concentration using Lipofectamine 3000 as per the manufacturer's protocol. 24h after WNV infection or 3h after ctDNA transfection cells were fixed with 4% paraformaldehyde for 15min at room temperature (RT). Cells were permeabilized with 0.1% Triton X-100 for 5min at RT. After blocking the cells for 30min with 3% BSA in PBS, immunofluorescent staining was performed overnight at 4°C with the following primary antibodies: rabbit-anti-STING (1:100, kind gift of Glen Barber), mouse-anti-dsRNA (J2, 1:800, Scicons, Budapest, Hungary). Nuclei were counterstained with 4',6-Diamidino-2-

Phenylindole, Dihydrochloride (DAPI, Thermo Fisher). Fluorophore coupled secondary antibodies (Thermo Fisher) were applied for 1h at RT. After washing with PBS samples were mounted onto glass slides using ProLong Gold (Thermo Fisher). Images were acquired with a Nikon Eclipse Ti confocal microscope equipped with a 60x oil immersion objective using the Nikon confocal software. Insets were captured with 4x enlargement of 600x images. Images were merged and processed using the Nikon confocal analysis software (Nikon, Melville, NY, USA).

2.16 FLOW CYTOMETRY

Mice were euthanized by isoflurane and perfused with 30-40mL PBS to ensure systemic removal of blood and residual intravascular leukocytes.

Spleens were homogenized, and single cell suspensions were treated with ACK lysis buffer to clear any remaining red blood cells, washed and resuspended in FACS buffer (1X PBS, 0.5% FBS). Cells were plated at 1E6 cells/well and stained for surface markers 15 minutes on ice. Cells were then fixed, permeabilized (Foxp3 Fixation/Permeabilization Concentrate and Diluent, Ebioscience) and stained intracellularly with antibodies for 30 minutes on ice. Flow cytometry was performed on a BD LSRII machine using BD FACSDiva software. Analysis was performed using FlowJo software. The following directly conjugated antibodies were used: CD3-BUV395 (145-2C11), CD4-BV605 (RM4-5), CD8-BV650 (53-6.7), Foxp3-Alexa700 (FJK-16S), CD44-FITC (IM7), CD73-BV421 (TY/11.8), CTLA-4-APC (UC10-4B9), CXCR3-PerCP eFluor710 (CXCR3-173), and the class I WNV NS4b tetramer-APC. AmCyan Live/dead stain (Invitrogen) was used in all panels for identification of live cells. Cells were counted by hemocytometer using trypan blue exclusion.

Brains were harvested into RPMI and mechanically suspended using a 70uM strainer. Each brain suspension was added to hypertonic Percoll to create a 30% Percoll solution, vortexed then

centrifuged at 1250 rpm for 30 minutes at 4ºC. Following centrifugation, the supernatant was aspirated and cell pellet treated with ACK lysis buffer to remove any residual red blood cells. Cells were then washed and filtered through a 70µm nylon mesh to remove residual debris and resuspended in FACS buffer. Cells were counted using beads during FACS analysis. Cells were plated at 1E6 cells/well and stained for surface markers 15 minutes on ice. Cells were then fixed and extracellularly stained with antibodies for 30 minutes on ice. Flow cytometry was performed on a BD LSRII machine using BD FACSDiva software. Analysis was performed using FlowJo software. The following directly conjugated antibodies were used: FITC-CD19, PerCP-Cy5.5-CD103, PE-CD3e, PE-Cy7-CD4, APC-WNV Tetramer (NS4b), BV421-CD8a

Chapter 3. STING IS REQUIRED FOR HOST DEFENSE AGAINST NEUROPATHOLOGICAL WEST NILE VIRUS INFECTION

3.1 INTRODUCTION

Encephalitic *Flavivirus* infections including West Nile virus (WNV), Japanese encephalitis virus (JEV), and Zika virus (ZIKV), are ongoing or emerging threats to global health [1, 10-13, 25, 121]. In particular, WNV continues to re-emerge in the Americas, causing neuropathology and death in the most severe cases [11, 24, 30, 36]. Since its emergence in the USA in 1999, annual outbreaks of WNV are impacted with fluctuations in neurovirulence attributed to the circulating strain [14, 15, 24, 25, 36]. Morbidity and mortality are dramatically increased in years where the circulating strain has enhanced neurovirulence, as exemplified by the 2012 outbreak in Texas [24, 122]. An analysis of CDC reports reveals that of all cases reported between 1999-2014, 9% of neurovirulent cases result in death, in contrast to 0.5% of non-neurovirulent WNV cases. Factors that limit WNV neurovirulence are not well understood but are critical to restrict pathology associated with WNV infections [24].

WNV infection in humans most commonly manifests as an asymptomatic or mild febrile illness known as West Nile Fever (WNF) with symptoms that include headache, generalized weakness, rash, fever or myalgia, and in some cases vomiting, diarrhea, joint or eye pain [11, 24, 30, 31, 33, 36, 123]. While most patients displaying WNF generally display symptoms for days to weeks, in some cases persistent symptoms continue to impact quality of life and cognitive abilities rendering a chronic disease outcome to WNV infection [33]. More serious disease occurs if the virus is able to cross the blood brain barrier and progress to West Nile Neuroinvasive Disease (WNND) [30]. WNND often involves neurologic disease symptoms including meningitis,

encephalitis, myelitis, marked with acute flaccid paralysis, gastric complications, tremors and Parkinson-like symptoms [30, 32, 33, 124-127]. Patients with WNND can maintain symptoms for weeks to months, with persistent symptoms including chronic fatigue, functional cognitive disorders or neuropsychiatric disabilities and physiological complications, particularly those who exhibited acute flaccid paralysis symptoms during acute infection [30, 33, 127]. Currently no therapeutics or vaccines are available for treatment of WNV infection or neuropathogenesis. Thus, there remains a critical need to understand the virus-host interactions of WNV neurovirulence.

Both the innate and adaptive immune response are required to clear WNV infection and to restrict immune mediated pathology [48]. In humans, infection with WNV typically occurs through subcutaneous inoculation from the bite of an infected mosquito. A parallel form of infection using sub-cutaneous challenge of WNV in a mouse model has been shown to replicate the progression, tissue involvement, and pathology of WNV infection that occurs in humans [48, 128-130]. In the mouse model, viral replication occurs at the subcutaneous site of entry followed by infection of the draining lymph node and splenic infection [48]. These processes trigger innate immune activation in the peripheral, non-central nervous system (CNS) sites of infection through viral recognition by the RIG-I-like receptors to induce IRF3 activation and the production of types I and III interferon (IFN) [53, 65, 131, 132]. Innate immune defenses triggered by RLR signaling and IFN actions serve to restrict the tissue tropism of WNV and are essential for protection against neuroinvasion [23, 48-50, 52-55, 57, 65, 133]. Type I and III IFN are essential to inform the innate and adaptive immune interface to balance development of effective immunity, protect the blood-brain barrier, and limit immune-related pathology in the CNS [48, 51, 53, 56, 65-67, 134]. In particular, type I IFN-dependent cytokine and chemokine signaling cascades are essential for functional development of the cytotoxic CD8+ T cell response, as well as its regulatory T cell

(Tregs; FoxP3+-CD4+ T cells) counterpart [53, 56, 66, 134-137]. While CD8+ T cells are required for controlling both peripheral and CNS viral load, CD4+ T cells, specifically Tregs, are essential for preventing symptomatic disease in the CNS [69, 135-137].

The adaptor protein, *St*imulator of *In*terferon *G*enes (STING), has also been implicated in host defense against WNV [71, 96, 97]. STING was first described as an essential defense mechanism against both RNA and DNA viruses [72, 73]. Since then, STING has been recognized for its role in generating a type I IFN response DNA detected in the cytoplasm, however its role in the defense against RNA viruses is poorly understood [72-76, 87, 111, 138]. Intriguingly, multiple RNA viruses, including Dengue virus, yellow fever virus, hepatitis C virus and coronaviruses, direct viral evasion strategies to disrupt the STING signaling pathway, reflecting a likely role for STING in host defense against RNA viruses [75]. STING was found to be required for host defense during infection with influenza A virus, as well as dengue virus, a closely related flavivirus to WNV [91, 139, 140]. Additionally, during infection with related flavivuses including JEV and Zika Virus, STING deficiency led to increased neuropathology *in vivo* and *in vitro*, suggesting a critical role for STING in CNS defense [98, 99]. The role for STING in the CNS has been implicated in multiple other neurodegenerative diseases including Aicardi-Goutières syndrome, sterile immune mediated CNS pathology and during chronic CNS diseases [32, 103-107, 125, 141, 142].

In this study, we investigated the hypothesis that STING plays a regulatory role in the immune response against WNV, thereby restricting viral neurotropism and neuropathology. We show that STING is essential for host defense against WNV in a mouse model of infection. Clinical and pathological analyses demonstrate a novel role for STING in conferring CNS defense against WNV *in vivo*. We found that tonic levels of type I IFN were decreased in STING$^{-/-}$ BMDM and

linked with increased susceptibility to WNV infection over WT cells. Following infection, we observed heightened immune responses *in vitro* and *in vivo* concomitant with increased viral load. STING deficiency led to the development of an aberrant adaptive immune response, with decreased activation of CD8+ cells and T regulatory cells (Tregs) in the spleen, and a decreased CD4/CD8 T cell ratio in the CNS coupled with neuropathology. Our observations imply an essential role for STING within the interface between the innate and adaptive immune responses for effective immune programming in the control of WNV infection and CNS disease.

3.2 STUDY DESIGN

In order to see if a similar phenotype was observed in genetically knocked-out (*Tmem173*$^{-/-}$; STING$^{-/-}$) mice, we inoculated mice via foot-pad injection with 100 PFU/mouse and monitored them for progression of clinical disease for 18 days post infection (dpi). Mice that met euthanasia criteria typically did so between 8-12 dpi, with any mice surviving 12 dpi surviving until the study end-point, 18 dpi (**Figure 3-1**). Mice used in the survival analysis were harvested for pathologic analysis at the point they met euthanasia criteria or at the study end-point. For subsequent virologic and immunologic studies, mice were harvested at 4 (peak of peripheral viremia) and 8 dpi (peak of detectible virus in the CNS). At 8 dpi, it is also possible to observe early adaptive immune responses in the CNS. Later time-points were examined initially but due to high levels of mortality were used for preliminary data only due to numbers of mice lost to the study.

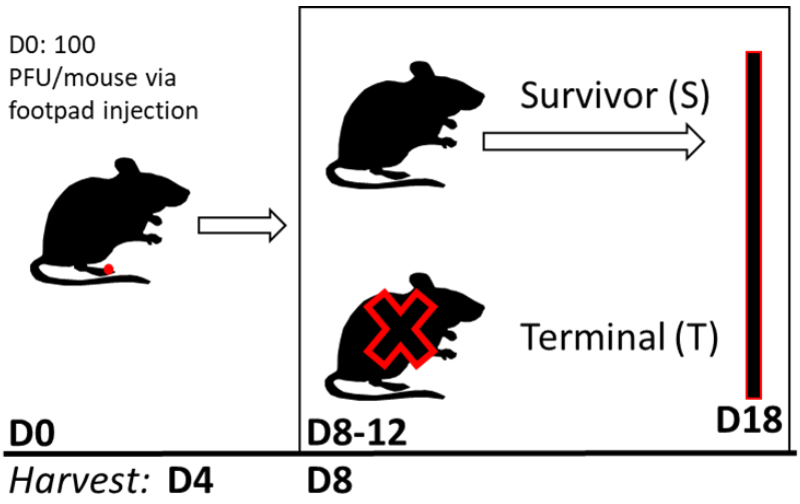

Figure 3-1: Schematic of infection and harvest time points
Mice were inoculated D0 (0 days post infection; dpi) via footpad inoculation with 100 PFU (Methods 2.8), or by intracranial inoculation (Methods 2.9). Mice were followed for survival analysis until D18 (18dpi); mice either met euthanasia criteria D8-12 (8-12 dpi) during the acute phase of disease or went on to survive until study endpoint (18 dpi). Mice that met euthanasia criteria (Terminal) and survived until study end (Survivors) were necropsied and formalin fixed for histopathological analysis. At $^{4\ DPI}$ (4 dpi) and D8 (8 dpi) mice were harvested for virologic and immunologic analysis.

3.3 Results: Identification of a Novel Role for STING in Host Defense against WNV

3.3.1 *Survival Analysis*

Previous studies demonstrated that mice defective in STING signaling experienced increased mortality during WNV infection, yet the linkage of STING to immune response programming for defense against WNV has not been defined [71]. Using genetically knocked-out *Tmem173* (STING$^{-/-}$) mice [112], we first performed a survival analysis to confirm the role of STING in host survival during WNV infection (**Figure 3-2A**). C57B/6J (B6, WT) and STING$^{-/-}$ mice were infected through subcutaneous virus challenge via foot-pad injection and monitored for 18 days post infection (dpi). Mice were scored daily for morbidity, marked as loss in body weight (**Figure 3-2B**) and increased clinical symptoms (clinical score) (**Figure 3-2C**). Consistently,

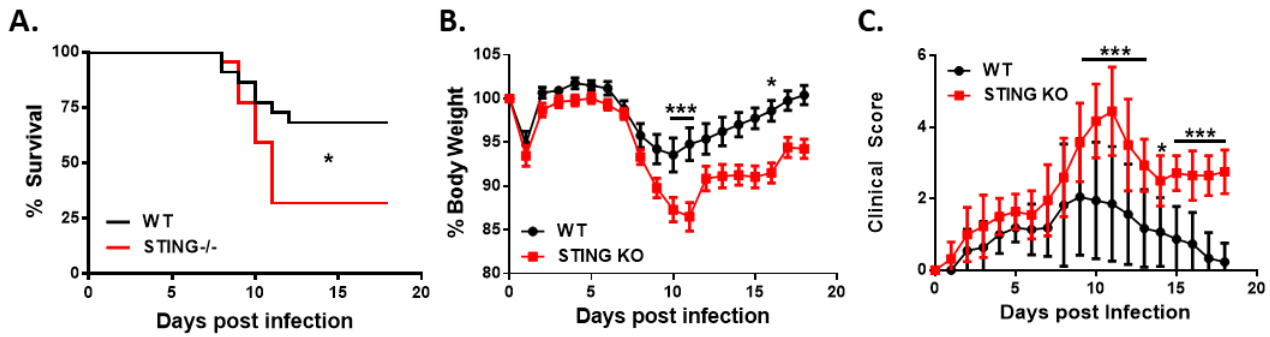

Figure 3-2: Morbidity and mortality analysis in WT vs. STING$^{-/-}$ mice
(A) Increased mortality in STING$^{-/-}$ mice. n = 22 per strain; Mantel-Cox analysis, p = 0.05*; p = 0.005**, p = 0.0005***. (B-C) Body weight loss (B) and clinical scores (C) are more pronounced in STING$^{-/-}$ mice, indicating increased morbidity during WNV infection. n = 22 per strain; two-way ANOVA, Bonferroni posttest; p = 0.05*; p = 0.005**, p = 0.0005***.

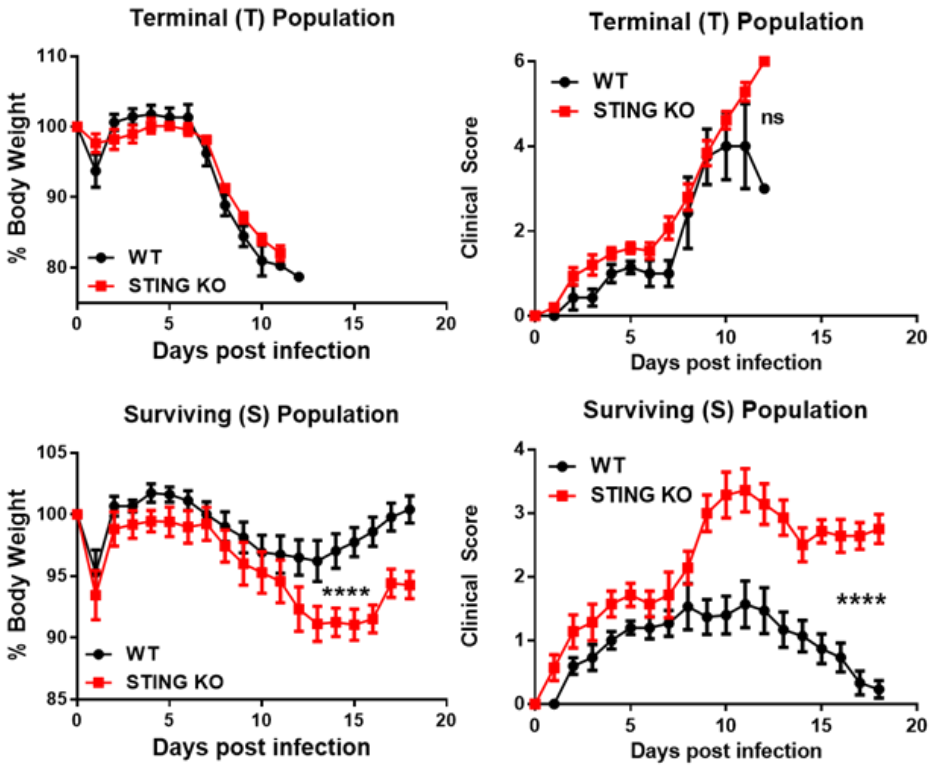

Figure 3-3: Stratification of clinical scores and loss of body weight between WT and STING$^{-/-}$ populations
Stratification of clinical scores and loss of bodyweight between WT and STING$^{-/-}$ populations. (Left) Body weight loss in (top) Terminal (T) vs (bottom) Survivor (S) populations. n = 22 per strain; two-way ANOVA. (Right) Clinical score analysis in (top) Terminal (T) vs (bottom) Survivor (S) populations. n = 22 per strain; two-way ANOVA.

between 8-12 dpi, mice either met euthanasia criteria (Terminal; T) or went on to survive (Survivors; S) through 18 dpi (study end-point) (**Figure 3-3**). Using this model, we confirmed the occurrence of increased susceptibility to WNV infection in the complete absence of *Sting* (**Figure 3-2A**), similar to what was previously described in STING$^{gt/gt}$ mice [71]. Additionally, we observed significantly increased clinical severity scores in the STING$^{-/-}$ mice including at the study-endpoint when WT mice had returned to a base-line clinical score (**Figure 3-2B-C**). In order to assess if this increased morbidity was equally or differentially represented by the Terminal and Survivor cohorts, we retrospectively stratified the groups and found that significant differences in body weight loss and clinical scores between WT and STING$^{-/-}$ mice were only observed in the Survivor cohort and not in the Terminal cohort (**Figure 3-3**).

3.3.2 *Clinical symptoms and observations*

Analysis of clinical symptoms revealed a strong CNS phenotype in the STING$^{-/-}$ mice, suggesting a role for STING in conferring neuropathological protection during WNV infection. STING$^{-/-}$ mice displayed increased neurological symptoms of disease, characterized by loss of balance, reduced muscle tone and reflexes predominantly in the pelvic limbs and increased paresis and paralysis, implicating severe damage to the hind-brain and spinal cord (**Figure 3-4**).

3.3.3 *CNS histopathology*

When we examined CNS histopathology, we found that in both WT and STING$^{-/-}$ mice, scores were higher in Survivor population (**Figure 3-5**). Intriguingly, while STING$^{-/-}$ Terminal mice displayed increased CNS pathology, the WT Terminal cohort had unexpectedly low clinical scores, suggesting that they met euthanasia criteria for reasons independent of severe encephalitis.

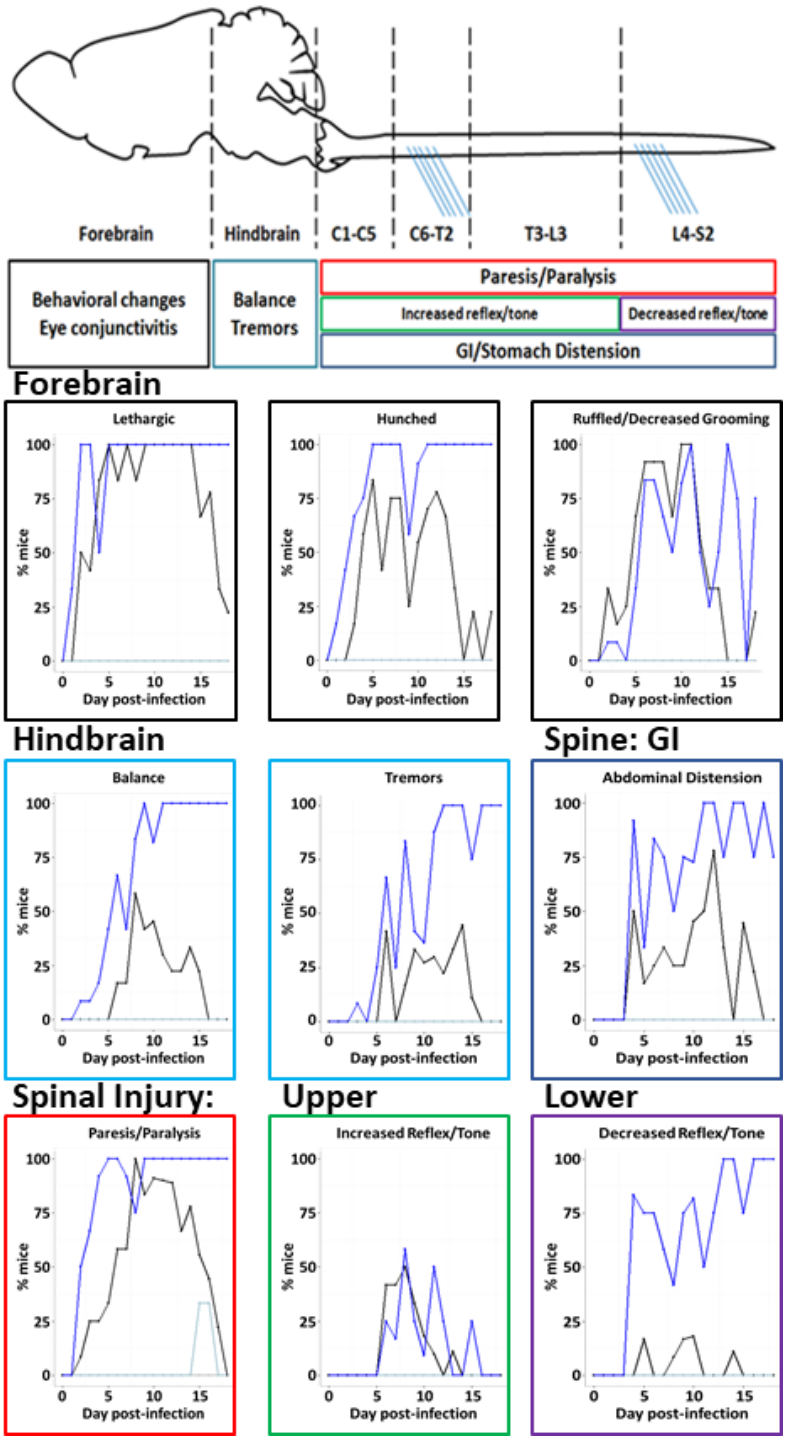

Figure 3-4: Clinical analysis of neurological symptoms in WNV infected WT vs STING$^{-/-}$ mice

(Schematic) Map of predicted clinical symptoms associated with WNV damage of CNS regions. Outline color of schematic correlates predicted damage with clinical symptom. (Graphs) Clinical symptoms observed during WNV infection of WT and STING$^{-/-}$ mice. n = 10 per strain. Graph Legend: (Gray) WT Mock-infected; (Light-blue) STING$^{-/-}$ Mock-infected; (Black) WT-WNV infected; (Dark Blue) STING$^{-/-}$ WNV-infected.

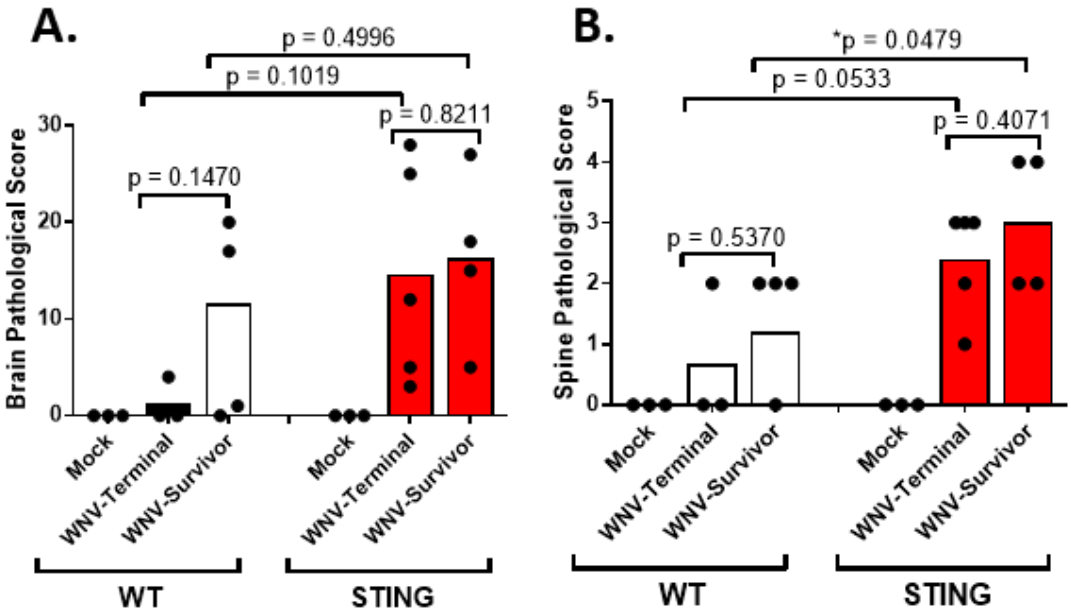

Figure 3-5: Combined (total) histopathological score in the brain (A) and spinal cord (B) Combined (total) histopathological score in the brain (A) and spinal cord (B). Histopathological damage observed in the brains (A) spinal cord (B) by H&E staining in WT and STING$^{-/-}$ Terminal (T) and Survivor (S) mice. n = 3-9 per condition; students t-test (unpaired).

Supplemental Figure 1

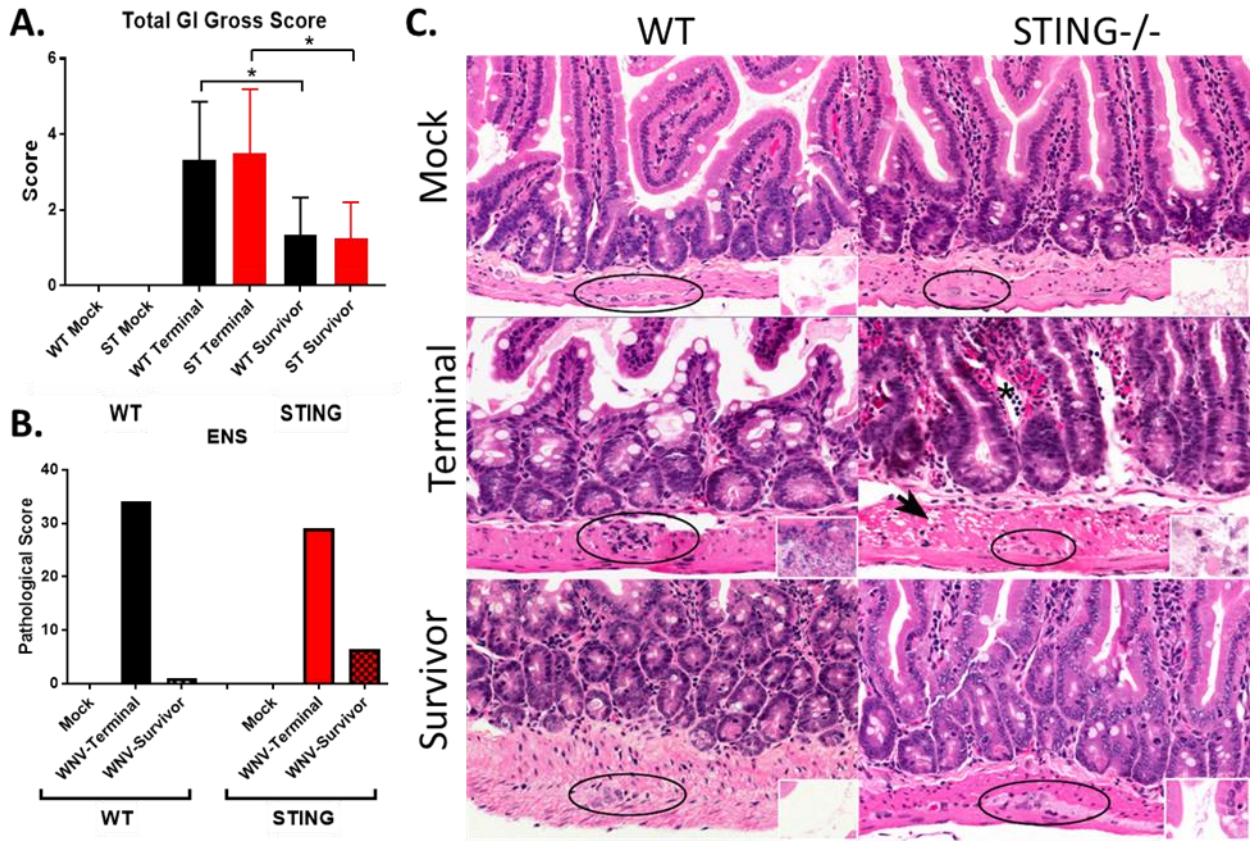

Figure 3-6: Pathology and clinical scoring the GI tract

A: Gross pathology scores of the GI tract from necropsied mice. Mice were visually examined at necropsy and scored. Scores were assigned to each mouse ranging from 0 (normal GI tract) to 3 (grossly distended or aberrant morphology). n = 3-9 per condition; students t-test (unpaired). * = 0.0500.

B: Histopathological analysis was performed on randomly selected representative mice. Sections of the GI were scored including sections from: 1) the duodenum and upper jejunum; 2) jejunum; 3) ileum; 4) cecum; 5) colon; 6) stomach. Graphed as the mean sum of all scores. n = 1-2 per condition.

C: Representative hematoxylin and eosin-stained small intestinal sections. Mock tissues are unremarkable with readily detectable myenteric ganglia (black ovals) and normal scant intestinal contents (inserts). Survivor mice have mild enteritis and minimal changes in the myenteric ganglia (ovals) with normal intestinal contents. In contrast, terminal mice have myenteric ganglia with neuritis, degeneration and loss. There is bacterial overgrowth and exudative material within the intestinal contents (inserts). In the STING$^{-/-}$ mice, there is readily observable vacuolation of the inner tunica muscularis (arrow), dilation of lacteals (asterisk) and intramucosal hemorrhage and lymphocytic and proliferative enteritis. All panels, original magnification 200X.

During necropsy, we observed that the gastrointestinal (GI) tract of Terminal mice exhibited gross distension or other aberrant phenotypes including stool compaction and increased friability (**Figure 3-6A**). Histopathologic analysis confirmed that Terminal mice display increased GI pathology that included bacterial overgrowth and neuronal degeneration and loss in the myenteric ganglia, particularly in STING$^{-/-}$ (**Figure 3-6B-C**). Previous studies have indicated that GI manifestations during WNV infections exist in both mice and humans and are positively correlated to increased neurotropism and mortality [124-126, 130]. This outcome may imply that WT mice are meeting euthanasia criteria following WNV infection due to severe GI disease rather than severe CNS involvement as previously thought. Further, these results demonstrate that STING plays a systemic role in host defense against WNV. These data also reveal that GI pathology, not CNS pathology, correlate with increases in mortality in both WT and STING$^{-/-}$ mice. Together, these results show an essential role for STING in host survival and neuropathological defense in the CNS during WNV infection.

3.3.4 *Virologic analysis in the CNS and Periphery*

To determine if STING is required for viral control in the CNS, we challenged mice with WNV via footpad injection and examined tissue viral load at 4 dpi (peak of peripheral viremia) and 8 dpi (peak of detectible virus in the CNS) (**Figure 3-7**). Mice were terminally anesthetized and whole-body saline-perfused prior to sacrifice and tissue harvest to ensure removal of blood from the tissues. Brains were macrodissected into gross anatomical regions including the cerebellum, brain-stem, cortex and regions contained within the cortex (sub-cortex). The spine was collected from the base of the skull through the pelvic junction and spinal cords were PBS pressure extracted. Viral titer of the extracted spinal cords was examined by plaque assay individually for each mouse in the cohort (**Figure 3-7**). Virus was not consistently found in the CNS of all mice

examined. There was however, a consistent trend toward increased numbers of infected mice with detectible virus in the CNS as well as increased viral titers in the CNS of STING$^{-/-}$ mice compared to WT.

To determine if the actions of STING might be restricted to the CNS for WNV protection, we performed an intracranial virus inoculation, bypassing the role of the peripheral immune response and physical barriers such as the blood-brain barrier to directly infect the brain with WNV (**Figure 3-8**). At 4 dpi, there was no difference in CNS viral load found in WT vs STING$^{-/-}$ mice nor was viral load different between STING$^{-/-}$ and WT mice. Taken together, our observations imply that the role of STING is not limited to mediating viral control in the CNS; instead STING has an essential role in the periphery that results in restriction of CNS pathology. It is possible that STING is therefore required in the development of a protective immune response in the periphery such that in the absence of STING the immune response is aberrantly programmed, leading to CNS immunopathology.

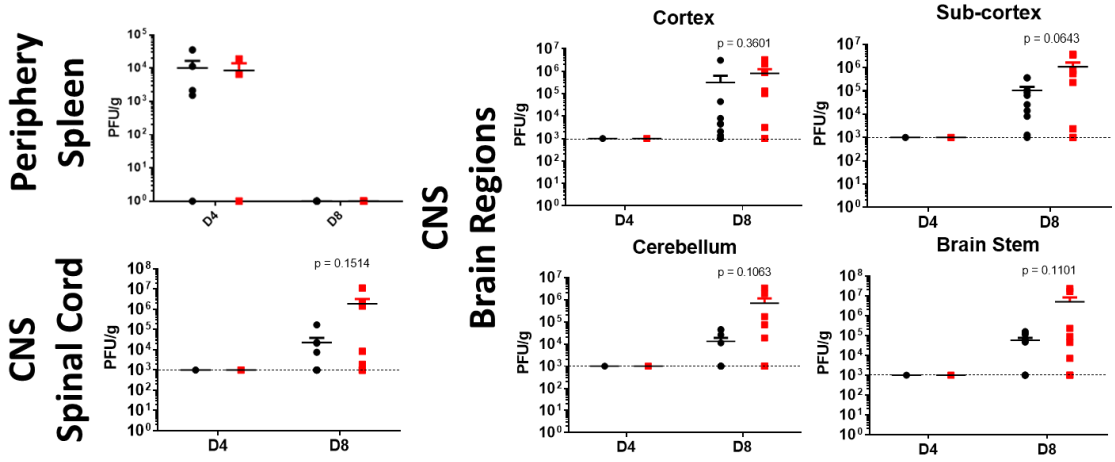

Figure 3-7: *In vivo* virologic analysis in CNS and peripheral tissues
WNV viral load in macro-dissected brain sections (cortex, sub-cortex, cerebellum and brain-stem), spinal cord and spleen of WT and STING$^{-/-}$ infected mice, 4 dpi and 8 dpi post infection. n = 6-10 per strain per time-point. Unpaired students t-test; p=0.05*; p=0.005**.

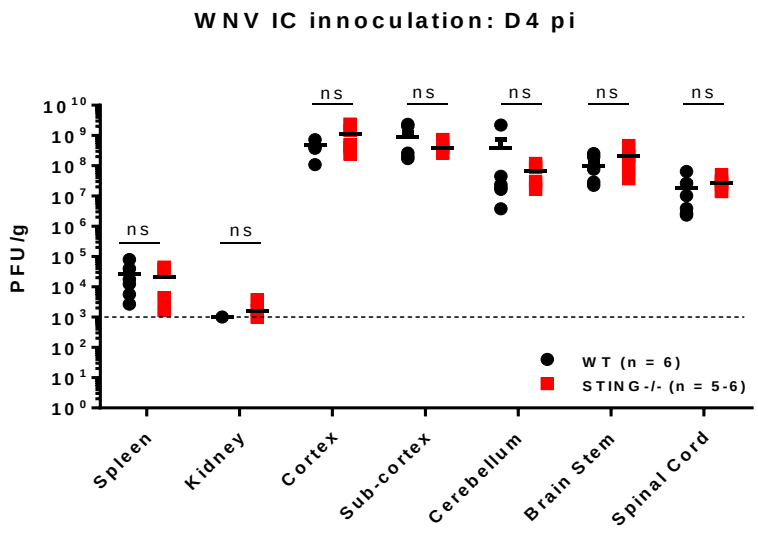

Figure 3-8: Intracranial inoculation to determine CNS role for STING
Titer in mice infected with WNV-TX via intracranial inoculation 4 dpi. n = 6 WT and n = 5-6 STING$^{-/-}$. Students t-test, p=0.05*; p=0.005**.

3.3.5 *STING is required for IFN/ISG homeostasis and control of WNV in BMDM*

Given that STING deficiency was associated with enhanced mortality (**Figure 3-2**) without a significant increase in CNS viral burden (**Figure 3-7**), we hypothesized that STING deficiency could result in defective antiviral innate immune signaling and lead to loss of viral control in the periphery, thereby leading to enhanced morbidity and mortality. We first tested the role of STING in bone-marrow derived macrophages (BMDM), as macrophages are a tropic cell and key modulator of peripheral viral control during WNV infection (**Figure 3-9**) [48]. As expected, WNV levels were significantly increased by 24 and 48 hours post inoculation (hpi). Unexpectedly however, STING$^{-/-}$ BMDM had increased innate immune and inflammatory gene expression, including enhanced level of type I IFN expression during WNV infection (**Figure 3-9**). This suggests that there may be a baseline deficit in tonic IFN levels, preventing cells from early antiviral responses. This implicates a potential role for STING-dependent IFN control of WNV both in early antiviral control and IFN dependent immune homeostasis.

A. WT vs STING BMDM infected with WNV

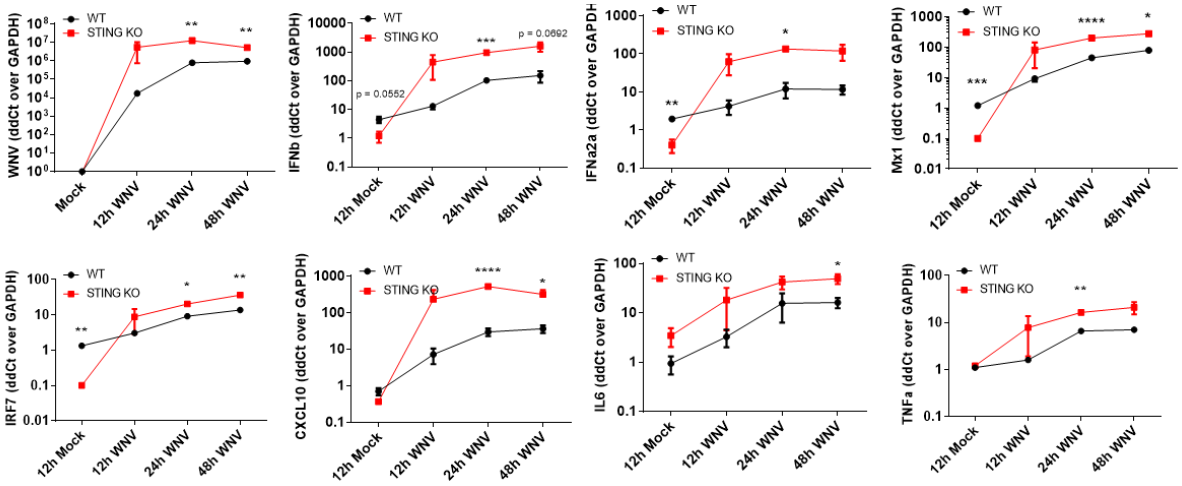

B. WT and STING$^{-/-}$ compared to MAVS$^{-/-}$ mice infected with WNV

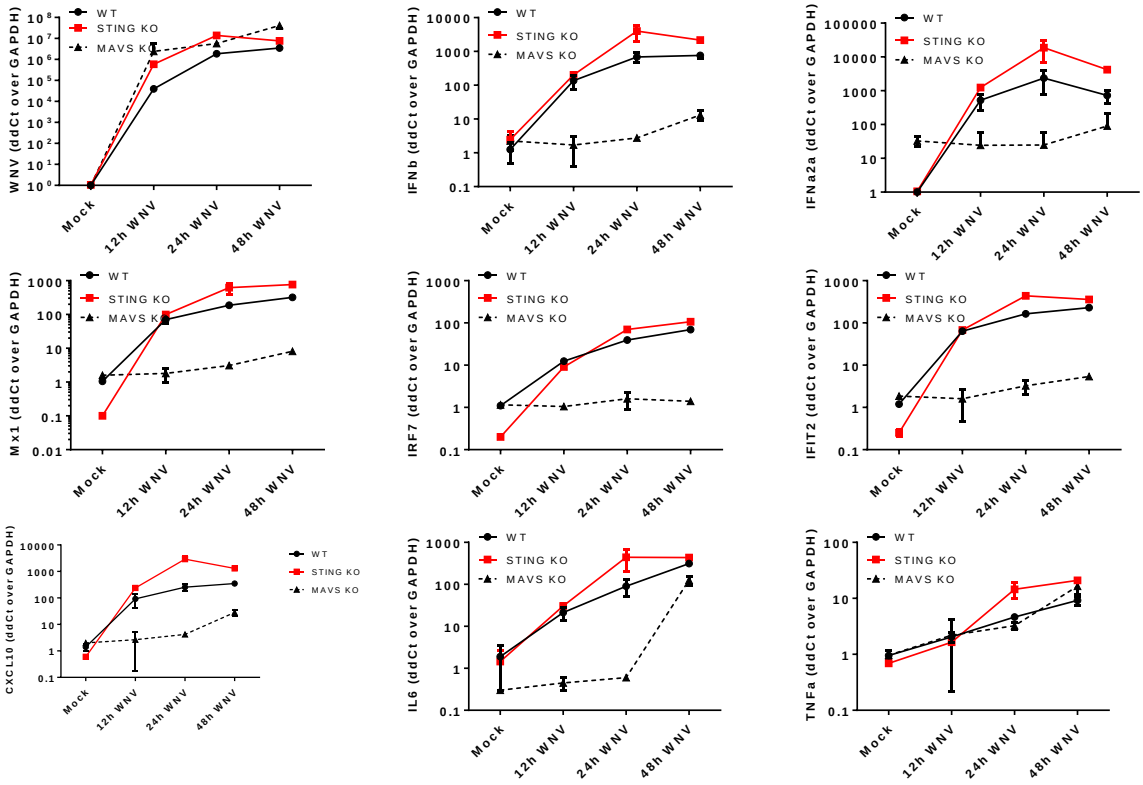

Figure 3-9: BMDM have decreased baseline IFN and ISG production and exacerbated signaling during WNV infection.

WNV detection in BMDM by RT-qPCR; innate immune response gene expression in WNV-infected BMDM over an infection time course. A) WT vs STING$^{-/-}$ BMDM showing significant differences between infectious replicates (n = 3). B) Viral and immune comparison between WT, STING$^{-/-}$ and MAVS$^{-/-}$ demonstrating early loss of viral control in STING$^{-/-}$; infectious replicates (n = 2). Bone marrow was harvested and differentiated into BMDM with mMCSF for 7 days. Cells were infected and harvested at the indicated time-points. Mock infected cells harvested at 12hpi. Results were reproducibly significant in multiple studies. Calculated as linear fold change over WT M. Unpaired students t-test; p=0.05*; p=0.005**, p=0.0005***.

3.3.6 *Innate immune response in vivo*

Given that STING deficiency was associated with enhanced mortality (**Figure 3-2**) without a significant increase in CNS viral burden (**Figure 3-7**), we hypothesized that STING deficiency could result in defective antiviral innate immune signaling and lead to loss of viral control in the periphery, thereby leading to enhanced morbidity and mortality. Similarly, to viral titers, viral RNA was detected equally in spleens of infected WT and STING$^{-/-}$ mice at 4 DPI, but the virus was largely cleared from the spleen by 8 dpi post infection. In the CNS however, both viral RNA and innate immune gene expression were increased in at 8 dpi in WNV-infected STING$^{-/-}$ mice (**Figure 3-10**). These data demonstrate that innate immune activation and the inflammatory response are exacerbated in both *in vitro* and *in vivo* STING deficient models, possibly culminating in enhanced immunopathology in STING$^{-/-}$ mice.

In order to determine if there was a systemic change in the innate immune profile in STING$^{-/-}$ mice, we examined the cytokine and chemokine profile in the serum of WT and STING$^{-/-}$ mice at the peak of peripheral viremia (4 dpi) and CNS viral burden (8 dpi). At 4 dpi, mock infected STING$^{-/-}$ mice had an increased basal production of multiple cytokines and chemokines, which appeared to have resolved partially by D8 that may be in response to inoculation even in the absence of virus (**Figure 3-11**). In WNV infected mice, we also observed significant increases in IL33, IL4, IL6, IL15, MCSF, Gro-alpha, while at 4 dpi IP-10 (CXCL10) was decreased in STING$^{-/-}$ compared to WT mice (**Figure 3-12**). While these cytokines have multiple roles in immune modulation, a common role among them is in activation and recruitment of T cells. These data suggest that STING is required for regulation of immune cytokine and chemokines that program immune cell trafficking and actions during WNV, as has been shown for STING in cancer immunity and autoimmune signaling [138].

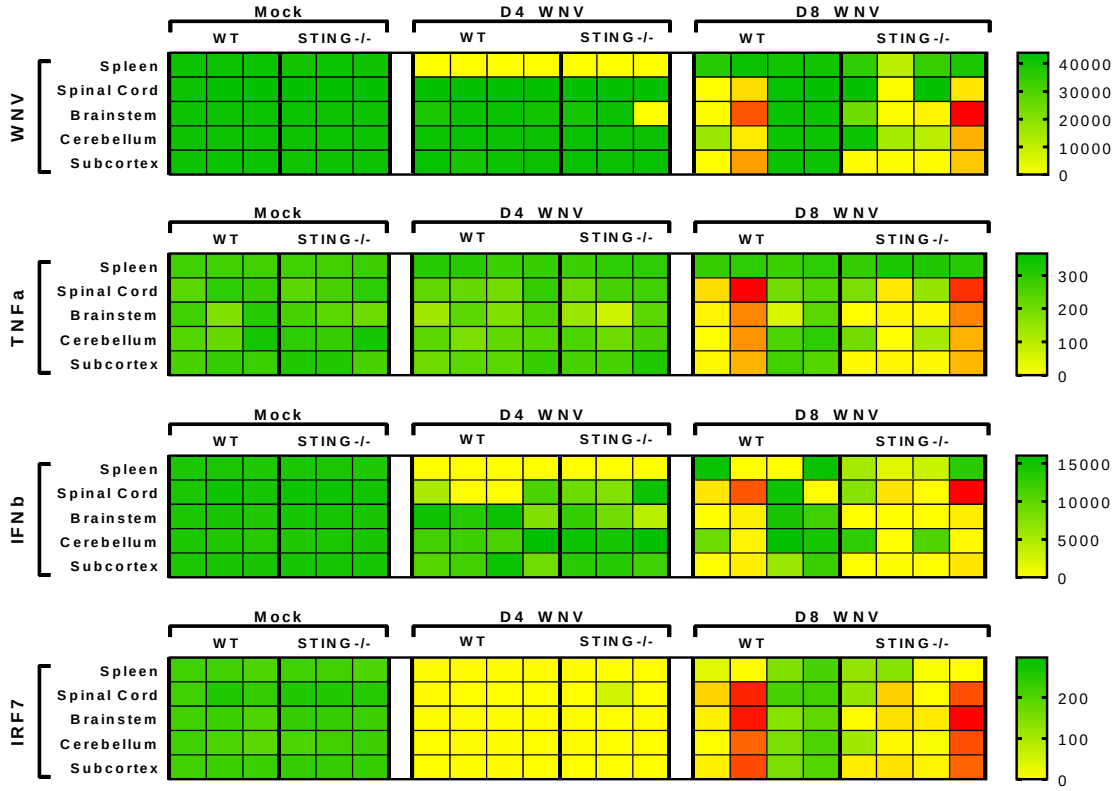

Figure 3-10: Innate immune profile *in vivo*

In vivo innate immune profile in splenic and CNS tissues. RT-qPCR detection of innate immune genes in the spleen, spinal cord and brain regions (brain stem, cerebellum, sub-cortex). Columns indicate individual mice; rows the different tissues. Calculated as linear fold change over GAPDH in WT Mock.

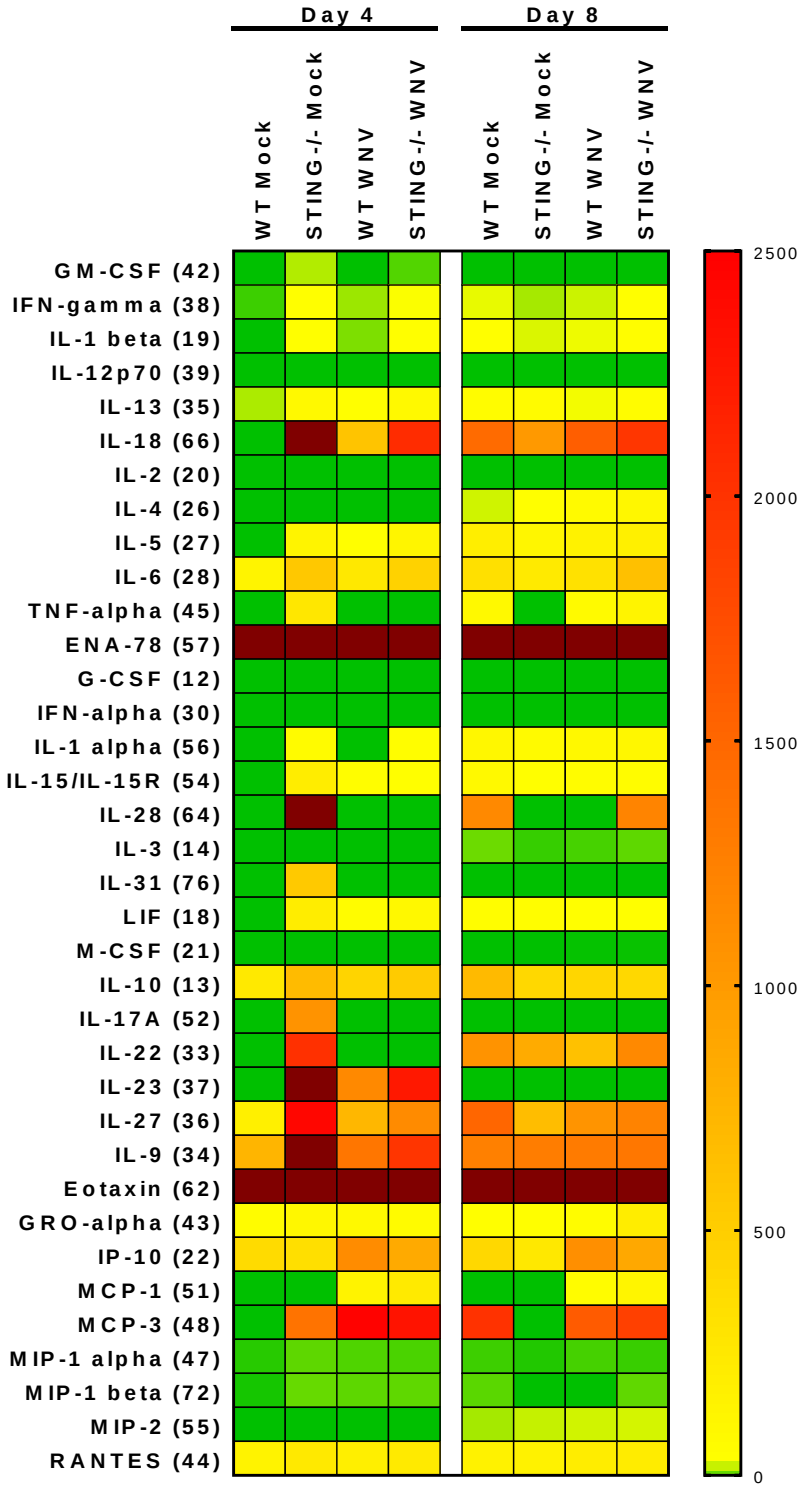

Figure 3-11: Luminex analysis in WT and STING$^{-/-}$ serum

Luminex analysis of cytokines and chemokines from serum in mock (PBS) and WNV infected mice at 4 and 8 dpi; n = 3-8 per condition.

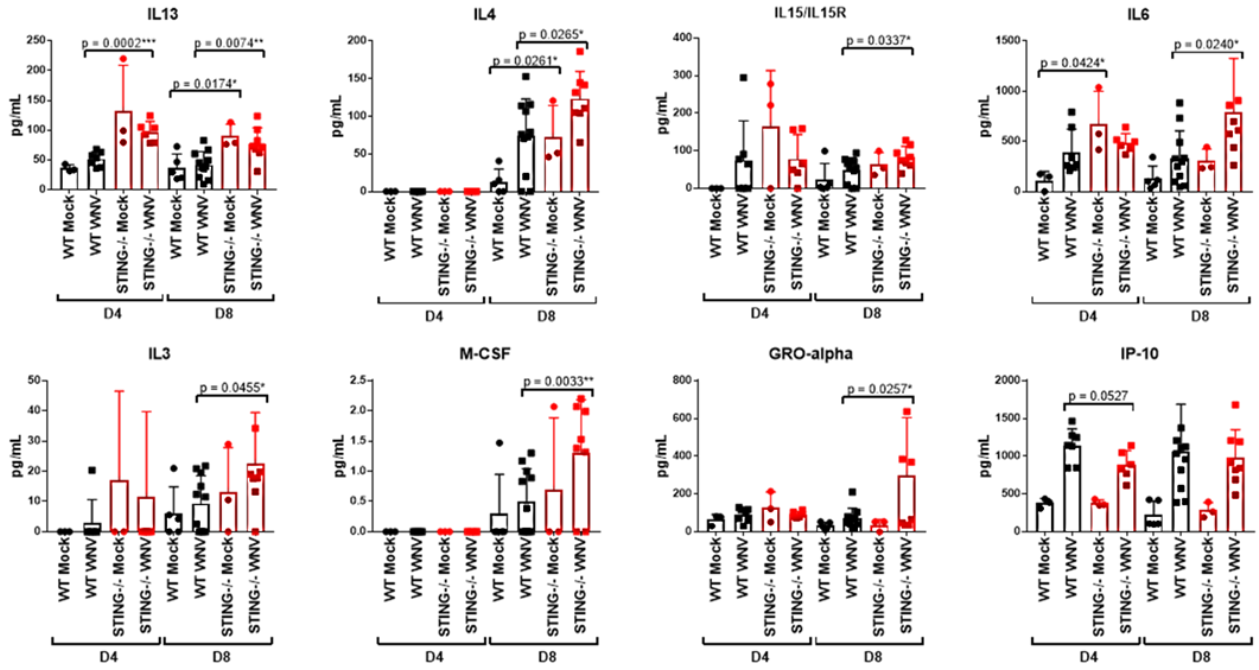

Figure 3-12: Differences in serum levels of WT and STING$^{-/-}$ innate immune signal
Serum Luminex results with statistically significant differences in response to WNV infection between WT and STING$^{-/-}$ mice *in vivo*. Unpaired students t-test; p = 0.05*; p = 0.005*; p = 0.0005***).

3.3.7 *Flow analysis in the spleen*

To determine if STING is required for proper programming of the T cell response during WNV infection, we examined splenic T cells from WT and STING$^{-/-}$ mice at 8 dpi, a time point when the adaptive immune response is established in WT mice [53]. We observed a reduction in the frequency of CD8 T cells, along with a trend toward decreased numbers of T cells in the spleens of STING$^{-/-}$ mice compared to WT during WNV infection (**Figure 3-13**). We also observed a significant increase in the frequency of CD4+ T cells in STING$^{-/-}$ mice (**Figure 3-13**), with a corresponding trend toward increased absolute numbers.

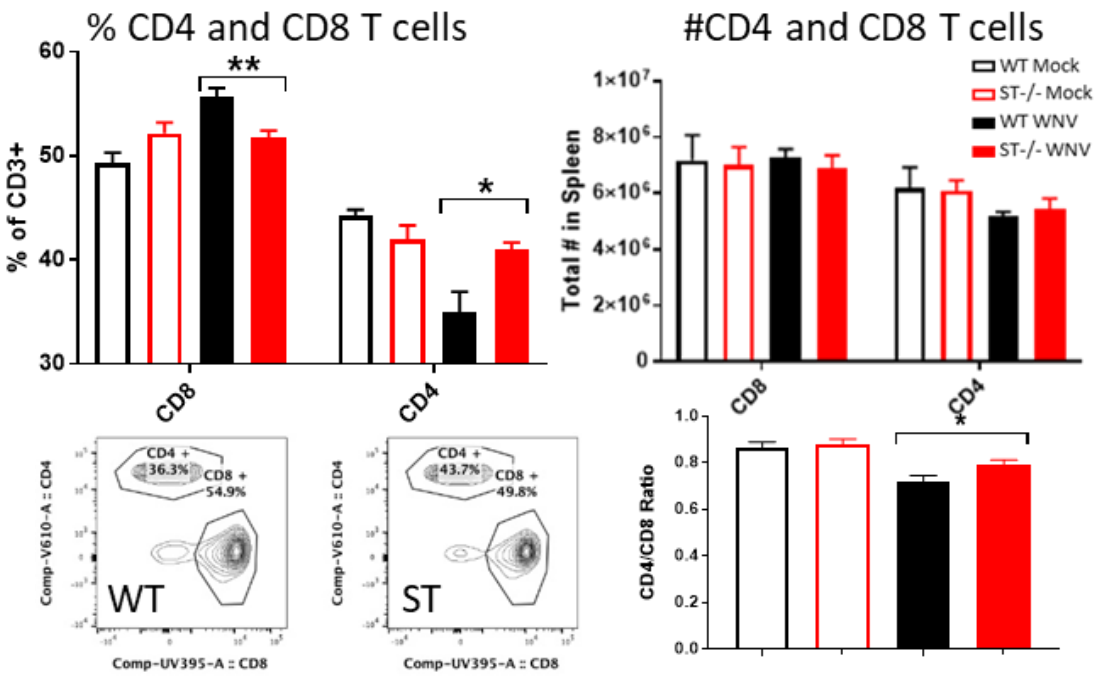

Figure 3-13: CD4 and CD8 in the spleen
CD4 and CD8 frequency and absolute number in D8 post infection spleens (top). Flow schematic (bottom left) and CD4/CD8 ratio (bottom right). n = 4-8 per condition. Unpaired students t-test; p = 0.05*; p = 0.005*; p = 0.0005***).

Additionally, within the CD8 T cell subset (**Figure 3-14**), there was a significant decrease in frequency of activated (CD44+) and CXCR3+ T cells, and we observed a consistent trend of decrease in the frequency of WNV-specific CD8+ T cells in the spleens of STING$^{-/-}$ mice compared to WT, suggesting that STING is required for optimal anti-WNV CD8+ T cell responses. While we observed a trend toward differences in the absolute number of most cell populations examined between WT and STING$^{-/-}$ mice, we found that significant differences most typically occurred in cell frequencies, suggesting that the balance of T cells subsets may be skewed in the absence of STING. In particular, we found skewing within the T regulatory cell (FoxP3+) populations (**Figure 3-15**), with significant deficits in Ki67, CD44 and CD73+ Tregs (**Figure 3-16**). These data suggest that STING is required for optimal programming of protective T cell responses and T cell frequencies during WNV infection in the spleen.

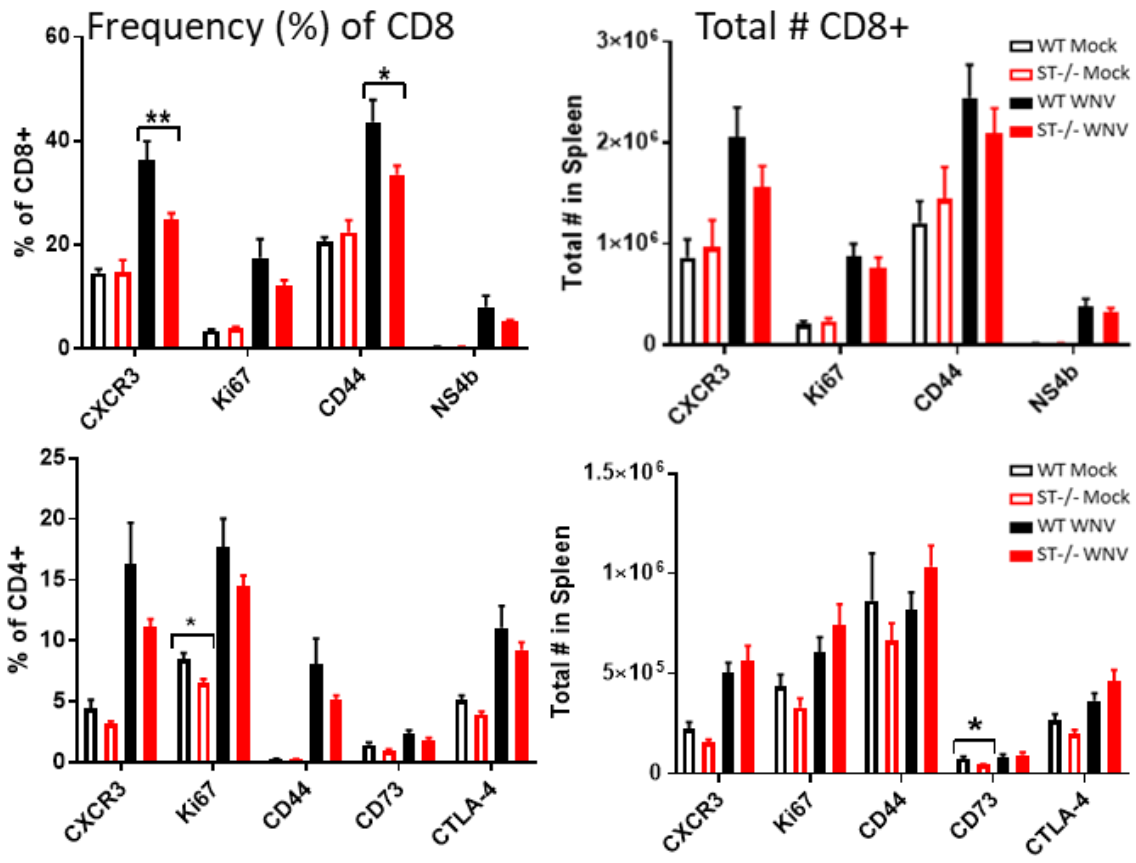

Figure 3-14: CD4 and CD8 activation in T cells

(Top) Characterization of D8 pi splenic CD8 sub-populations (CXCR3, Ki67, CD44 and NS4b). Left: frequency; Right: Absolute number. n = 4-8 per condition. Unpaired students t-test; p = 0.05*; p = 0.005*; p = 0.0005***). (Bottom) Characterization of D8 pi splenic CD4 sub-populations (CXCR3, Ki67, CD44, CD73 and CTLA-4). Left: frequency; Right: Absolute number. n = 4-8 per condition. Unpaired students t-test; p = 0.05*; p = 0.005*; p = 0.0005***).

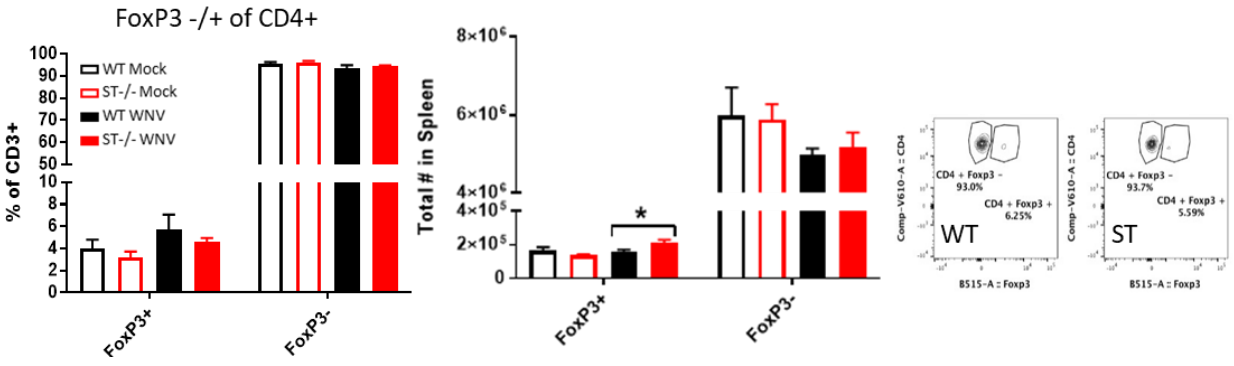

Figure 3-15: Treg population of CD4

Splenic FoxP3- and FoxP3+ CD4+ T cells. Left: frequency; Middle; absolute number; Right: gating scheme. n = 4-8 per condition. Unpaired students t-test; p = 0.05*; p = 0.005*; p = 0.0005***).

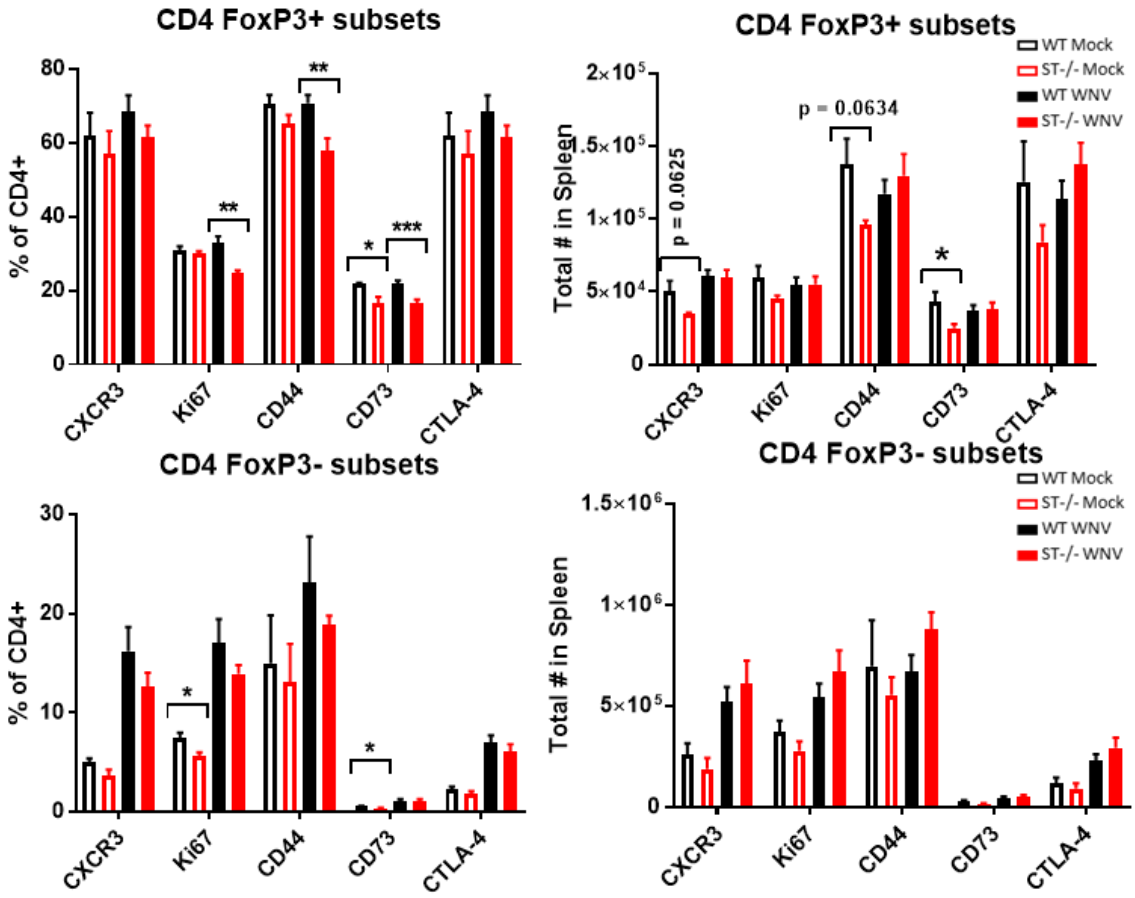

Figure 3-16: Treg markers

Analysis of FoxP3+ (Top) and FoxP3- (Bottom) subpopulations (CXCR3, Ki67, CD44, CD73 and CTLA-4). Left: frequency; Right: Absolute number. n = 4-8 per condition. Unpaired students t-test; p = 0.05*; p = 0.005*; p = 0.0005***).

3.3.8 *Cellular infiltration in the CNS and neuronal death in STING$^{-/-}$ mice*

The increase in clinical disease and histopathological damage observed in the STING$^{-/-}$ versus WT mice, particularly in Survivors, could be due to an aberrant adaptive immune response resulting in CNS damage in after initial viral insult. We found that CNS lesions in WT mice is largely restricted to the cortex and meninges, while STING$^{-/-}$ mice display increased pathology in the cerebellum and hind/mid brain regions in addition to the cortex and meninges (**Figure 3-17**). We then performed a CD3 IHC stain in the brains of Survivors, we found increased clusters of CD3 infiltrate in the hind and mid-brain regions; at the same localization we observed robust histopathology (**Figure 3-18**). On serial sections of the same tissues, we examined the brains of Terminal vs Survivor mice for the presence of WNV antigen via immunostain of formalin-fixed tissue (**Figure 3-19**). WNV foci were found in the brains of WT and STING$^{-/-}$ Terminal mice but were not apparent in WT or STING$^{-/-}$ Survivors, suggesting that either the virus had cleared or that surviving mice did not have CNS infection. However, we did observe continued gliosis, suggesting that a potential immunopathology may occur in the brain of STING$^{-/-}$ mice infected with WNV. Localization of CD3 and WNV staining in STING$^{-/-}$ mice in the hind-brain correlates with both the location of pathological lesions increased symptoms such as loss of balance and tremors (**Figure 3-4**). These observations suggest that STING plays a role in directing or maintaining the T cell response to specific loci within the CNS or that initial viral infection led to increased recruitment of a localized adaptive immune response that resulted in immunopathology. Furthermore, pathology in the spine was more diffuse, suggesting that STING has a widespread protective role in the CNS during WNV infection (**Figure 3-18**).

3.3.9 *STING in the CNS*

To determine where in the CNS STING is localized and if this tissue localization correlates to the location of the cellular infiltrate noted histopathologically, we utilized the Allen Brain Institute database to search for *Tmem173* (STING) localization in the mouse brain [143]. Within the brain, STING expression is found within the olfactory bulb, thalamus/midbrain, brainstem and cerebellum, as well as low levels throughout the cortex, overlapping areas that are affected most severely by WNV infection (**Figure 3-20**) [32, 143]. These regions of brain affected correlate with the clinical symptoms we observed including loss of balance, tremors, and loss of motor function (**Figure 3-4**). Histopathologically and by TUNEL staining, neuronal death was observed in both WT and STING$^{-/-}$ Survivors; however, it was more pronounced in STING$^{-/-}$ Terminal mice, suggesting STING may have a role in protecting neurons in the CNS (**Figure 3-21**).

In order to determine if STING is required for neuronal defense against WNV, primary cortical neurons were isolated and cultured, followed by infection with WNV to determine viral growth kinetics under conditions of single and multi-step growth (**Figure 3-22**). Surprisingly, no difference was detected between in WNV replication in WT and STING$^{-/-}$ primary cortical neurons (**Figure 3-23**).

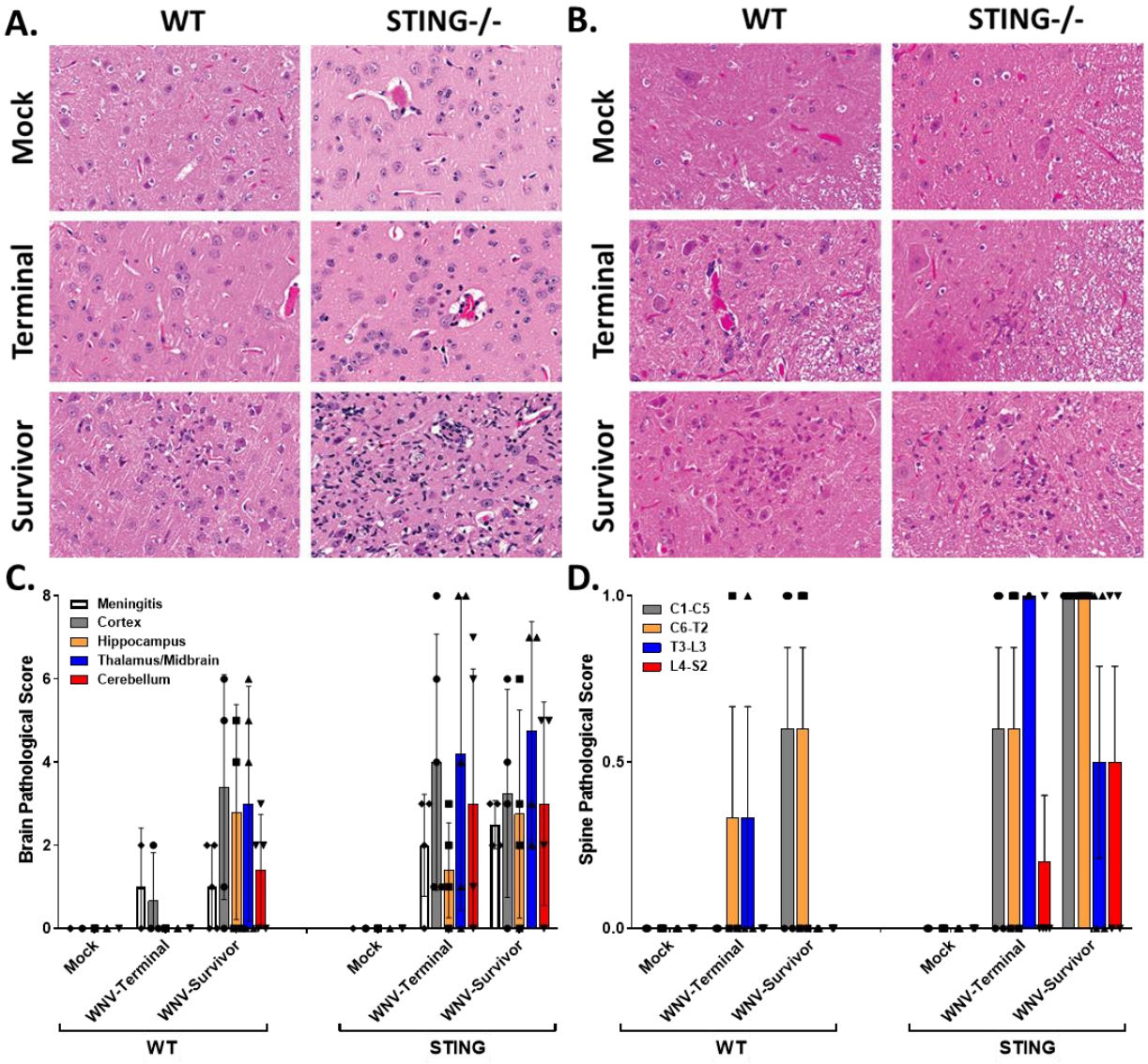

Figure 3-17: Histopathology in CNS of WT vs STING$^{-/-}$ mice

(A-B) Representative H&E of histopathological lesions and cellular infiltration in Brain (A) and Spinal Cord (B). (A) Mock tissues are unremarkable. Terminal mice have minimal lesions, observable in STING$^{-/-}$ as perivascular mononuclear cells and minimal gliosis. For both genotypes, survivor mice have readily observable neuropathology which is severe in the STING$^{-/-}$ mice with intense gliosis, neuronal degeneration and death, and perivascular cuffing with mononuclear cells. In the WT survivors, there is a mild focus of gliosis and neuronal degeneration. All panels, original magnification 200X. (B) Mock tissues are unremarkable. Terminal mice have minimal lesions, observable as perivascular mononuclear cells. For both genotypes, survivor mice have readily observable infiltration of mononuclear cells and neuronal degeneration. All panels, original magnification 200X. (C-D) Regional analysis of pathology in WT and STING$^{-/-}$ brains (C) and spinal cords (D) in Terminal (mice meeting euthanasia criteria) and Surviving (harvested at study endpoint) mice. n = 3-5 per condition.

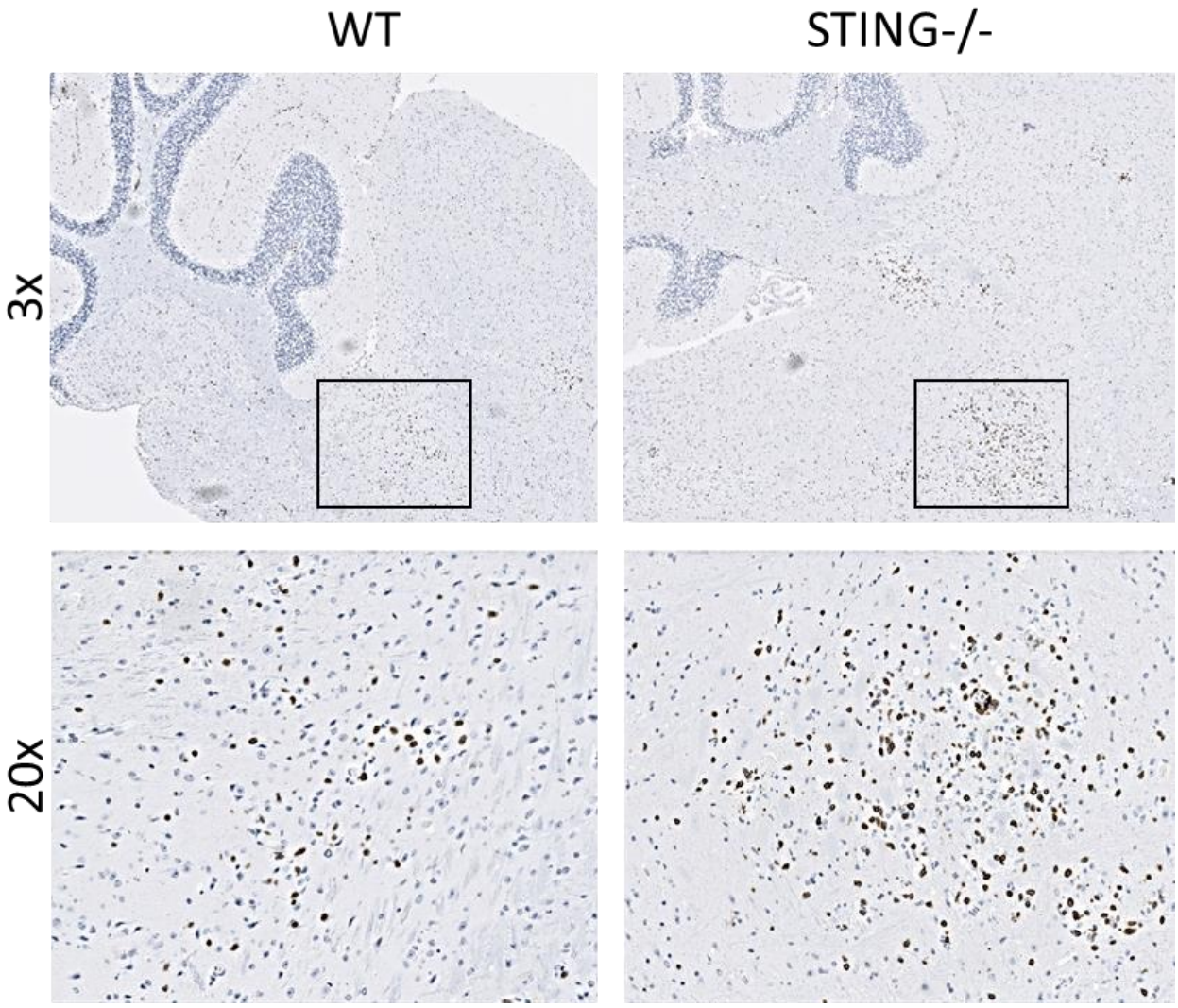

Figure 3-18: CD3 infiltrate in the brain
CD3 IHC of WNV infected brains. Boxed regions, higher magnification, lower panel. T cells stain brown; hematoxylin counterstain.

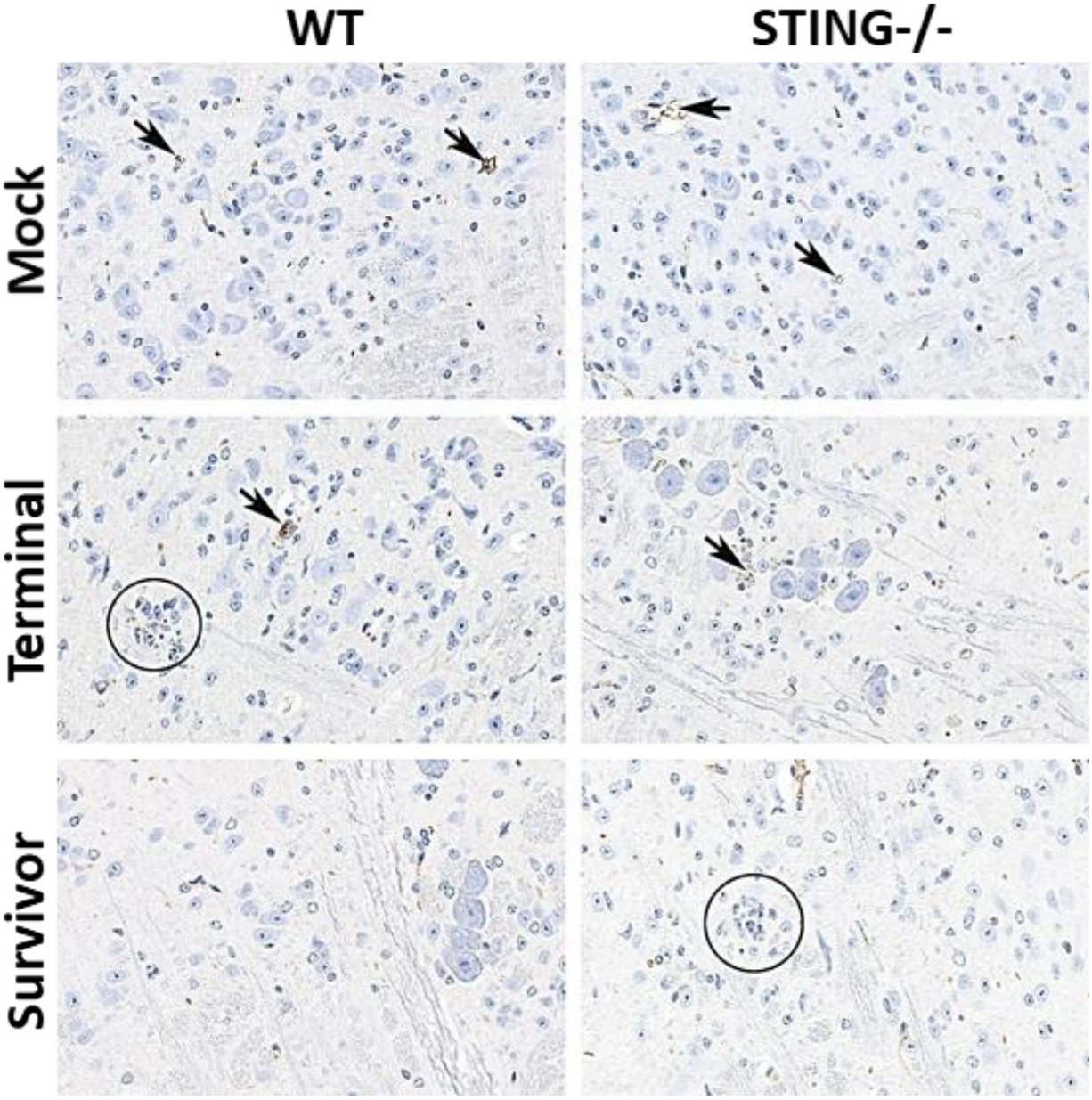

Figure 3-19: WNV IHC

WNV IHC in the brains of mock infected and WNV infected WT and STING$^{-/-}$ Terminal and Survivor populations. Mock tissues are unremarkable with non-specific staining of capillaries (arrows). Terminal mice have punctate staining near foci of gliosis (WT, circle) or neuronal degeneration (WT and STING$^{-/-}$, arrows). No discernable specific signal for WNV antigen was observed in either WT or STING$^{-/-}$ survivors, despite observable gliosis in STING$^{-/-}$ (circle). All panels, original magnification 200X.

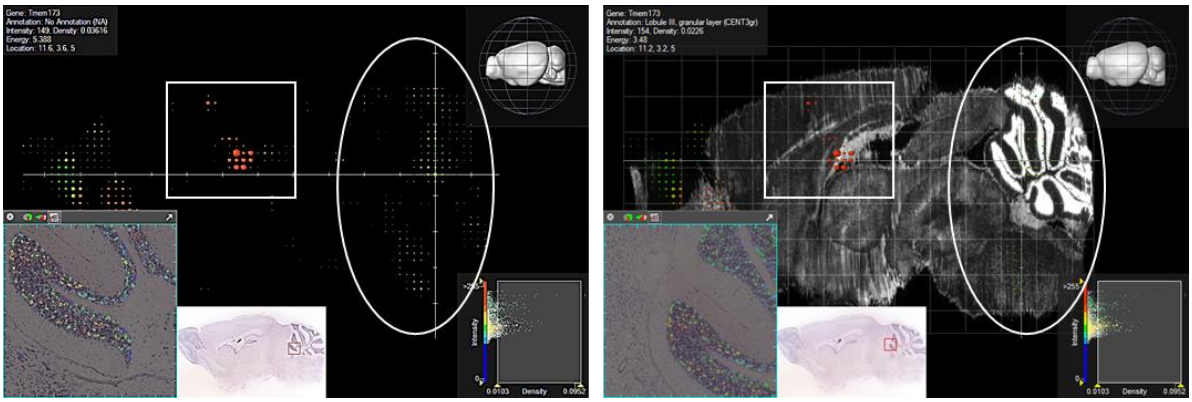

Figure 3-20: Localization of STING in the brain

STING localization in the brain is centralized to the hind/mid-brain, hippocampus, primary motor-cortex and olfactory bulb in the brain. Square: midbrain/thalamus region. Oval: hindbrain (cerebellum and brain-stem). © [2004] Allen Institute for Brain Science. [Allen Mouse Brain Atlas]. Available from: [http://mouse.brain-map.org/gene/show/48353]. Images acquired using [Allen Brain Institute Brain Explorer 2]. Available from: [http://mouse.brain-map.org/static/brainexplorer].

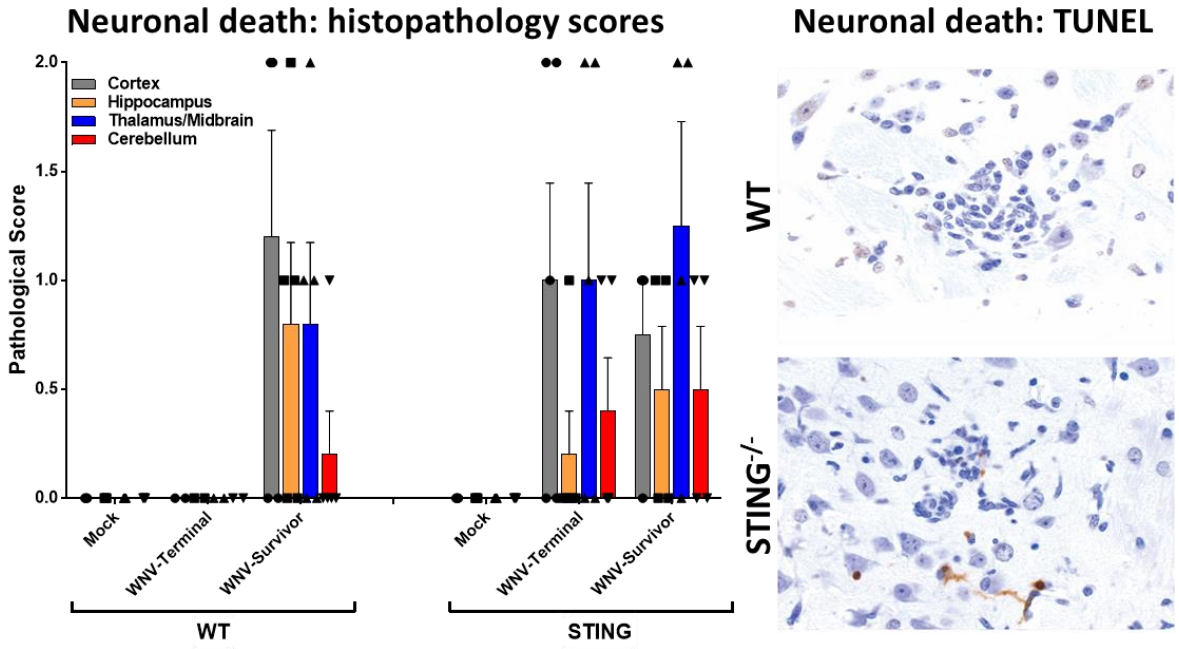

Figure 3-21: Neuronal death

(Left) Histoathological score of neuronal death observed by H&E staining. (Right) TUNEL staining; representative images of WT (top) and STING$^{-/-}$ (bottom) survivors showing neuronal death.

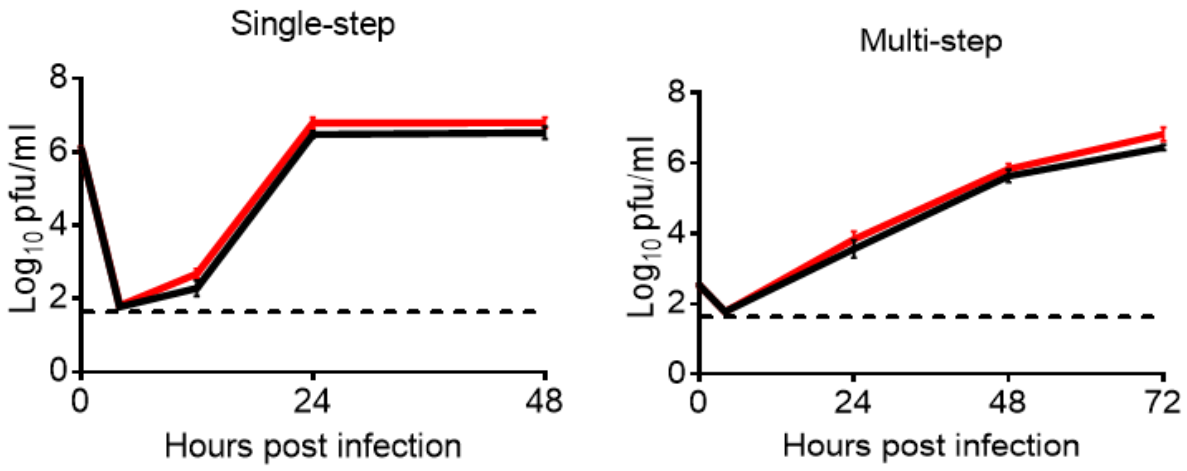

Figure 3-22:Viral load in primary cortical neurons

Single and multistep virologic analysis of primary cortical neurons from WT and STING$^{-/-}$ mice. Pooled samples of 3 embryos per genotype.

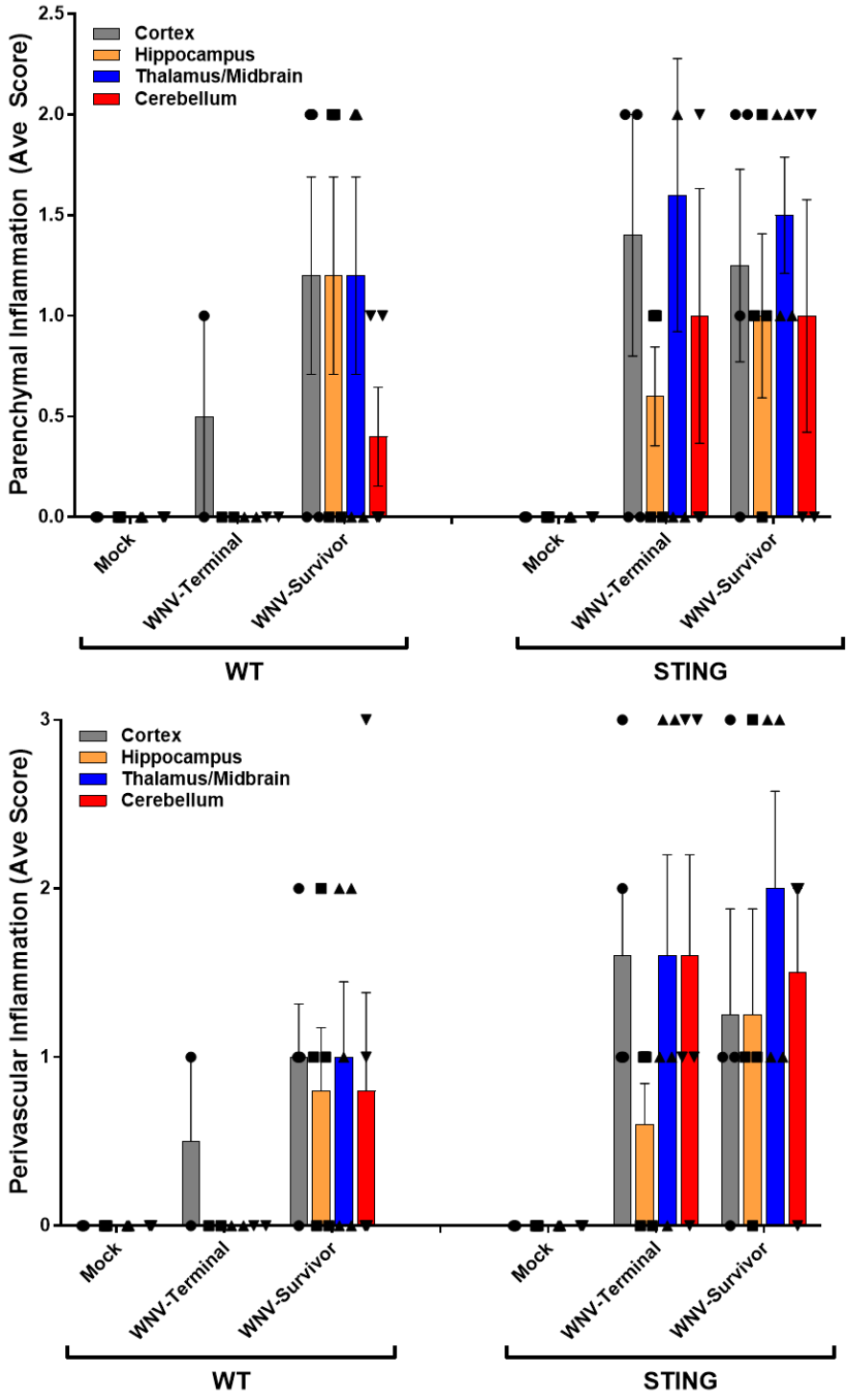

Figure 3-23: Cellular infiltrate in the CNS of WNV infected mice (WT and STING$^{-/-}$)
Cellular infiltrate in the brain in Terminal and Survivor mice by histopathological review of H&E. (Top) parenchymal inflammation; (bottom) perivascular inflammation. n = 3-5.

Because of the heightened innate immune profile and aberrant programming of the T cell responses in spleens of STING$^{-/-}$ mice, we examined the CNS-specific T cell profile across mouse lines. Histological analyses revealed trends toward increases in perivascular and parenchymal mononuclear infiltrate, suggesting the CNS pathology may be immune-mediated (**Figure 3-23**). Cumulatively, these data suggest that STING has an essential role in maintaining immune response homeostasis and immune programming in initial defense against WNV infection. Without STING, immunopathology occurs, leading to exacerbated CNS disease and clinical sequelae.

3.3.10 *Flow analysis in the brain*

Previous studies indicated that cellular infiltrate in the brain is predominantly comprised of CD3+ T cells during WNV infection [144]. Therefore, we characterized T cell responses of WT and STING$^{-/-}$ mice in the CNS on 4 dpi to examine baseline differences and 8 dpi when WNV and leukocytes are both present in the CNS (**Figure 3-24**). By 8 dpi however, we found statistically significant decreases in the frequency and numbers of CD4+ T cells in STING $^{-/-}$ mice (**Figure 3-25Figure 3-25**). Although there was no difference in the total numbers of CD8+ T cells, there was a statistically significant increase in the frequency of CD8+ T cells in the CNS of STING$^{-/-}$ mice, likely due to overall trend to decreased numbers of lymphocytes in the brain (**Figure 3-25**). Intriguingly, by 8 dpi, these changes resulted in a significantly decreased CD4/CD8 ratio of T cells, indicating development of an aberrant T cell response to WNV in the CNS of STING$^{-/-}$ mice (**Figure 3-26**). Of cells that made it to the brain by 8 dpi, no differences were found in activated (CD44+) or WNV-specific (NS4b-Tetramer+) CD8+ T cells (**Figure 3-27**). This outcome suggests that while a WNV-specific cytotoxic CD8+ T cell occurs in the CNS in both WT and STING$^{-/-}$ mice, STING plays an essential role in modulating a protective rather than immunopathogenic response in the CNS during WNV infection.

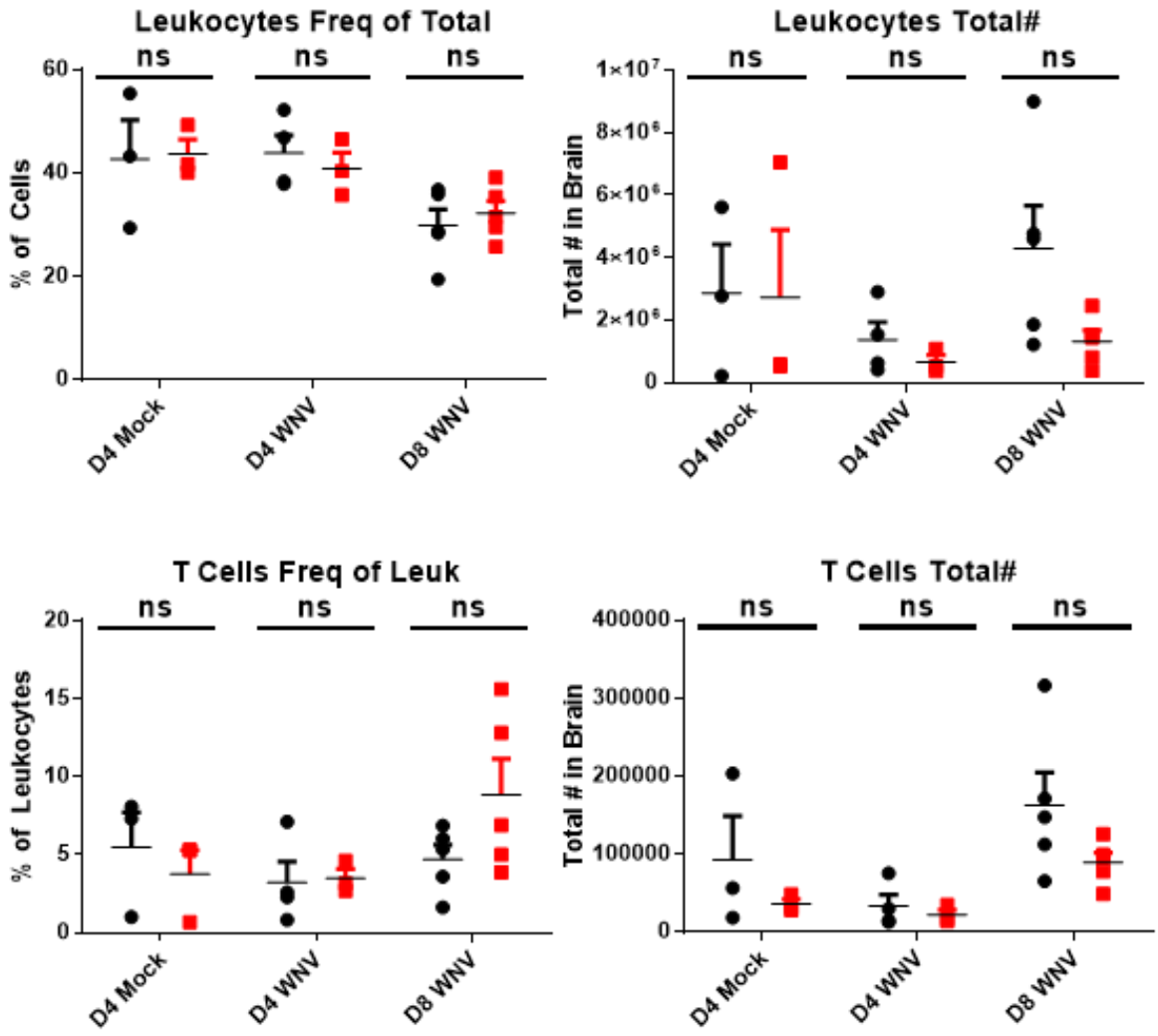

Figure 3-24: CNS Leukocyte and T cell infiltration

Flow analysis of brain lymphocytes. Left: frequency; Right: Absolute number. N = 3-5 per condition. Unpaired students t-test; p = 0.05*; p = 0.005*; p = 0.0005***).

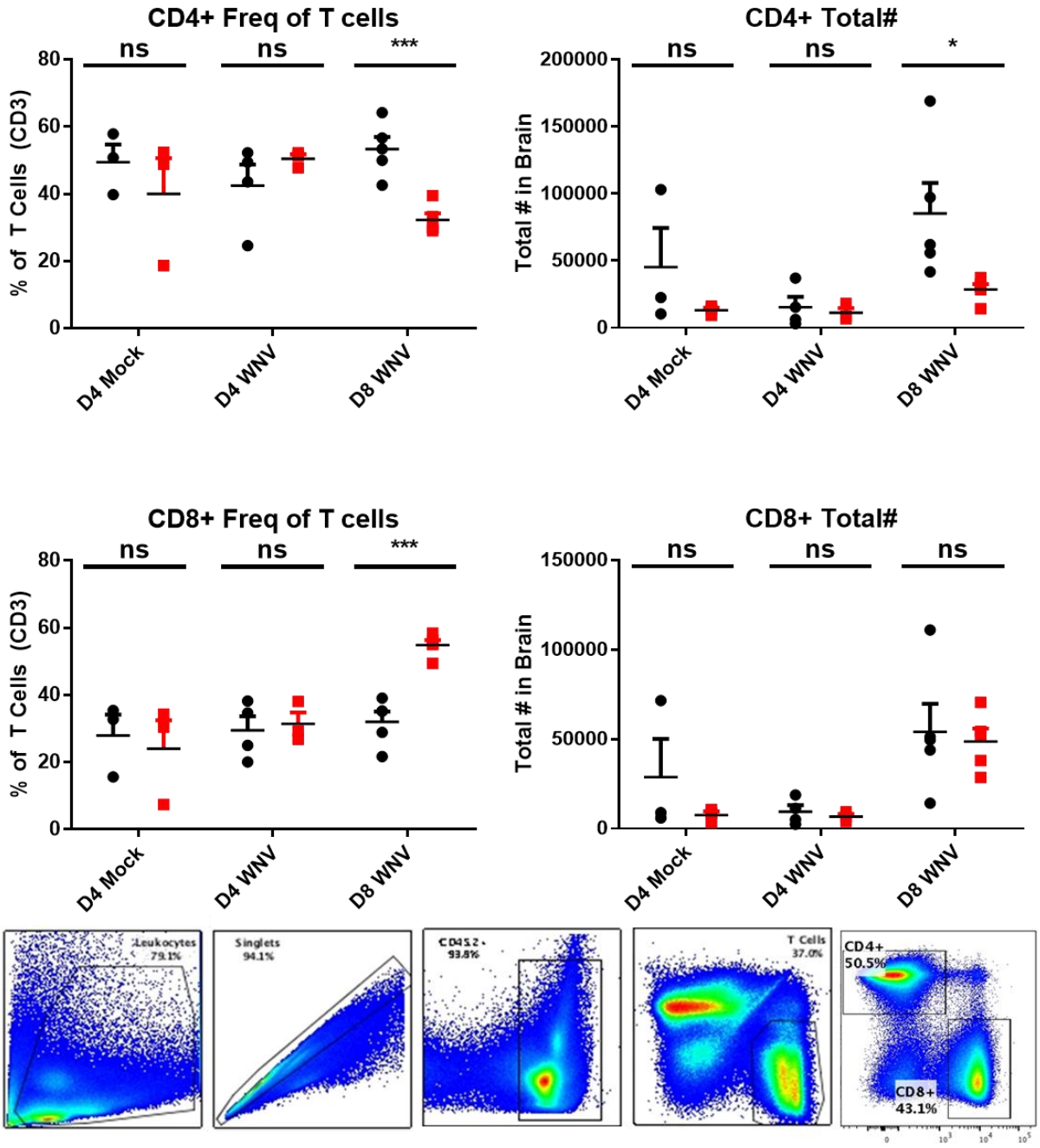

Figure 3-25: CD4 and CD8 T cells in the brain

Flow analysis of brain lymphocytes. Left: frequency; Right: Absolute number. N = 3-5 per condition. Unpaired students t-test; p = 0.05*; p = 0.005*; p = 0.0005***.

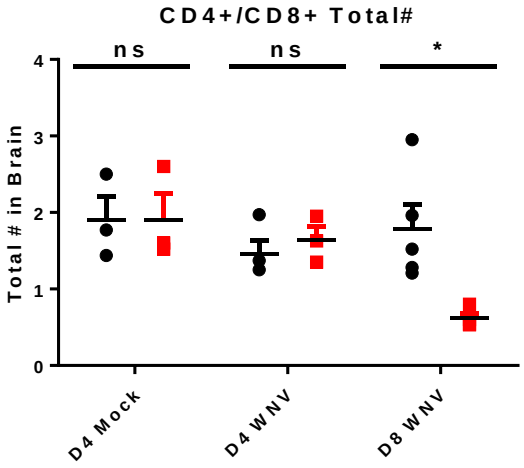

Figure 3-26: CD4/CD8 Ratio in the CNS

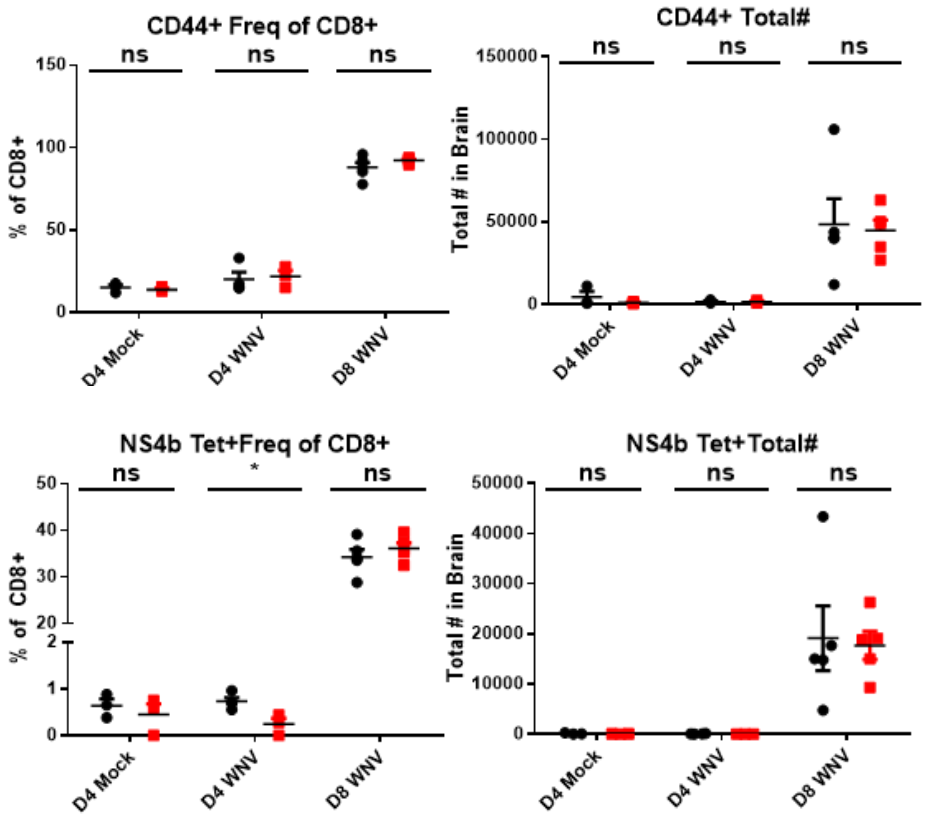

Figure 3-27: Activated (CD44+) and WNV-specific (NS4b-Tet+) CD8 in the CNS
Characterization of CD8 sub-populations (CD44 and NS4b Tetramer). Left: frequency; Right: Absolute number. N = 3-5 per condition. Unpaired students t-test; p = 0.05*; p = 0.005*; p = 0.0005***).

3.4 DISCUSSION

Recent years have seen a marked increase in the global health threat presented by emerging and re-emerging encephalitic viruses, particularly those with increased neurotropism and neuropathology such as WNV [1, 11-13, 122]. Previous studies indicated an important role for STING in host survival during WNV infection [71], however it is unclear what role STING plays in conferring host defense against RNA viruses [75, 111]. Here, we demonstrate that STING is essential to prevent host morbidity and mortality during WNV infection where it plays a role in immune homeostasis and programming. However, STING is not canonically activated *in vitro* upon infection with WNV, revealing a novel function for STING during infection with RNA viruses. Furthermore, we show that STING is essential for host neuropathological defense against WNV through regulation of the innate- adaptive immune interface *in vivo*.

We found that STING deficient mice exhibit increased mortality and morbidity including increased and sustained neurological clinical symptoms, particularly in mice that survive infection. These data were corroborated by pathological analysis, which also revealed distinct differences in CNS pathology. Intriguingly, there seems to be a stratification in clinical and pathological findings between the STING$^{-/-}$ mice that meet euthanasia criteria and those that go on to survive. This outcome has been previously observed in the WNV model and is a critical factor to consider when performing time course vs. end-point experiments [145]. Unexpectedly, these studies also revealed that there was minimal CNS pathology in WT mice that met euthanasia criteria. It is typically assumed that mice meeting euthanasia criteria do so because of neuroinvasion and subsequent encephalitis. Our data instead indicates that both WT and STING$^{-/-}$ Terminal mice have severe GI abnormalities and corroborating abnormalities on histopathology, which may be the proximate cause of morbundity and meeting euthanasia criteria (**Figure 3-6**). GI complications during WNV

have been previously described, however further study is necessary to understand the implications of GI pathology on WNV induced morbidity and mortality [124-126, 146]. Together, these data demonstrate that STING has a neuroprotective role during WNV infection, although it is unclear if STING is directly involved in sensing and producing an antiviral response against WNV or if a non-canonical role is involved.

WNV typically is cleared through development of an innate immune response and effective T cell immunity [48]. To prevent progression to neuroinvasion, both the innate and adaptive immune response are critical to control WNV viremia, and prevent viral induced pathology [20, 21, 58, 70]. Because the known function of STING is to initiate a type I IFN response to both PAMPs and DAMPs, we anticipated that the type I IFN response would be diminished both *in vivo* and *in vitro* explaining the increased viral loads. Surprisingly, we actually observed an increased inflammatory and antiviral innate immune response in STING$^{-/-}$ mice in the CNS during WNV infection. This same increase in the cytokine-chemokine response was also observed in BMDM (**Figure 3-9**) and in serum of infected mice (**Figure 3-11**). These outcomes were highly unexpected as the most commonly described role for STING is known as initiating a type I IFN response [71-73, 111, 138]. In particular, STING was shown previously to facilitate the actions of the ELF4 transcription factor to promote type I IFN expression from WNV-infected cells wherein loss of STING associated with reduced IFN and ISG expression (49). While we observed significant increases in IFN and ISG expression in BMDM lacking STING, it is likely that STING imparts cell type-specific actions for regulation of innate immune signaling, similar to other pathogen recognition receptors that govern innate immune signaling against WNV , likely explaining this discrepancy between studies [48]. It is also important to note that our studies employed STING$^{-/-}$ mice produced through classical gene targeting approach [73] while the

previous study used STING$^{gt/gt}$ mutant mice produced from N-ethyl-N-Nitrosourea mutagenesis and encoding a T596A point mutation of STING [147], highlighting that genetic differences between mouse lines might impact findings. Importantly, both mouse lines exhibit increased susceptibility to lethal WNV infection, and together reveal expanded roles for STING in immune regulation during WNV infection.

Our data also suggest that STING has a role in controlling WNV replication and tropism, as we found increased viral loads in BMDM (**Figure 3-9**), as well as a trend toward increased viral load in the CNS, particularly in the hindbrain regions, but not in the spleens of infected mice lacking STING (**Figure 3-7**). Furthermore, the requirement for STING in viral control is not restricted to neurons or the CNS, as no difference was observed in the viral load of STING$^{-/-}$ primary cortical neurons or intracranial infection (**Figure 3-22**). This outcome suggests that while there is a peripheral requirement for STING in conferring CNS protection, it is not due to complete inhibition of viral control in the periphery. Intriguingly, base-line expression of type I IFN and ISGs were significantly reduced in STING$^{-/-}$ BMDM compared to WT, but not other inflammatory genes (**Figure 3-9**). It is possible that this reduction in baseline IFN allows WNV to establish an earlier and more robust infection, that is later controlled by the RIG-I dependent antiviral response [65, 133]. However, we favor that STING plays a role in innate immune homeostasis, as in its absence the control of the inflammatory response is lost, thus leading to immune-mediated pathology. This function for STING may explain why we had a trend but not significant increase in viral load in the CNS; it is possible that virus is able to establish a stronger infection in the CNS earlier on, but is cleared through an exacerbated innate inflammatory and antiviral response in the absence of STING. Following these events, it is likely that subsequent T cell recruitment and

clearance of the virus occurs in some STING$^{-/-}$ mice but in a manner that leads to enhanced immunopathology and lack of recovery from clinical illness by 18 dpi.

In addition to its role in mounting a type I IFN response to PAMPs and DAMPs, recent studies demonstrated an essential role for STING in developing antitumor T cell responses [138]. These studies suggested that dead and dying cells are phagocytosed by dendritic cells, which requires STING to present antigen and produce a type I IFN signaling cascade that informs and develops the adaptive immune response. Upon examining the CNS of infected mice, particularly in STING$^{-/-}$ with ongoing symptoms, we observed increases in mononuclear cellular infiltrate, which, if unregulated, may exacerbate immunopathology. Previous studies have shown that there is an essential requirement for both CD8+ and CD4+FoxP3+ (Treg) T cells to control WNV and prevent immunopathology [69, 137, 144]. Examining the programming of the adaptive immune response in spleens (**Figure 3-14**) we found that CD8+ T cells had statistically lower CXCR3 and CD44 levels, which are markers of activated T cells capable of migrating to the CNS, suggesting that STING is involved in programming the adaptive CNS response to WNV. Furthermore, expression of Ki67, CD44 and CD73 in splenic FoxP3+CD4+ Tregs were impaired, implicating a role for STING in the proliferation, activation and suppressive potential of Tregs. Upon examining the brains of mice at baseline (4 dpi) and following infection (8 dpi), we observed no differences at baseline between WT and STING$^{-/-}$ mice, however the CD4/CD8 ratio was significantly decreased in STING$^{-/-}$ mice, suggesting that there is a defective recruitment or maintenance of T cells in the brain, characterized by increased frequency of CD8+ T cells and decreased frequency of CD4+ T cells. These data suggest that the cytotoxic effect of CD8+ T cells may not be controlled adequately in the absence of STING. We found that in STING$^{-/-}$ survivors there were large clusters of CD3+ cells in the same vicinity as we observed increased pathology and where STING is

localized in the brain (**Figure 3-18**). Together, these data suggest that STING is required to appropriately program the adaptive immune response to restrict WNV infection while minimizing pathology. Further, our study reveals an essential role for STING in restricting WNV neuropathogenesis.

Chapter 4. DIFFERENTIAL REQUIREMENT FOR THE cGAS AND STING IN HOST DEFENSE AGAINST WNV

4.1 INTRODUCTION

The mechanism by which STING acts during WNV infection could be either direct sensing of viral PAMPs, indirect sensing within an infected cell through recognition of DAMPs or alternatively in a multi-cell mechanism where phagocytic cells detect DAMPs upon engulfing dead and dying cells. The canonical STING sensing pathway is dependent on upstream recognition of DNA danger- or pathogen-associated molecular patterns (DAMP, PAMP) such as DNA viruses, cell-free or mitochondrial DNA, by cyclic GMP-AMP synthase (cGAS). In mammals, cGAS binding to dsDNA activates its synthase activity to produce a cyclic di-nucleotide, cGAMP (cyclic guanosine monophosphate-adenosine monophosphate), which binds to STING, initiating downstream activation of STING by phosphorylation, STING relocalization from diffuse cytosolic to punctate pattern, and subsequent induction of innate immune signaling and IFN production [72, 73, 80, 86, 138]. During RNA virus infections however, the role for STING defense has not been well-characterized. Prior studies have suggested multiple potential mechanisms leading to a STING-dependent immune response to RNA viruses (**Figure 4-1**). First, the STING signaling pathway directly responds to viral PAMPs, either genomic or lipid. Lipid binding to cell membranes has been shown to activate STING in the absence of a nucleic acid PAMP or DAMP. Studies have also indicated that only enveloped, and not non-enveloped RNA viruses are capable of activating STING [91, 139]. Further, virus-like particles (VLPs) in the absence of any genomic material are sufficient to activate STING, suggesting that lipid membranes alone are sufficient to activate STING [139]. Secondly, studies have implicated interaction between the RLR and STING signaling pathways in the case of RNA virus detection and signaling. In this pathway, RIG-I binds

RNA and signals through a multimeric interaction involving both STING and MAVS, activating a downstream type I IFN response [75]. A third pathway suggests utilization of the cGAS-STING signaling pathway either through direct detection of viral factors or through detection of host factors released during infection such as mitochondrial or nuclear DNA [75, 96, 97].

Here, we sought to examine the hypothesis that STING signaling is dependent on upstream sensor cGAS to confer host defense against WNV using the same approach to study cGAS$^{-/-}$ mice that was used to examine STING$^{-/-}$ mice (Chapter 3). Prior studies have demonstrated that WNV activates STING in an overexpression model of STING-Flag in Hela cells [71] and additionally that cGAS is essential for survival during WNV infection [96, 97]. These data suggest that it is possible that WNV activates STING through the canonical cGAS-STING signaling pathway, either directly through viral sensing or indirectly through host DAMPs.

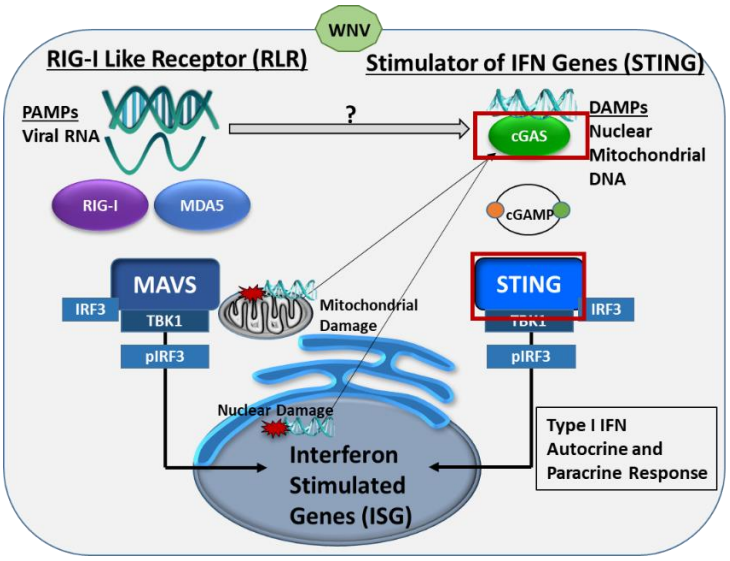

Figure 4-1: Model for cGAS-STING signaling during RNA virus infection
The role for STING is not well characterized during RNA viral infection, however several possible pathways have been described. It is possible that 1) viral PAMPs including viral RNA are directly sensed and activate STING similar to the DNA sensing pathway. 2) It is also possible that the RLR and STING pathways are interrelated, leading to activation of STING following RLR detection of viral RNA. A third pathway, 3) is that viral infection leads to downstream intracellular damage resulting in the release of mitochondrial or nuclear DNA, which then go on to activate the cGAS-STING pathway. In the event of STING activation, a downstream type I IFN response would be initiated, inducing both autocrine and paracrine signaling.

4.2 cGAS SURVIVAL, CLINICAL DATA

Utilizing the same study design as that in the STING$^{-/-}$ analysis (Chapter 3), we sought to determine the clinical profile of cGAS$^{-/-}$ and if clinical scores or body weight loss tracked with Terminal vs. Survivor populations similarly to STING$^{-/-}$ mice. We performed a survival analysis, tracking the clinical scores and loss in body weight daily and then retrospectively stratified the Terminal and Survivor populations. Utilizing our IACUC approved scoring criteria, we did not see a difference in survival, unlike what has been previously reported [97]. Further, there was no difference between WT and cGAS$^{-/-}$ in loss of body weight. What was distinct between WT and cGAS$^{-/-}$ however, was the clinical progression of disease. In the cGAS$^{-/-}$, we found that there were no significant differences in mortality nor loss of body-weight compared to WT mice. There was however, a significant increase in clinical scores, surprising in that the mice maintained high clinical scores for several days and then rapidly began to recover, something that has not been seen in WT mice (**Figure 4-2**). When examining the difference between Terminal and Survivor cohorts, we saw no stratification between cGAS and WT cohorts in loss of body-weight, but increased clinical symptoms were observed in both cohorts over WT (**Figure 4-3**).

Most profoundly, cGAS$^{-/-}$ did not develop significant hind-limb paresis/paralysis as observed in the STING$^{-/-}$. Instead, they displayed grossly distended abdomen, severe parkinsonism, bulging eyes, and a 'frozen' face [30, 148, 149]. These data suggesting increased encephalitis but without the motor-neuron or spinal complications that lead to IACUC approved euthanasia criteria. Further, while there was clear abdominal distension, stool compaction and other GI issues were not readily observed by abdominal palpation examination, which was distinctly different than the cGAS$^{-/-}$ mice (**Figure 4-4**).

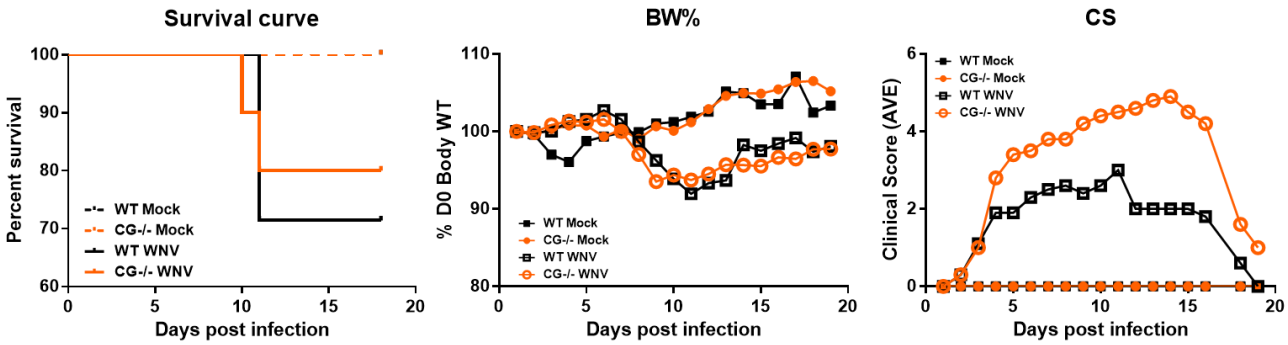

Figure 4-2: cGAS survival

No significant difference in survival noted between WT and cGAS$^{-/-}$ strains infected with WNV. Representative of 3 individual experiments; Body weight loss (BW%) was not different between WT and cGAS$^{-/-}$, although clinical scores (CS) are dramatically more pronounced in STING$^{-/-}$ mice, although they are nearly resolved by study endpoint.

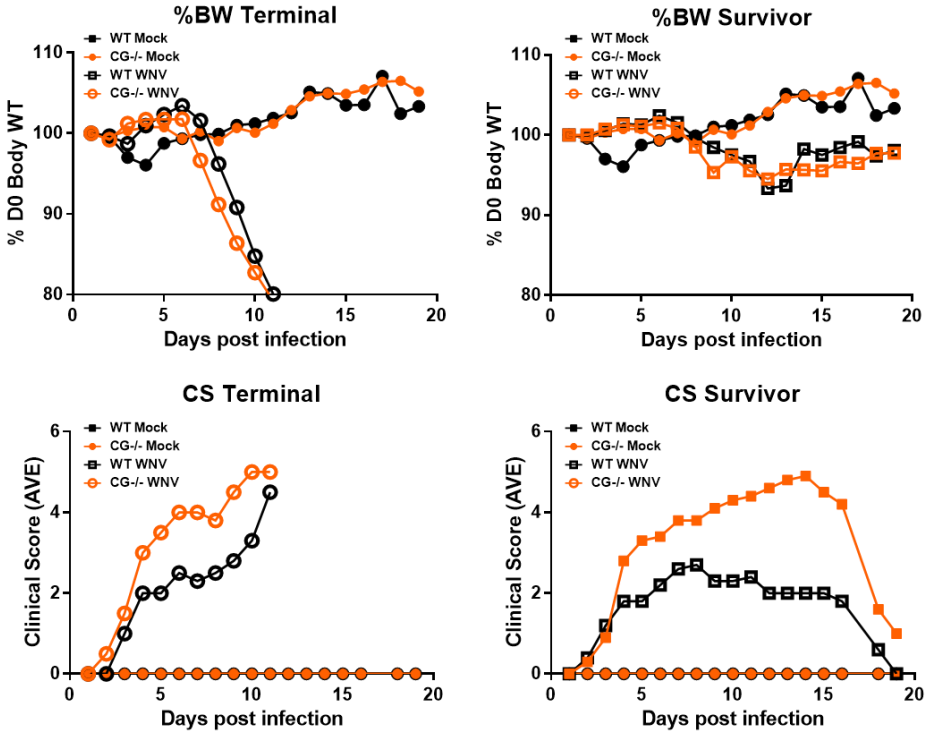

Figure 4-3: cGAS$^{-/-}$ clinical score and body-weight Terminal vs Survivor

Stratification of clinical scores and loss of bodyweight between WT and STING$^{-/-}$ populations. Body weight loss (%BW) and clinical scores (CS) in Terminal (T) vs Survivor (S) populations.

4.3 cGAS CLINICAL MANIFESTATIONS

During the survival analysis, we observed distinctly different clinical progression in the cGAS$^{-/-}$ mice than that observed in the STING$^{-/-}$ mice (**Figure 4-4**). Predominant symptoms in STING$^{-/-}$ include eye disease such as conjunctivitis, opaqueness or build-up, severe balance issues, moderate tremors, severe paresis and paralysis, and abdominal distension. Paresis and paralysis typically begins with increased reflex and tone in the hind-quarters but progresses to a flaccid phenotype characterized by decreased reflexes and tone. Abdominal distension occurs, with clear swelling in the small intestine, ceacum and stool compaction (**Figure 3-4**). cGAS$^{-/-}$ however, often have bulopthalmia without conjunctivitis, opaqueness or build-up, mild issues in balance, severe parkinsonism, symptoms where the mouse continually experiences visible tremors, mild-to-moderate paresis and paralysis and trends toward increased reflexes and tone in both the fore and hind limbs. Flaccid paralysis is rarely observed in cGAS$^{-/-}$, nor was true paralysis regularly observed. Severe abdominal distension was observed and upon necropsy, the GI tract appeared pale, distended and friable. Unlike STING-/- mice, stool compaction and seizure of the GI tract were not commonly observed. These data suggest that cGAS and STING may have essential but distinct and independent roles during WNV infection.

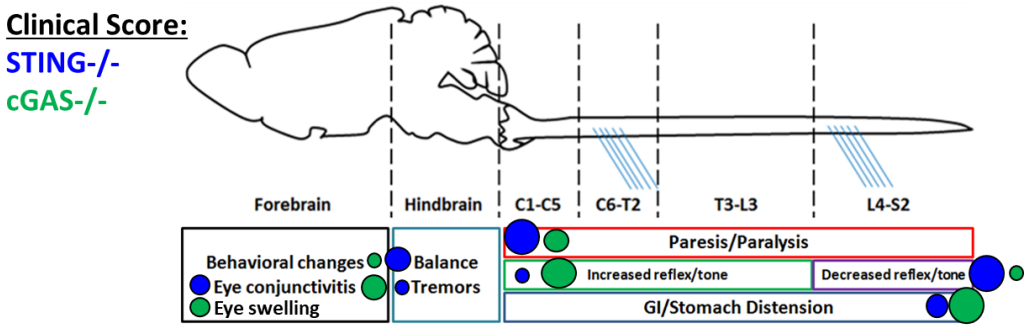

Figure 4-4: Differential clinical manifestations in cGAS and STING$^{-/-}$ models of WNV infection.
Size of circle represents observed severity of symptoms. (Blue) STING$^{-/-}$; (Green) cGAS$^{-/-}$.

4.4 cGASxSTING$^{GT/GT}$ Analysis

To determine if the clinical phenotypes observed in cGAS$^{-/-}$ and STING$^{-/-}$ are distinct and additive, we sought to infect mice with defective cGAS and STING signaling. Initially, we sought to infect the cGAS$^{-/-}$xSTING$^{-/-}$ (DKO) line, however what was available was the cGAS$^{-/-}$ xSTING$^{gt/gt}$ line, so we utilized this for preliminary study while the DKO line was generated. Importantly, our studies employed STING$^{-/-}$ mice produced through classical gene targeting approach [73] while STING$^{gt/gt}$ mutant mice produced from N-ethyl-N-Nitrosourea mutagenesis and encoding a T596A point mutation of STING [147], so direct comparisons between the strains may be limited as genetic differences between mouse lines might impact findings. During infection, mice did not present with the typical clinical manifestations observed during WT infection such as 20% loss of body-weight or morbundity/refusal to move. Clinical symptoms appeared to be a mix of those observed in both STING and cGAS$^{-/-}$, suggesting that they act in distinct ways to provide host defense against WNV. As the infection progressed, the cGAS$^{-/-}$ xSTING$^{gt/gt}$ mice developed severe abdominal distension, however paralysis or morbundity was not observed. One mouse in particular was unusually symptomatic without loss of body weight or paresis/paralysis typically accompanying WNV infection. Abdominal palpation did not reveal hardness or compaction of the GI typically associated with WNV infection. At necropsy, the mouse had severely distended small intestine and caecum. Enlarged caecum are not uncommon during WNV infection, however the marked distention and friability of the small intestine was notable. Stool compaction in the intestines were not observed. This is in direct comparison with WT and STING$^{-/-}$ mice, which have a rigidness in the GI tract of infected mice displaying a GI phenotype, accompanied by a build-up of stool and a darkening of the GI tract.

There was a second mouse that had similar although not as severe of a phenotype, and the UW veterinary staff requested a full diagnostic necropsy and compete histopathology. The necropsy was performed in conjunction with a laboratory animal veterinary resident with histopathology conducted by P.M. Treuting. Histopathological lesions were limited to the central nervous system and myenteric ganglia, segmentally, in the intestine. Morphological diagnoses were for the gastrointestinal tract: segmental moderate lymphocytic and necrotizing myenteric ganglioneuritis consistent with WNV infection with secondary intestinal dilatation and dysbiosis; marked focal proliferative and ulcerative enterocolitis; marked *Spironucleus* bloom distal ileum and the for the brain and spinal cord: multifocal minimal to mild lymphocytic and lesser neutrophilic myeloencephalitis, subacute with minimal cerebral hemorrhage and mild edema, consistent with experimental infection with WNV. It was considered that the cause of the clinical signs of marked GI distension is the viral infection of the enteric nervous system with secondary ileus and dysbiosis. Given these preliminary findings, examination of the microbiome in $cGAS^{-/-}$, $STING^{-/-}$ and mice deficient in both cGAS and STING may warrant further study.

No further survival studies were conducted on this line or are recommended to be conducted without changes in clinical scoring and euthanasia criteria to include GI distress. For future analysis, tissues were harvested at 4 and 8 dpi from this line to determine viral load and are stored at -80^{o}C. Further work is recommended to proceed with the $cGAS^{-/-}$ x $STING^{-/-}$ (double knock-out; DKO) line once generated, so direct comparisons can be made with the $cGAS^{-/-}$ and $STING^{-/-}$ results. Preliminarily, the clinical symptoms of $cGAS^{-/-}$ and $STING^{-/-}$ seem to be distinct and additive, suggesting novel and independent roles in host defense against WNV.

4.5 cGAS INNATE IMMUNE SIGNALING

During WNV infection, STING$^{-/-}$ mice have trends toward increased viral load and expanded tropism in the CNS, correlated to increased innate immune signaling (**Figure 3-10**). To see if cGAS$^{-/-}$ have the same phenotype, tissues were harvested at 4 and 8 dpi and their immunologic profiles examined (**Figure 4-5**). Unexpectedly, where a clear increase in viral load was observed in both the numbers of mice and within each tissue in STING$^{-/-}$ mice, cGAS$^{-/-}$ did not have this phenotype. Instead, the innate immune profile was indistinguishable from WT. Similarly, with the exception of one cGAS$^{-/-}$ mouse that had increased viral load and signaling, there was nothing that differentiated WT and cGAS$^{-/-}$ strains. These data suggest that the role of STING is not dependent on cGAS, and that while cGAS is critical for host defense against WNV it is not through canonical STING activation.

4.6 cGAS VS STING ADAPTIVE SPLENIC RESPONSES

We then performed an initial assessment of splenic CD8 T cells in the WT vs STING$^{-/-}$ and cGAS$^{-/-}$ mice. While we did not see the same results in the innate immune profile in cGAS$^{-/-}$ we observed in the STING$^{-/-}$, the adaptive immune deficits seem to be enhanced. Interestingly, where there is an almost significant increase in the frequency of T cells among all CD45+ cells in the spleen, there is a significant decrease in the frequency of CD8 T cells (**Figure 4-6**). Further, activation of CD8 T cells appears to be compromised (**Figure 4-7**). There is a significant decrease in the

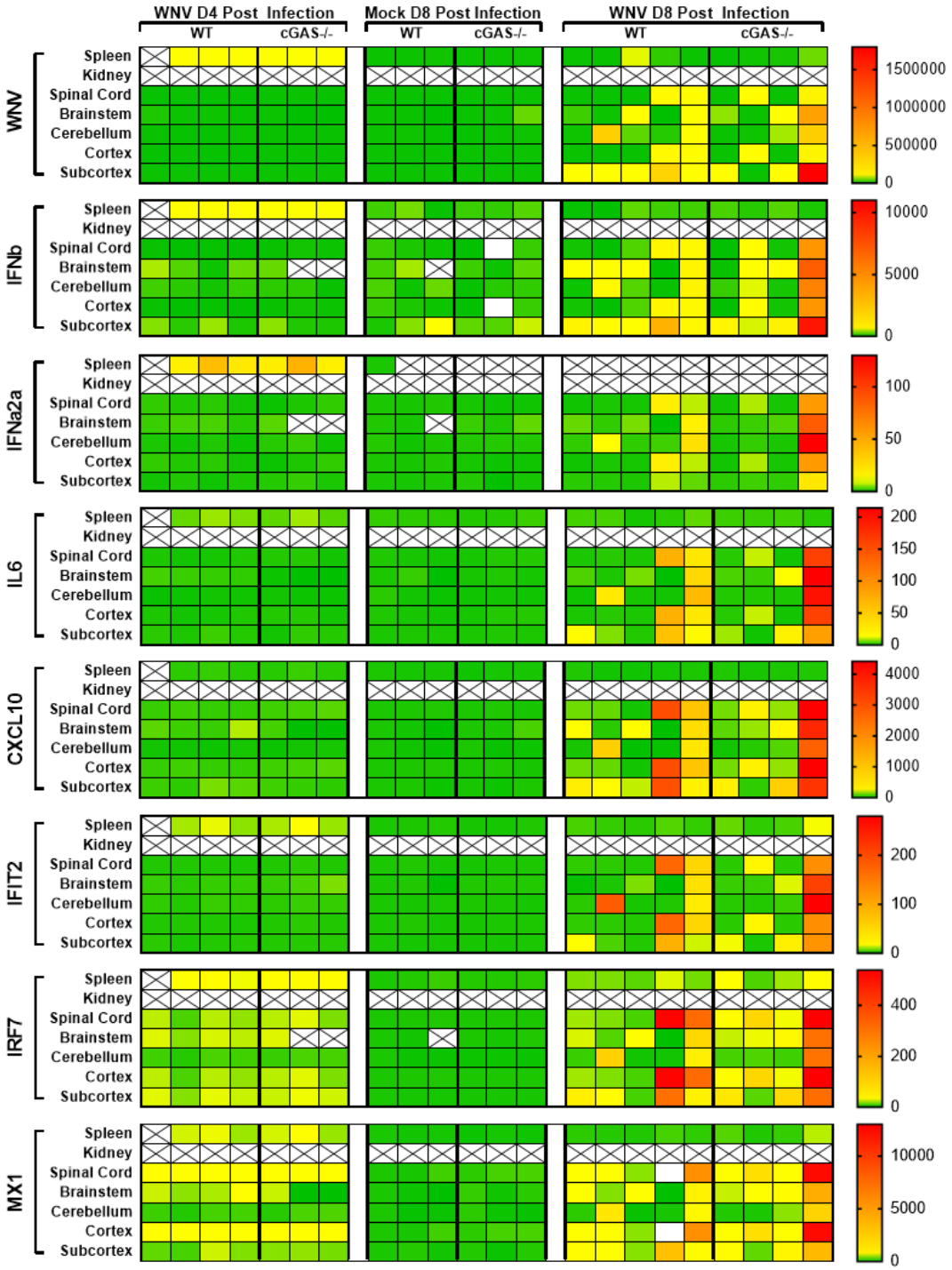

Figure 4-5: RT-qPCR analysis of cGAS$^{-/-}$ tissues

In vivo innate immune profile in splenic and CNS tissues. RT-qPCR detection of innate immune genes in the spleen, spinal cord and brain regions (brain stem, cerebellum, sub-cortex, cortex). Columns indicate individual mice; rows the different tissues. Calculated as linear fold change over GAPDH in WT Mock. Boxes with X have been harvested but not analyzed by RT-qPCR.

frequency of both the CD44 and CD44+NS4b+ CD8+ T cells, and a corresponding trend in absolute numbers. Evaluation of the cGAS$^{-/-}$ adaptive response including CD4+ subsets has yet to be done but may reveal novel functions for cGAS and STING during WNV infection, where they may have multiple functions resulting in both independent and dependent roles to provide host defense against WNV.

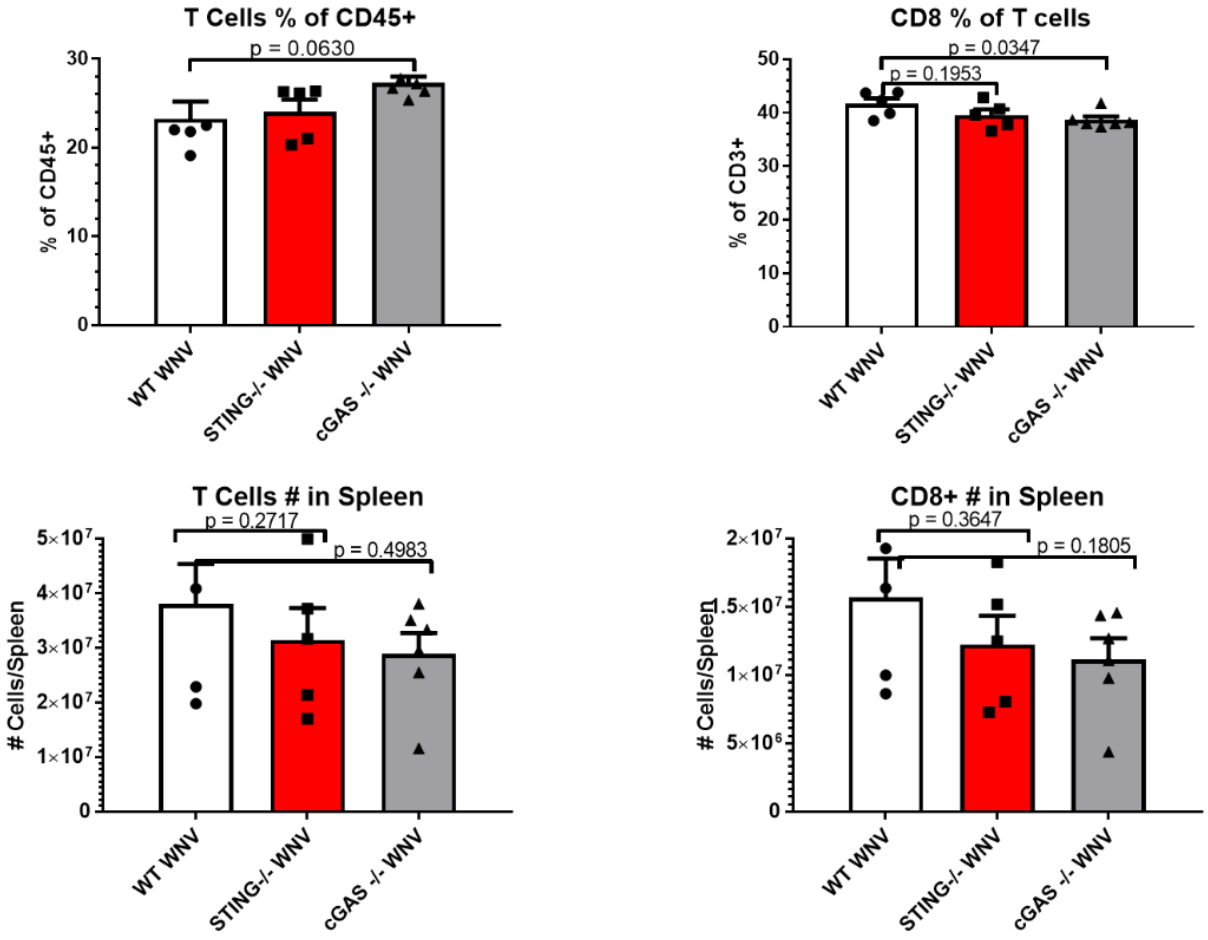

Figure 4-6: cGAS vs STING$^{-/-}$ splenic CD8 T cell response
Left: CD45 and Right: CD8 frequency (top) and absolute number (bottom) in D10 post infection spleens. n = 3-5 per condition. Unpaired students t-test; p = 0.05*; p = 0.005*; p = 0.0005***.

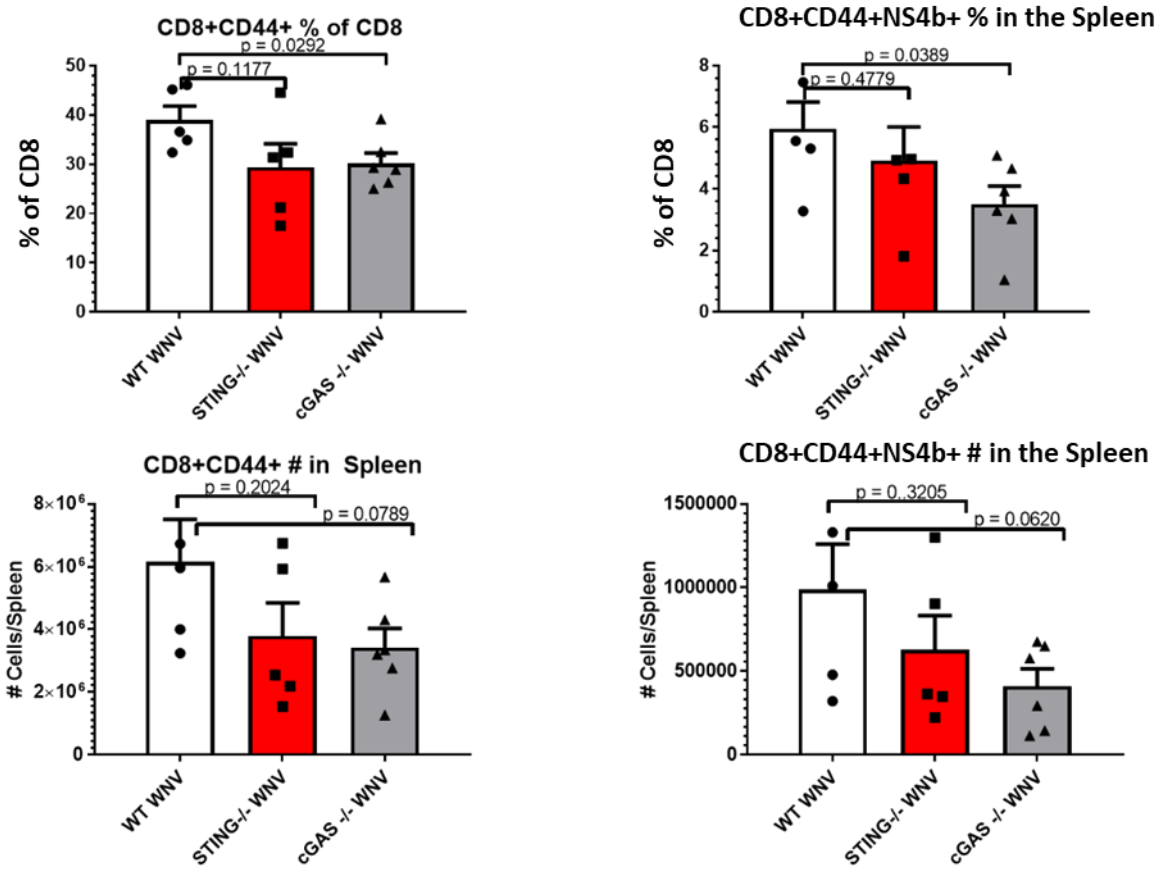

Figure 4-7: Activation and WNV-specific CD8 T cell response in cGAS vs STING$^{-/-}$ mice
Left: activated CD8 (CD44) and Right: WNV-specific activated CD8 (CD44+NS4b-Tet+) frequency (top) and absolute number (bottom) in D10 post infection spleens. n = 3-5 per condition. Unpaired students t-test; p = 0.05*; p = 0.005*; p = 0.0005***.

4.7 STING ACTIVATION

With the differences observed in survival analysis, clinical phenotype and innate immune signaling, we hypothesized a possible novel role for STING, other than canonical activation through cGAS. At the start of these studies, we hypothesized that cGAS was essential for STING activation, which provided downstream Type I IFN antiviral responses and host defense following infection with WNV. To evaluate the activation of STING during WNV infection, we utilized a recently described telomerase reverse transcriptase human foreskin fibroblasts (HFF) model to assess activation of endogenous STING by phosphorylation and relocalization from the cytoplasm

to the perinuclear space during WNV infection [150]. Transfection of interferon-stimulated DNA (ISD; calf-thymus DNA) into HFFs initiated re-localization of STING as previously reported by 3hpi [73, 150]. Intriguingly however, STING was not relocalized in WNV infected cells (**Figure 4-8A**).

It is possible that the kinetics of STING activation are different during WNV infection, so we performed a time course experiment to detect STING activation by phosphorylation status [88], looking at a range of times from 1-24 hpi at MOI = 1 (**Figure 4-8B**). Similar to what was observed by IFA, STING phosphorylation was not observed at any time point during WNV infection, although an innate immune response developed in response to infection. To determine if activation was dependent on viral load, we infected tertHFF with an MOI = 1 and MOI = 10 of WNV but also observed no STING activation as measured by phosphorylation (**Figure 4-8C**). These data suggest that STING is not canonically activated during WNV infection *in vitro* and that STING has a novel function in host defense during infection with WNV-TX.

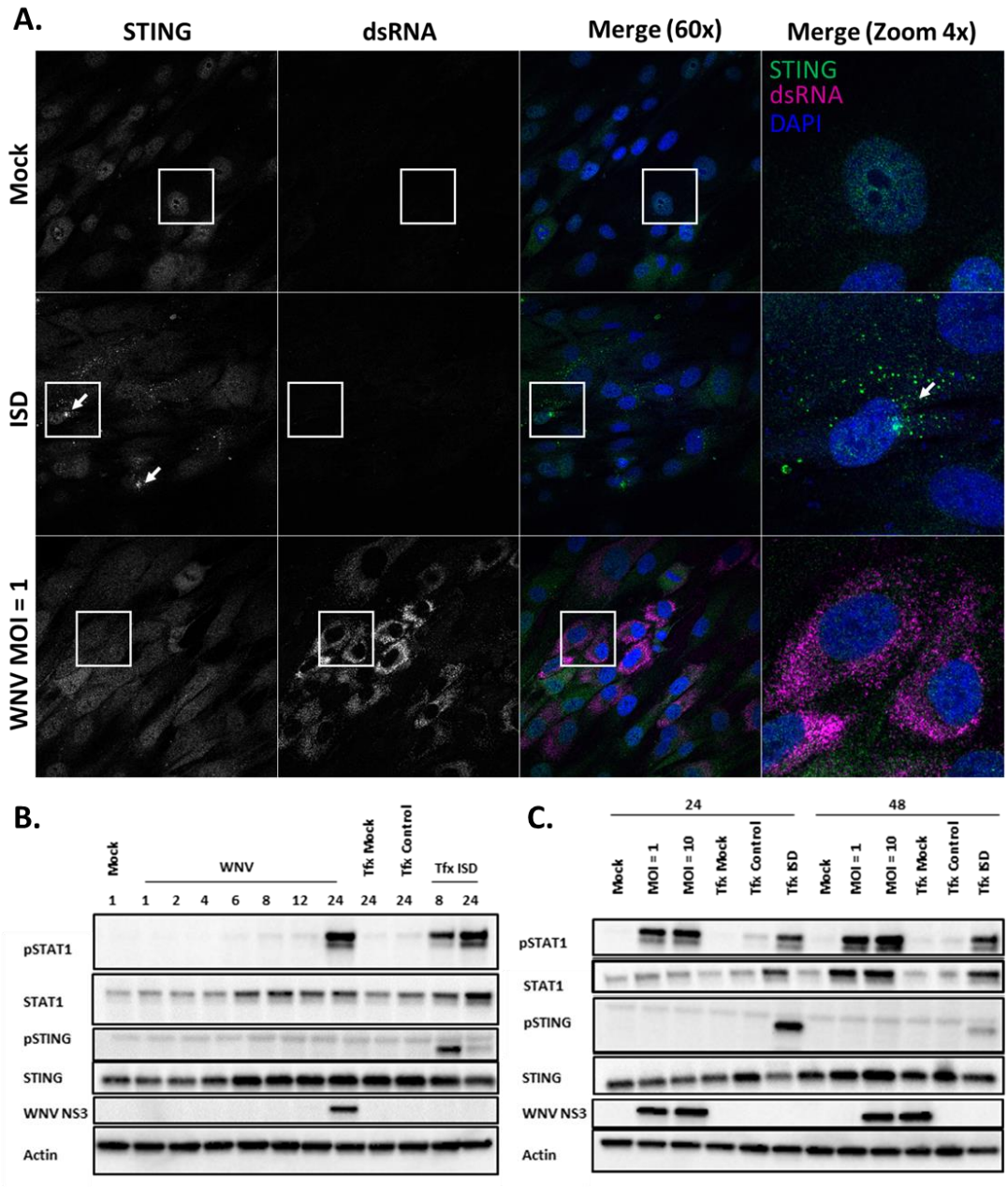

Figure 4-8: Assessment of STING activation during WNV infection

(A) Immunofluorescence STING re-localization assay to assess STING activation. HFF cells were treated with PBS (Mock), transfected with ctDNA for 3hr infected with WNV for 24h (MOI = 1). Cells were stained for endogenous STING and dsRNA. The data are representative for two independent experiments.
(B) Western blot to detect activation of endogenous STING during WNV infection. (B) HFF were infected with WNV MOI = 1 and harvested at the indicated times post inoculation (hpi). (C) HFF cells were infected with WNV (MOI = 1, MOI = 10) and lysed at 24 and 48 hpi. In parallel, HFFs were transfected with ctDNA and harvested at the indicated times (B-C). The data are representative of three replicate experiments.

4.8 DISCUSSION

The goal of this study was to uncover the pathway by which STING is activated during WNV infection. While PAMP and DAMP sensors upstream of STING have been suggested to activate signaling and induction of a type I IFN response, the best characterized is the cGAS-STING pathway. Previous work implicated a role for both cGAS and STING in host defense against WNV, suggesting that the cGAS-STING pathway was essential for host defense against WNV. When we tested this hypothesis, we immediately saw differences in the progression of clinical illness, as well as the disease outcome. Compared to both WT and STING$^{-/-}$, cGAS have increased tremors, decreased facial responses, enlarged and protruding eyes and abdominal distension. They also tend to have increased reflexes in both the pelvic and thoracic responses that do not resolve to a decreased reflex as observed in the STING$^{-/-}$. Unlike STING$^{-/-}$ mice, cGAS$^{-/-}$ do not have increased loss in body weight, nor do they have increased paresis or paralysis compared to WT. They become rotund as their GI swells over the course of infection and will often score a clinical score = 5 for days without becoming moribund. Uniquely to the cGAS$^{-/-}$ mice however, mice that receive high clinical scores for several days will recover by the study end-point, almost to WT level. Recovery after severe disease such as observed with the cGAS$^{-/-}$ has not been seen in either WT nor STING$^{-/-}$ mice, suggesting important differences in disease progression and pathology. Prolonged neurological symptoms as observed in the STING$^{-/-}$ were not seen in the cGAS$^{-/-}$.

Although direct comparisons cannot be made between STING$^{-/-}$ and cGAS$^{-/-}$xSTING$^{gt/gt}$ mice, these data suggest that the phenotypes observed in STING$^{-/-}$ and cGAS$^{-/-}$ mice may be additive, so distinct. Future studies using the STING$^{-/-}$ x cGAS$^{-/-}$ DKO will be intriguing and worth pursuing, once generated. The clinical symptoms observed in this line appeared to be additive;

with both increased GI and paresis observed. Upon pathological review, both the CNS and GI were severely impacted, while all other organs examined appeared to have no significant damage. Further analysis is recommended, moving forward with the DKO line to see if the phenotype is the same, but with a modified protocol that incorporates inclusion of GI distress/abdominal bloating as a clinical sign of disease.

While there is a clear role for cGAS in providing a protective role against WNV, it was very surprising to see that there did not appear to be increased virus, nor innate immune response in the CNS as observed in STING$^{-/-}$ (**Figure 4-5**). This suggests that STING is acting in a novel function, because if the cGAS-STING pathway was being utilized to provide the increased signaling observed in STING$^{-/-}$ mice, we would expect to see the same in cGAS$^{-/-}$ mice. Conversely, the deficits in the adaptive immune response appears to be enhanced in cGAS$^{-/-}$, even over the difference we see in STING$^{-/-}$. Combined with the clinical data, it may suggest that cGAS and STING have distinct but essential roles in conferring host defense against WNV.

Chapter 5. CONCLUSIONS AND FUTURE DIRECTIONS

5.1 CONCLUSIONS

In this study, we sought to identify essential host immune determinants of neurologic defense. We examined the cGAS-STING signaling pathway, because both cGAS and STING had been shown to have essential roles in host survival against WNV. Further, we sought to understand what the role of cGAS-STING signaling is in the broader context of an RNA virus infection, something which is relatively poorly understood. Going into this study, we hypothesized that cGAS would sense a host or viral factor, generate cGAMP and activate STING downstream antiviral response. This hypothesis was supported based on the fact that both cGAS and STING have been shown to have decreased survival during WNV infection than WT mice.

What we found instead is that there appears to be a differential requirement for STING and cGAS, that is complimentary but not necessarily co-dependent. STING$^{-/-}$ mice infected with WNV have increased paresis/paralysis, mortality, clinical symptoms and loss of body-weight particularly in mice that go on to survive, trend toward increased CNS viral load with no change in the periphery and both peripheral and CNS increases in innate immune profiles. cGAS$^{-/-}$ do not have increased paresis/paralysis or mortality compared to WT unless GI is utilized as a euthanasia criteria. Both terminal and survivor cohorts display increased clinical symptoms, where only the surviving cohort in STING$^{-/-}$ displayed increased symptoms. cGAS$^{-/-}$ have no difference in their innate immune profile compared to WT mice. Where STING and cGAS have similar phenotypes is in the adaptive immune profile. Both strains have defective CD8 signaling, with cGAS having a more consistent and possibly increased deficit. These data suggest that there is a differential role for STING and cGAS, potentially resulting in host defense in different anatomical regions. The

fact that both strains have a deficit in the adaptive immune response suggests that it is also possible that cGAS-STING signaling occurs. This could implicate a novel concept that cGAS and STING have both independent and dependent roles during WNV infection. Additionally, these data suggest a novel role for STING that may not result in canonical activation. To test this, relocalization and phosphorylation of STING was assayed in the context of WNV, over a timecourse and with different concentrations of virus. At no point tested was STING either phosphorylated or relocalize during WNV infection, although the control treatment with DNA transfection caused both relocalization and phosphorylation of STING.

5.2 FUTURE DIRECTIONS

The results from this study show that STING has a critical and novel role in host defense against an RNA virus, WNV. Previous studies have indicated STING is necessary for host defense against multiple RNA viruses, including ZIKV, JEV, dengue, influenza, VSV and others, however the role STING plays in conferring protection has been ambiguous. In this study, we show that STING is required at multiple levels; from initial virologic control in BMDM, to maintaining homeostasis even in the absence of infection, interplay between the innate and adaptive responses to WNV to achieve protective, not pathogenic immunity. Further, our data suggests that there may be different functions for cGAS and STING during WNV infection, implicating potential novel and independent functions. We also found a correlate between GI disfunction and mortality, independent of CNS pathology in WT mice. In the GI of mice that met euthanasia criteria we saw increased pathology as well as dysbiosis of the microbiome. Given the increased Th2 response by Luminex even at background levels and the changes observed in the adaptive immune phenotype, it would be interesting to look into both the B cell and ILC2 responses. Given the protozoan overgrowth in the $cGAS^{-/-}xSTING^{gt/gt}$ mice, it would especially be worth looking into the ILC2

response in both cGAS$^{-/-}$ and STING$^{-/-}$. Additionally, examining the baseline response between WT, STING$^{-/-}$ and cGAS$^{-/-}$ mice would be critical to understand the underlying differences in steady-state immune responses that may influence later development of the immune response to WNV.

5.2.1 *cGAS vs STING signaling during WNV infection*

The differences we observed clinically, immunologically and virologically between cGAS$^{-/-}$ and STING$^{-/-}$ mice are intriguing and indicative that while both proteins are critical, they have distinct roles in conferring host defense from WNV. In STING$^{-/-}$ mice, we saw increased clinical symptoms, increased trend toward virus and innate immune profiles in the CNS and prolonged clinical symptoms. cGAS$^{-/-}$ mice had buphthalmoses and grossly distended abdomens, without the severe paresis and paralysis seen in STING$^{-/-}$. Furthermore, while cGAS$^{-/-}$ mice were acutely symptomatic, they recovered unlike STING$^{-/-}$. In both strains, aberrant adaptive immune profiles were observed in the spleen, suggesting that there may be both distinct and co-dependent roles for cGAS and STING during WNV infection.

It would be intriguing to examine the innate immune profile in BMDM in cGAS$^{-/-}$ in comparison to WT, MAVS$^{-/-}$ and STING$^{-/-}$ mice. In particular, it would be interesting to see if there is a baseline deficit in ISG signaling as we observed in STING$^{-/-}$, or if early control of the virus is also limited. Completion of a virologic analysis from cGAS$^{-/-}$ as well as pathological characterization will confirm if there are differences in CNS viral load and pathology.

A recent paper discusses a IL1b-IRF3-STING axis, that may also be important in the context of WNV infections [150]. This possibility and others suggest potential novel functions and signaling pathways dependent on either or both cGAS and STING. To understand the underlying differences between cGAS$^{-/-}$ and STING$^{-/-}$ signaling, initial studies using RNAseq to

examine both baseline and infected mice will result in an objective way to look for novel signaling pathways, interactions or differences that may explain the differences observed clinically. It would be particularly interesting to examine the signaling changes against MAVS$^{-/-}$ as well, to see how these pathways-both characterized to initiate type I IFN responses-are both similar and different. Additionally, generation and analysis of a STING$^{-/-}$ x cGAS$^{-/-}$ line will enable further analysis of whether and which pathways are either dependent, co-dependent or independent of cGAS and STING signaling.

5.2.2 *cGAS-STING RNAseq*

At this point in the literature, there is very little reference to known pathways for cGAS outside of STING signaling, though multiple studies have shown that they do have independent roles. Similarly, while multiple pathways have been implicated for STING activation, the best characterized is cGAS-STING signaling in the context of DNA sensing. Autoimmune and cancer literature has shown an essential role for STING in developing the adaptive immune response, however the mechanism outside of IFN signaling is not well understood. At this point, a discovery approach using meta-data analysis would be the best, to approach the data in an unbiased manner and examine overlapping, dependent and independent roles of cGAS and STING-dependent signaling. To do this, samples have been generated and processed from WT and STING$^{-/-}$ mice from brain hemispheres, spleens and spinal cords for RNA and protein/ELISA/Luminex or plaque assay analysis. Corresponding samples of serum were also collected for Luminex analysis. cGAS$^{-/-}$ samples still need to be generated, and then RNA sent for RNAseq. Initial bioinformatics analysis should examine the differential signaling at baseline, in mock-infected animals and see if there is a baseline deficit in IFN signaling in STING$^{-/-}$ mice, something that may explain the background phenotype we observed in BMDM and also in the overall development of STING$^{-/-}$ mice,

something that is not observed in cGAS$^{-/-}$ mice. After the initial analysis, D4 and D8 infected comparisons should be made. Once this is done, a multi-data analysis incorporating clinical, innate and adaptive profiles may be used to further inform the bioinformatics analysis and see if novel roles for cGAS and STING can be discovered.

5.2.3 *Virologic and innate immune response in STING$^{-/-}$ mice*

The BMDM data demonstrate an early spike in viral load, at the same rate as MAVS$^{-/-}$, but then was brought back to WT levels as the infection progressed, unlike MAVS$^{-/-}$ which continued to increase. We also found that ISGs were decreased at background levels, something that was not observed in other chemokines or cytokines outside of the type I IFN pathway. It is possible that this decrease in antiviral ISGs generates a more permissive environment for the virus, either allowing for earlier entry, establishment of viral replicons, viral replication or increased production of virus at early timepoints. Our data suggests that the initial response resulting in increased viral loads occurs by 12 hpi and then viral load begins to come into control by 24-48 hpi. This timing suggests that a deficit occurs in STING$^{-/-}$ BMDM to control early infection, which then may be brought into control by RLR signaling, which is the point at which MAVS$^{-/-}$ is still not able to bring viral load under control. It would be intriguing to perform a virologic analysis in WT vs STING$^{-/-}$ BMDM, particularly at early timepoints to access what stage of viral entry, replication or release is impacted by STING signaling. It also would be interesting to examine early innate immune responses to determine if there is continued reduction of antiviral responses. Comparing also with cGAS$^{-/-}$ BMDM may also assist in revealing differential mechanisms between signaling pathways *in vitro.*

Of additional interest, in a subset of STING$^{-/-}$ mice, virus isolated from the CNS formed both heterogenous and abnormally large plaques. Not all mice had these enlarged plaques, but of

the ones that did it would be intriguing to refer to their clinical record and see if there are correlates with symptoms. In mice with heterogeneous populations, it would be interesting to isolate and sequence virus from plaques of different sizes to see what viral proteins were mutated and where. Particularly in the enlarged plaques, it would be intriguing to know whether they 1) replicated faster, 2) produced more virus or 3) caused increased CPE upon release; or if there was another factor responsible for the enlarged plaques. It is also intriguing to know what host factors changed that caused selective pressure to either force or enable the virus to change; both from mice with heterogeneous plaques and in those with enlarged plaques.

Lastly, preliminary studies looked at viral load in 10 dpi and 12 dpi WT and STING-/. These studies are difficult to do, because so many mice meet euthanasia criteria between 8-12 dpi, particularly in STING$^{-/-}$. It also complicates the data because these later timepoints selects for mice that will survive. However, it appeared that there was a trend toward decreased virus in the CNS of STING$^{-/-}$ compared to WT mice. If these data are true, it is possible that there is sufficient clearance of virus in the CNS, but may be at the cost of immunopathology. More work needs to be done at later timepoints to determine the virologic outcome in WT vs. STING$^{-/-}$ mice. To do this and resolve bias that may come from only harvesting mice that survive to later timepoints, one possibility is to harvest mice as they meet euthanasia criteria for virologic and immune analysis, and then of mice that survive look at later timepoints such as 12 and 18 dpi to see if the virologic response has resolved or not, as well as the corresponding immune response.

5.2.4 *Adaptive immune response*

We saw intriguing differences in the development of the adaptive immune response to WNV in both STING$^{-/-}$ and cGAS$^{-/-}$ compared to WT mice. These differences suggest that there is a potential defecit in the priming or informing of early responses. Cancer literature has suggested

a role for STING in priming the adaptive response through cross-talk with dendritic cells. It is possible that one function of STING during WNV infection is in DCs, where STING signaling is required for antigen presentation and activation of T cells. This has been previously shown where STING deficient DCs exposed to dead and dying tumor cells were unable to present antigen to T cells, thereby restricting appropriate development of the adaptive response and restriction in clearing the tumor. It is possible that in the same way, that STING$^{-/-}$ DC phagocytose dead and dying infected cells but are unable to present antigen or inform T cells effectively. Studies looking into T cell activation and proliferation during DC priming studies, as well as potential bone marrow chimeras would help in determining the mechanism behind the adaptive immune deficit we observed here.

5.2.5 *CNS and ENS during WNV infection*

Most studies with WNV in a murine model assume that WT mice meet euthanasia criteria due to encephalitis because virus was found in brain tissue, but no study to date has examined the complete histopathology in mice that meet euthanasia criteria vs. those that go on to survive prior to this study. This has been brought up as an issue previously [145], where concerns were that there may be intrinsic differences between populations. While we do not see pathology in the brain associated with Terminal criteria in WT mice, we do see GI pathology as a correlate with mortality. This is in stark contrast with WT mice that survive, where we see some but not excessive GI symptoms, but instead we do see encephalitis in some mice. Further study would be neededto characterize the encephalitic response in the CNS that go on to survive, and also to extend the study endpoint past 18 dpi to see if the encephalitic phenotype resolves. Similarly, it would be worth further study of the GI phenotype to see if WNV is detected as well as to characterize the immune cellular and signaling profiles. One particularly interesting study would be to examine

innate lymphoid cell 2 (ILC2) responses, in both WT and STING$^{-/-}$ mice to see if there is an exacerbated response with excessive recruitment of eosinophils, mast, and other cells recruited with a Th2 profile.

Another evolving research area to examine would be the potential for an ENS to CNS route of infection in mice, and possibly in humans. It is possible that the GI is infected and virus travels to the spine through axonal transfer, from the ENS through the spine and then progresses upwards to the brainstem. Clinically the mice typically experience increased innervation of the pelvic muscles followed in STING$^{-/-}$ by decreased reflexes and tone, as well as balance. Further, pathology was only noted in the lower spine in mice that went on to survive. This may suggest that the virus is able to spread further throughout the GI and access the spine lower at the lumbar/sacral nerve junction, initiating pathology and inflammation in the lower spine, causing subsequent and sustained hind-limb paresis and paralysis. Preliminary analysis could start with sectioning the spine and GI of formalin fixed Terminal and Survivor mice, and looking for virus, cellular infiltrate and pathology by H&E and IHC.

Focusing on cGAS and STING signaling, the differences in clinical symptoms and innate immune signaling suggest differences between the two in conferring CNS defense and differences in GI pathology. STING seems to have a critical role in protecting the CNS, not just with WNV but also from a wide variety of other diseases. Using mixed-data types including pathology, IHC, RNAseq, virologic and molecular analysis it would be intriguing to determine what signaling pathways are different between cGAS and STING deficient mice and determine specifically what pathways and factors are critical for conferring neurological protection during WNV infection.

5.2.6 *STING and RNA viruses*

Given our results demonstrating an essential role for STING in providing host defense against WNV, and other studies demonstrating a role for STING with other flaviviruses, it would be interesting to examine related viruses and compare their results with WNV. Initially, studies in BMDM generated from WT, STING$^{-/-}$, cGAS$^{-/-}$ and MAVS$^{-/-}$ mice would be a comprehensive initial screen to see if the same kinetics are observed with influenza A, ZIKV, dengue, JEV, poliovirus, rhinovirus and mouse hepatitis virus (coronavirus). This would give a range of RNA viruses including negative and positive sense viruses, enveloped and non-enveloped and from different viral families including orthomyxoviruses, flaviviruses, picornaviruses, and coronaviruses. Using these viruses as tools, it may be possible to examine the mechanism of STING-dependent protection *in vitro* and then extend this work to an *in vivo* model.

BIBLIOGRAPHY

1. Chow, F.C. and C.A. Glaser, *Emerging and reemerging neurologic infections.* Neurohospitalist, 2014. **4**(4): p. 173-84.
2. Ekstrand, J.J., *Neurologic complications of influenza.* Semin Pediatr Neurol, 2012. **19**(3): p. 96-100.
3. Tsai, J.P. and A.J. Baker, *Influenza-associated neurological complications.* Neurocrit Care, 2013. **18**(1): p. 118-30.
4. Algahtani, H., A. Subahi, and B. Shirah, *Neurological Complications of Middle East Respiratory Syndrome Coronavirus: A Report of Two Cases and Review of the Literature.* Case Rep Neurol Med, 2016. **2016**: p. 3502683.
5. Wiwanitkit, V., *Neurological Problem in Ebola: A Topic in Neurology.* Acta Neurol Taiwan, 2015. **24**(2): p. 69-70.
6. Liner, K.J., 2nd, C.D. Hall, and K.R. Robertson, *Impact of human immunodeficiency virus (HIV) subtypes on HIV-associated neurological disease.* J Neurovirol, 2007. **13**(4): p. 291-304.
7. Oliveira, D.B., et al., *Infection of the central nervous system with dengue virus 3 genotype I causing neurological manifestations in Brazil.* Rev Soc Bras Med Trop, 2016. **49**(1): p. 125-9.
8. Verma, R., R. Sahu, and V. Holla, *Neurological manifestations of dengue infection: a review.* J Neurol Sci, 2014. **346**(1-2): p. 26-34.
9. Solomon, T., et al., *Neurological manifestations of dengue infection.* Lancet, 2000. **355**(9209): p. 1053-9.

10. Johnson, R.T., *Emerging viral infections of the nervous system.* J Neurovirol, 2003. **9**(2): p. 140-7.

11. Petersen, L.R., A.C. Brault, and R.S. Nasci, *West Nile virus: review of the literature.* JAMA, 2013. **310**(3): p. 308-15.

12. Beckham, J.D., et al., *Zika Virus as an Emerging Global Pathogen: Neurological Complications of Zika Virus.* JAMA Neurol, 2016.

13. Carod-Artal, F.J., *Epidemiology and neurological complications of infection by the Zika virus: a new emerging neurotropic virus.* Rev Neurol, 2016. **62**(7): p. 317-328.

14. Nash, D., et al., *The outbreak of West Nile virus infection in the New York City area in 1999.* N Engl J Med, 2001. **344**(24): p. 1807-14.

15. Fine, A. and M. Layton, *Lessons from the West Nile viral encephalitis outbreak in New York City, 1999: implications for bioterrorism preparedness.* Clin Infect Dis, 2001. **32**(2): p. 277-82.

16. May, F.J., et al., *Phylogeography of West Nile virus: from the cradle of evolution in Africa to Eurasia, Australia, and the Americas.* J Virol, 2011. **85**(6): p. 2964-74.

17. Davis, C.T., et al., *Phylogenetic analysis of North American West Nile virus isolates, 2001-2004: evidence for the emergence of a dominant genotype.* Virology, 2005. **342**(2): p. 252-65.

18. Bondre, V.P., et al., *West Nile virus isolates from India: evidence for a distinct genetic lineage.* J Gen Virol, 2007. **88**(Pt 3): p. 875-84.

19. Jungbauer, C., et al., *West Nile virus lineage 2 infection in a blood donor from Vienna, Austria, August 2014.* J Clin Virol, 2015. **64**: p. 16-9.

20. Papa, A., et al., *West Nile virus lineage 2 from blood donor, Greece.* Emerg Infect Dis, 2012. **18**(4): p. 688-9.

21. Brinton, M.A., *Replication cycle and molecular biology of the West Nile virus.* Viruses, 2014. **6**(1): p. 13-53.

22. Berthet, F.X., et al., *Extensive nucleotide changes and deletions within the envelope glycoprotein gene of Euro-African West Nile viruses.* J Gen Virol, 1997. **78 (Pt 9)**: p. 2293-7.

23. Cho, H. and M.S. Diamond, *Immune responses to West Nile virus infection in the central nervous system.* Viruses, 2012. **4**(12): p. 3812-30.

24. Lindsey, N.P., et al., *West nile virus and other arboviral diseases - United States, 2013.* MMWR Morb Mortal Wkly Rep, 2014. **63**(24): p. 521-6.

25. Reimann, C.A., et al., *Epidemiology of neuroinvasive arboviral disease in the United States, 1999-2007.* Am J Trop Med Hyg, 2008. **79**(6): p. 974-9.

26. Troupin, A. and T.M. Colpitts, *Overview of West Nile Virus Transmission and Epidemiology.* Methods Mol Biol, 2016. **1435**: p. 15-8.

27. Komar, N., et al., *Experimental infection of North American birds with the New York 1999 strain of West Nile virus.* Emerg Infect Dis, 2003. **9**(3): p. 311-22.

28. Kilpatrick, A.M., et al., *Host heterogeneity dominates West Nile virus transmission.* Proc Biol Sci, 2006. **273**(1599): p. 2327-33.

29. Kilpatrick, A.M., et al., *Temperature, viral genetics, and the transmission of West Nile virus by Culex pipiens mosquitoes.* PLoS Pathog, 2008. **4**(6): p. e1000092.

30. Sejvar, J.J., et al., *Neurologic manifestations and outcome of West Nile virus infection.* JAMA, 2003. **290**(4): p. 511-5.

31. Zou, S., et al., *West Nile fever characteristics among viremic persons identified through blood donor screening.* J Infect Dis, 2010. **202**(9): p. 1354-61.

32. Russo, M.V. and D.B. McGavern, *Immune Surveillance of the CNS following Infection and Injury.* Trends Immunol, 2015. **36**(10): p. 637-50.

33. Sejvar, J.J., et al., *Neurocognitive and functional outcomes in persons recovering from West Nile virus illness.* J Neuropsychol, 2008. **2**(Pt 2): p. 477-99.

34. Davis, L.E., et al., *West Nile virus neuroinvasive disease.* Ann Neurol, 2006. **60**(3): p. 286-300.

35. Weber, I.B., et al., *Completeness of West Nile virus testing in patients with meningitis and encephalitis during an outbreak in Arizona, USA.* Epidemiol Infect, 2012. **140**(9): p. 1632-6.

36. Petersen, L.R., et al., *Estimated cumulative incidence of West Nile virus infection in US adults, 1999-2010.* Epidemiol Infect, 2013. **141**(3): p. 591-5.

37. Lim, P.Y., et al., *Keratinocytes are cell targets of West Nile virus in vivo.* J Virol, 2011. **85**(10): p. 5197-201.

38. Schneider, B.S. and S. Higgs, *The enhancement of arbovirus transmission and disease by mosquito saliva is associated with modulation of the host immune response.* Trans R Soc Trop Med Hyg, 2008. **102**(5): p. 400-8.

39. Johnston, L.J., G.M. Halliday, and N.J. King, *Langerhans cells migrate to local lymph nodes following cutaneous infection with an arbovirus.* J Invest Dermatol, 2000. **114**(3): p. 560-8.

40. Wang, T., et al., *Toll-like receptor 3 mediates West Nile virus entry into the brain causing lethal encephalitis.* Nat Med, 2004. **10**(12): p. 1366-73.

41. Verma, S., et al., *Reversal of West Nile virus-induced blood-brain barrier disruption and tight junction proteins degradation by matrix metalloproteinases inhibitor.* Virology, 2010. **397**(1): p. 130-8.

42. Wang, P., et al., *Matrix metalloproteinase 9 facilitates West Nile virus entry into the brain.* J Virol, 2008. **82**(18): p. 8978-85.

43. Diamond, M.S., et al., *Innate and adaptive immune responses determine protection against disseminated infection by West Nile encephalitis virus.* Viral Immunol, 2003. **16**(3): p. 259-78.

44. Getts, D.R., et al., *Ly6c+ "inflammatory monocytes" are microglial precursors recruited in a pathogenic manner in West Nile virus encephalitis.* J Exp Med, 2008. **205**(10): p. 2319-37.

45. Terry, R.L., et al., *Inflammatory monocytes and the pathogenesis of viral encephalitis.* J Neuroinflammation, 2012. **9**: p. 270.

46. Samuel, M.A., et al., *Axonal transport mediates West Nile virus entry into the central nervous system and induces acute flaccid paralysis.* Proc Natl Acad Sci U S A, 2007. **104**(43): p. 17140-5.

47. Samuel, M.A. and M.S. Diamond, *Pathogenesis of West Nile Virus infection: a balance between virulence, innate and adaptive immunity, and viral evasion.* J Virol, 2006. **80**(19): p. 9349-60.

48. Suthar, M.S., M.S. Diamond, and M. Gale, Jr., *West Nile virus infection and immunity.* Nat Rev Microbiol, 2013. **11**(2): p. 115-28.

49. Quicke, K.M. and M.S. Suthar, *The innate immune playbook for restricting West Nile virus infection.* Viruses, 2013. **5**(11): p. 2643-58.

50. Fredericksen, B.L., et al., *Establishment and maintenance of the innate antiviral response to West Nile Virus involves both RIG-I and MDA5 signaling through IPS-1.* J Virol, 2008. **82**(2): p. 609-16.

51. Lazear, H.M., et al., *IRF-3, IRF-5, and IRF-7 coordinately regulate the type I IFN response in myeloid dendritic cells downstream of MAVS signaling.* PLoS Pathog, 2013. **9**(1): p. e1003118.

52. Samuel, M.A. and M.S. Diamond, *Alpha/beta interferon protects against lethal West Nile virus infection by restricting cellular tropism and enhancing neuronal survival.* J Virol, 2005. **79**(21): p. 13350-61.

53. Suthar, M.S., et al., *IPS-1 is essential for the control of West Nile virus infection and immunity.* PLoS Pathog, 2010. **6**(2): p. e1000757.

54. Fredericksen, B.L. and M. Gale, Jr., *West Nile virus evades activation of interferon regulatory factor 3 through RIG-I-dependent and -independent pathways without antagonizing host defense signaling.* J Virol, 2006. **80**(6): p. 2913-23.

55. Keller, B.C., et al., *Resistance to alpha/beta interferon is a determinant of West Nile virus replication fitness and virulence.* J Virol, 2006. **80**(19): p. 9424-34.

56. Lazear, H.M., et al., *Pattern recognition receptor MDA5 modulates CD8+ T cell-dependent clearance of West Nile virus from the central nervous system.* J Virol, 2013. **87**(21): p. 11401-15.

57. Suthar, M.S., et al., *A systems biology approach reveals that tissue tropism to West Nile virus is regulated by antiviral genes and innate immune cellular processes.* PLoS Pathog, 2013. **9**(2): p. e1003168.

58. Isaacs, A. and J. Lindenmann, *Virus interference. I. The interferon.* Proc R Soc Lond B Biol Sci, 1957. **147**(927): p. 258-67.

59. Porterfield, J.S., *A SIMPLE PLAQUE INHIBITION TEST FOR ANTIVIRAL AGENTS : APPLICATION TO ASSAY OF INTERFERON.* The Lancet. **274**(7098): p. 326-327.

60. Kell, A.M. and M. Gale, Jr., *RIG-I in RNA virus recognition.* Virology, 2015. **479-480**: p. 110-21.

61. Ramos, H.J. and M. Gale, Jr., *RIG-I like receptors and their signaling crosstalk in the regulation of antiviral immunity.* Curr Opin Virol, 2011. **1**(3): p. 167-76.

62. Saito, T. and M. Gale, Jr., *Differential recognition of double-stranded RNA by RIG-I-like receptors in antiviral immunity.* J Exp Med, 2008. **205**(7): p. 1523-7.

63. Loo, Y.M. and M. Gale, Jr., *Immune signaling by RIG-I-like receptors.* Immunity, 2011. **34**(5): p. 680-92.

64. Jiang, F., et al., *Structural basis of RNA recognition and activation by innate immune receptor RIG-I.* Nature, 2011. **479**(7373): p. 423-7.

65. Errett, J.S., et al., *The essential, nonredundant roles of RIG-I and MDA5 in detecting and controlling West Nile virus infection.* J Virol, 2013. **87**(21): p. 11416-25.

66. Suthar, M.S., et al., *The RIG-I-like receptor LGP2 controls CD8(+) T cell survival and fitness.* Immunity, 2012. **37**(2): p. 235-48.

67. Pinto, A.K., et al., *Deficient IFN signaling by myeloid cells leads to MAVS-dependent virus-induced sepsis.* PLoS Pathog, 2014. **10**(4): p. e1004086.

68. Larsen, M.V., et al., *Identification of CD8+ T cell epitopes in the West Nile virus polyprotein by reverse-immunology using NetCTL.* PLoS One, 2010. **5**(9): p. e12697.

69. Lanteri, M.C., et al., *Tregs control the development of symptomatic West Nile virus infection in humans and mice.* J Clin Invest, 2009. **119**(11): p. 3266-77.

70. Stewart, B.S., et al., *Persistence of virus-specific immune responses in the central nervous system of mice after West Nile virus infection.* BMC Immunol, 2011. **12**: p. 6.

71. You, F., et al., *ELF4 is critical for induction of type I interferon and the host antiviral response.* Nat Immunol, 2013. **14**(12): p. 1237-46.

72. Ishikawa, H. and G.N. Barber, *STING is an endoplasmic reticulum adaptor that facilitates innate immune signalling.* Nature, 2008. **455**(7213): p. 674-8.

73. Ishikawa, H., Z. Ma, and G.N. Barber, *STING regulates intracellular DNA-mediated, type I interferon-dependent innate immunity.* Nature, 2009. **461**(7265): p. 788-92.

74. Ma, Z. and B. Damania, *The cGAS-STING Defense Pathway and Its Counteraction by Viruses.* Cell Host Microbe, 2016. **19**(2): p. 150-8.

75. Maringer, K. and A. Fernandez-Sesma, *Message in a bottle: lessons learned from antagonism of STING signalling during RNA virus infection.* Cytokine Growth Factor Rev, 2014. **25**(6): p. 669-79.

76. Bhat, N. and K.A. Fitzgerald, *Recognition of cytosolic DNA by cGAS and other STING-dependent sensors.* Eur J Immunol, 2014. **44**(3): p. 634-40.

77. Cai, X., Y.H. Chiu, and Z.J. Chen, *The cGAS-cGAMP-STING pathway of cytosolic DNA sensing and signaling.* Mol Cell, 2014. **54**(2): p. 289-96.

78. Takaoka, A., et al., *DAI (DLM-1/ZBP1) is a cytosolic DNA sensor and an activator of innate immune response.* Nature, 2007. **448**(7152): p. 501-5.

79. Veeranki, S. and D. Choubey, *Interferon-inducible p200-family protein IFI16, an innate immune sensor for cytosolic and nuclear double-stranded DNA: regulation of subcellular localization.* Mol Immunol, 2012. **49**(4): p. 567-71.

80. Wu, J., et al., *Cyclic GMP-AMP is an endogenous second messenger in innate immune signaling by cytosolic DNA.* Science, 2013. **339**(6121): p. 826-30.

81. Stratmann, S.A., et al., *The innate immune sensor IFI16 recognizes foreign DNA in the nucleus by scanning along the duplex.* Elife, 2015. **4**.

82. Unterholzner, L., et al., *IFI16 is an innate immune sensor for intracellular DNA.* Nat Immunol, 2010. **11**(11): p. 997-1004.

83. Civril, F., et al., *Structural mechanism of cytosolic DNA sensing by cGAS.* Nature, 2013. **498**(7454): p. 332-7.

84. Diner, E.J., et al., *The innate immune DNA sensor cGAS produces a noncanonical cyclic dinucleotide that activates human STING.* Cell Rep, 2013. **3**(5): p. 1355-61.

85. Gao, P., et al., *Cyclic [G(2',5')pA(3',5')p] is the metazoan second messenger produced by DNA-activated cyclic GMP-AMP synthase.* Cell, 2013. **153**(5): p. 1094-107.

86. Sun, L., et al., *Cyclic GMP-AMP synthase is a cytosolic DNA sensor that activates the type I interferon pathway.* Science, 2013. **339**(6121): p. 786-91.

87. Burdette, D.L. and R.E. Vance, *STING and the innate immune response to nucleic acids in the cytosol.* Nat Immunol, 2013. **14**(1): p. 19-26.

88. Liu, S., et al., *Phosphorylation of innate immune adaptor proteins MAVS, STING, and TRIF induces IRF3 activation.* Science, 2015. **347**(6227): p. aaa2630.

89. Deng, L., et al., *STING-Dependent Cytosolic DNA Sensing Promotes Radiation-Induced Type I Interferon-Dependent Antitumor Immunity in Immunogenic Tumors.* Immunity, 2014. **41**(5): p. 843-52.

90. Gao, D., et al., *Activation of cyclic GMP-AMP synthase by self-DNA causes autoimmune diseases.* Proc Natl Acad Sci U S A, 2015. **112**(42): p. E5699-705.

91. Holm, C.K., et al., *Influenza A virus targets a cGAS-independent STING pathway that controls enveloped RNA viruses.* Nat Commun, 2016. **7**: p. 10680.

92. Li, T., et al., *Antitumor Activity of cGAMP via Stimulation of cGAS-cGAMP-STING-IRF3 Mediated Innate Immune Response.* Sci Rep, 2016. **6**: p. 19049.

93. West, A.P., et al., *Mitochondrial DNA stress primes the antiviral innate immune response.* Nature, 2015. **520**(7548): p. 553-7.

94. Woo, S.R., et al., *STING-dependent cytosolic DNA sensing mediates innate immune recognition of immunogenic tumors.* Immunity, 2014. **41**(5): p. 830-42.

95. Herzner, A.M., et al., *Sequence-specific activation of the DNA sensor cGAS by Y-form DNA structures as found in primary HIV-1 cDNA.* Nat Immunol, 2015. **16**(10): p. 1025-33.

96. Schoggins, J.W., et al., *Corrigendum: Pan-viral specificity of IFN-induced genes reveals new roles for cGAS in innate immunity.* Nature, 2015. **525**(7567): p. 144.

97. Schoggins, J.W., et al., *Pan-viral specificity of IFN-induced genes reveals new roles for cGAS in innate immunity.* Nature, 2014. **505**(7485): p. 691-5.

98. Nazmi, A., et al., *STING mediates neuronal innate immune response following Japanese encephalitis virus infection.* Sci Rep, 2012. **2**: p. 347.

99. Liu, Y. and S. Cherry, *Zika virus infection activates sting-dependent antiviral autophagy in the Drosophila brain.* Autophagy, 2019. **15**(1): p. 174-175.

100. Aspelund, A., et al., *A dural lymphatic vascular system that drains brain interstitial fluid and macromolecules.* J Exp Med, 2015. **212**(7): p. 991-9.

101. Louveau, A., T.H. Harris, and J. Kipnis, *Revisiting the Mechanisms of CNS Immune Privilege.* Trends Immunol, 2015. **36**(10): p. 569-77.

102. Louveau, A., et al., *Structural and functional features of central nervous system lymphatic vessels.* Nature, 2015. **523**(7560): p. 337-341.

103. Chiu, R.W., T.H. Rainer, and Y.M. Lo, *Circulating nucleic acid analysis: diagnostic applications for acute pathologies.* Acta Neurochir Suppl, 2005. **95**: p. 471-4.

104. de Rivero Vaccari, J.P., W.D. Dietrich, and R.W. Keane, *Activation and regulation of cellular inflammasomes: gaps in our knowledge for central nervous system injury.* J Cereb Blood Flow Metab, 2014. **34**(3): p. 369-75.

105. Liimatainen, S.P., et al., *The concentration of cell-free DNA in focal epilepsy.* Epilepsy Res, 2013. **105**(3): p. 292-8.

106. Tsai, N.W., et al., *The value of serial plasma nuclear and mitochondrial DNA levels in patients with acute ischemic stroke.* Clin Chim Acta, 2011. **412**(5-6): p. 476-9.

107. Field, R., et al., *Systemic challenge with the TLR3 agonist poly I:C induces amplified IFNalpha/beta and IL-1beta responses in the diseased brain and exacerbates chronic neurodegeneration.* Brain Behav Immun, 2010. **24**(6): p. 996-1007.

108. Wang, R., B. Yang, and D. Zhang, *Activation of interferon signaling pathways in spinal cord astrocytes from an ALS mouse model.* Glia, 2011. **59**(6): p. 946-58.

109. Cox, D.J., et al., *DNA sensors are expressed in astrocytes and microglia in vitro and are upregulated during gliosis in neurodegenerative disease.* Glia, 2015. **63**(5): p. 812-25.

110. Gray, E.E., et al., *Cutting Edge: cGAS Is Required for Lethal Autoimmune Disease in the Trex1-Deficient Mouse Model of Aicardi-Goutieres Syndrome.* J Immunol, 2015. **195**(5): p. 1939-43.

111. Ni, G., Z. Ma, and B. Damania, *cGAS and STING: At the intersection of DNA and RNA virus-sensing networks.* PLoS Pathog, 2018. **14**(8): p. e1007148.

112. Gall, A., et al., *Autoimmunity initiates in nonhematopoietic cells and progresses via lymphocytes in an interferon-dependent autoimmune disease.* Immunity, 2012. **36**(1): p. 120-31.

113. Muller, D.M., M.P. Pender, and J.M. Greer, *A neuropathological analysis of experimental autoimmune encephalomyelitis with predominant brain stem and cerebellar involvement and differences between active and passive induction.* Acta Neuropathol, 2000. **100**(2): p. 174-82.

114. Miller, S.D. and W.J. Karpus, *Experimental autoimmune encephalomyelitis in the mouse.* Curr Protoc Immunol, 2007. **Chapter 15**: p. Unit 15 1.

115. Palle, P., et al., *The more the merrier? Scoring, statistics and animal welfare in experimental autoimmune encephalomyelitis.* Lab Anim, 2016. **50**(6): p. 427-432.

116. Pierson, E.R., I.M. Stromnes, and J.M. Goverman, *B cells promote induction of experimental autoimmune encephalomyelitis by facilitating reactivation of T cells in the central nervous system.* J Immunol, 2014. **192**(3): p. 929-39.

117. Treuting, P.M. and J.M. Snyder, *Mouse Necropsy.* Curr Protoc Mouse Biol, 2015. **5**(3): p. 223-33.

118. Daniels, B.P., et al., *RIPK3 Restricts Viral Pathogenesis via Cell Death-Independent Neuroinflammation.* Cell, 2017. **169**(2): p. 301-313 e11.

119. Klein, R.S., et al., *Neuronal CXCL10 directs CD8+ T-cell recruitment and control of West Nile virus encephalitis.* J Virol, 2005. **79**(17): p. 11457-66.

120. Brien, J.D., H.M. Lazear, and M.S. Diamond, *Propagation, quantification, detection, and storage of West Nile virus.* Curr Protoc Microbiol, 2013. **31**: p. 15D 3 1-15D 3 18.

121. Carteaux, G., et al., *Zika Virus Associated with Meningoencephalitis.* N Engl J Med, 2016. **374**(16): p. 1595-6.

122. Griffin, D.E., *Emergence and re-emergence of viral diseases of the central nervous system.* Prog Neurobiol, 2010. **91**(2): p. 95-101.

123. Carson, P.J., et al., *Neuroinvasive disease and West Nile virus infection, North Dakota, USA, 1999-2008.* Emerg Infect Dis, 2012. **18**(4): p. 684-6.

124. Harris, K., *Gastrointestinal manifestations of acute West Nile virus infection in humans*, in *School of Public Health*. 2016, The University of Texas: Texas Medical Center Dissertations (via ProQuest).

125. Armah, H.B., et al., *Systemic distribution of West Nile virus infection: postmortem immunohistochemical study of six cases.* Brain Pathol, 2007. **17**(4): p. 354-62.

126. Watson, J.T., et al., *Clinical characteristics and functional outcomes of West Nile Fever.* Ann Intern Med, 2004. **141**(5): p. 360-5.

127. Leis, A.A., et al., *Clinical spectrum of muscle weakness in human West Nile virus infection.* Muscle Nerve, 2003. **28**(3): p. 302-8.

128. Graham, J.B., J.L. Swarts, and J.M. Lund, *A Mouse Model of West Nile Virus Infection.* Curr Protoc Mouse Biol, 2017. **7**(4): p. 221-235.

129. Graham, J.B., et al., *A Mouse Model of Chronic West Nile Virus Disease.* PLoS Pathog, 2016. **12**(11): p. e1005996.

130. Bingham, J., et al., *Evaluation of a mouse model for the West Nile virus group for the purpose of determining viral pathotypes.* J Gen Virol, 2014. **95**(Pt 6): p. 1221-32.

131. Lazear, H.M., et al., *Interferon-lambda restricts West Nile virus neuroinvasion by tightening the blood-brain barrier.* Sci Transl Med, 2015. **7**(284): p. 284ra59.

132. Daffis, S., et al., *Cell-specific IRF-3 responses protect against West Nile virus infection by interferon-dependent and -independent mechanisms.* PLoS Pathog, 2007. **3**(7): p. e106.

133. Loo, Y.M., et al., *Distinct RIG-I and MDA5 signaling by RNA viruses in innate immunity.* J Virol, 2008. **82**(1): p. 335-45.

134. Pinto, A.K., et al., *A temporal role of type I interferon signaling in CD8+ T cell maturation during acute West Nile virus infection.* PLoS Pathog, 2011. **7**(12): p. e1002407.

135. Shrestha, B. and M.S. Diamond, *Role of CD8+ T cells in control of West Nile virus infection.* J Virol, 2004. **78**(15): p. 8312-21.

136. Sitati, E.M. and M.S. Diamond, *CD4+ T-cell responses are required for clearance of West Nile virus from the central nervous system.* J Virol, 2006. **80**(24): p. 12060-9.

137. Wang, Y., et al., *CD8+ T cells mediate recovery and immunopathology in West Nile virus encephalitis.* J Virol, 2003. **77**(24): p. 13323-34.

138. Barber, G.N., *STING: infection, inflammation and cancer.* Nat Rev Immunol, 2015. **15**(12): p. 760-70.

139. Holm, C.K., et al., *Virus-cell fusion as a trigger of innate immunity dependent on the adaptor STING.* Nat Immunol, 2012. **13**(8): p. 737-43.

140. Aguirre, S., et al., *DENV inhibits type I IFN production in infected cells by cleaving human STING.* PLoS Pathog, 2012. **8**(10): p. e1002934.

141. Abdullah, A., et al., *STING-mediated type-I interferons contribute to the neuroinflammatory process and detrimental effects following traumatic brain injury.* J Neuroinflammation, 2018. **15**(1): p. 323.

142. Ahn, J. and G.N. Barber, *Self-DNA, STING-dependent signaling and the origins of autoinflammatory disease.* Curr Opin Immunol, 2014. **31**: p. 121-6.

143. *Allen Mouse Brain Atlas*. 2004 [cited 2019 January 21]; Tmem173-/- (STING) in the mouse brain]. Available from: http://mouse.brain-map.org/gene/show/48353.

144. Kelley, T.W., et al., *The neuropathology of West Nile virus meningoencephalitis. A report of two cases and review of the literature.* Am J Clin Pathol, 2003. **119**(5): p. 749-53.

145. Suen, W.W., et al., *End-point disease investigation for virus strains of intermediate virulence as illustrated by flavivirus infections.* J Gen Virol, 2016. **97**(2): p. 366-77.

146. Thackray, L.B., et al., *Oral Antibiotic Treatment of Mice Exacerbates the Disease Severity of Multiple Flavivirus Infections.* Cell Rep, 2018. **22**(13): p. 3440-3453 e6.

147. Sauer, J.D., et al., *The N-ethyl-N-nitrosourea-induced Goldenticket mouse mutant reveals an essential function of Sting in the in vivo interferon response to Listeria monocytogenes and cyclic dinucleotides.* Infect Immun, 2011. **79**(2): p. 688-94.

148. Jang, H., et al., *Viral parkinsonism.* Biochim Biophys Acta, 2009. **1792**(7): p. 714-21.

149. Robinson, R.L., et al., *Transient parkinsonism in West Nile virus encephalitis.* Am J Med, 2003. **115**(3): p. 252-3.

150. Aarreberg, L.D., et al., *Interleukin-1β induces mitochondrial DNA release to activate innate immune signaling via cGAS-STING.* In Press Molecular Cell, 2019.

151. Terry, R.L., I. Ifergan, and S.D. Miller, *Experimental Autoimmune Encephalomyelitis in Mice.* Methods Mol Biol, 2016. **1304**: p. 145-60.

152. Bebo, B.F., Jr., et al., *Gender differences in experimental autoimmune encephalomyelitis develop during the induction of the immune response to encephalitogenic peptides.* J Neurosci Res, 1998. **52**(4): p. 420-6.

153. Lessler, J., et al., *Assessing the global threat from Zika virus.* Science, 2016.

154. *Zika virus outbreaks in the Americas.* Wkly Epidemiol Rec, 2015. **90**(45): p. 609-10.

155. Campos, G.S., A.C. Bandeira, and S.I. Sardi, *Zika Virus Outbreak, Bahia, Brazil.* Emerg Infect Dis, 2015. **21**(10): p. 1885-6.

156. Cardoso, C.W., et al., *Outbreak of Exanthematous Illness Associated with Zika, Chikungunya, and Dengue Viruses, Salvador, Brazil.* Emerg Infect Dis, 2015. **21**(12): p. 2274-6.

157. Macnamara, F.N., *Zika virus: a report on three cases of human infection during an epidemic of jaundice in Nigeria.* Trans R Soc Trop Med Hyg, 1954. **48**(2): p. 139-45.

158. Dick, G.W., *Zika virus. II. Pathogenicity and physical properties.* Trans R Soc Trop Med Hyg, 1952. **46**(5): p. 521-34.

159. Dick, G.W., S.F. Kitchen, and A.J. Haddow, *Zika virus. I. Isolations and serological specificity.* Trans R Soc Trop Med Hyg, 1952. **46**(5): p. 509-20.

160. Simpson, D.I., *Zika Virus Infection in Man.* Trans R Soc Trop Med Hyg, 1964. **58**: p. 335-8.

161. Bowen, E.T., et al., *Large scale irrigation and arbovirus epidemiology, Kano Plain, Kenya. II. Preliminary serological survey.* Trans R Soc Trop Med Hyg, 1973. **67**(5): p. 702-9.

162. Rodhain, F., et al., *Arbovirus infections and viral haemorrhagic fevers in Uganda: a serological survey in Karamoja district, 1984.* Trans R Soc Trop Med Hyg, 1989. **83**(6): p. 851-4.

163. Fagbami, A.H., *Zika virus infections in Nigeria: virological and seroepidemiological investigations in Oyo State.* J Hyg (Lond), 1979. **83**(2): p. 213-9.

164. Darwish, M.A., et al., *A sero-epidemiological survey for certain arboviruses (Togaviridae) in Pakistan.* Trans R Soc Trop Med Hyg, 1983. **77**(4): p. 442-5.

165. Olson, J.G., et al., *A survey for arboviral antibodies in sera of humans and animals in Lombok, Republic of Indonesia.* Ann Trop Med Parasitol, 1983. **77**(2): p. 131-7.

166. Olson, J.G., et al., *Zika virus, a cause of fever in Central Java, Indonesia.* Trans R Soc Trop Med Hyg, 1981. **75**(3): p. 389-93.

167. McCrae, A.W. and B.G. Kirya, *Yellow fever and Zika virus epizootics and enzootics in Uganda.* Trans R Soc Trop Med Hyg, 1982. **76**(4): p. 552-62.

168. Lee, V.H. and D.L. Moore, *Vectors of the 1969 yellow fever epidemic on the Jos Plateau, Nigeria.* Bull World Health Organ, 1972. **46**(5): p. 669-73.

169. Haddow, A.J., et al., *Twelve Isolations of Zika Virus from Aedes (Stegomyia) Africanus (Theobald) Taken in and above a Uganda Forest.* Bull World Health Organ, 1964. **31**: p. 57-69.

170. McIntosh, B.M., C.B. Worth, and R.H. Kokernot, *Isolation of Semliki Forest virus from Aedes (Aedimorphus) argenteopunctatus (Theobald) collected in Portuguese East Africa.* Trans R Soc Trop Med Hyg, 1961. **55**: p. 192-8.

171. Weinbren, M.P. and M.C. Williams, *Zika virus: further isolations in the Zika area, and some studies on the strains isolated.* Trans R Soc Trop Med Hyg, 1958. **52**(3): p. 263-8.

172. Marchette, N.J., R. Garcia, and A. Rudnick, *Isolation of Zika virus from Aedes aegypti mosquitoes in Malaysia.* Am J Trop Med Hyg, 1969. **18**(3): p. 411-5.

173. Monlun, E., et al., *[Surveillance of the circulation of arbovirus of medical interest in the region of eastern Senegal]*. Bull Soc Pathol Exot, 1993. **86**(1): p. 21-8.

174. Fagbami, A., *Epidemiological investigations on arbovirus infections at Igbo-Ora, Nigeria.* Trop Geogr Med, 1977. **29**(2): p. 187-91.

175. Moore, D.L., et al., *Arthropod-borne viral infections of man in Nigeria, 1964-1970.* Ann Trop Med Parasitol, 1975. **69**(1): p. 49-64.

176. Althouse, B.M., et al., *Impact of climate and mosquito vector abundance on sylvatic arbovirus circulation dynamics in Senegal.* Am J Trop Med Hyg, 2015. **92**(1): p. 88-97.

177. Duffy, M.R., et al., *Zika virus outbreak on Yap Island, Federated States of Micronesia.* N Engl J Med, 2009. **360**(24): p. 2536-43.

178. Foy, B.D., et al., *Probable Non-Vector-borne Transmission of Zika Virus, Colorado, USA.* Emerging Infectious Diseases, 2011. **17**(5): p. 880-882.

179. Cao-Lormeau, V.M., et al., *Zika virus, French polynesia, South pacific, 2013.* Emerg Infect Dis, 2014. **20**(6): p. 1085-6.

180. Cao-Lormeau, V.M., et al., *Guillain-Barre Syndrome outbreak associated with Zika virus infection in French Polynesia: a case-control study.* Lancet, 2016. **387**(10027): p. 1531-9.

181. Schuler-Faccini, L., et al., *Possible Association Between Zika Virus Infection and Microcephaly - Brazil, 2015.* MMWR Morb Mortal Wkly Rep, 2016. **65**(3): p. 59-62.

182. WHO, *WHO Director-General summarizes the outcome of the Emergency Committee regarding clusters of microcephaly and Guillain-Barré syndrome.* 2016.

183. CDC, *Countries and Territories with Active Local Zika Virus Transmission.*

184. Petersen, L.R., et al., *Zika Virus.* N Engl J Med, 2016. **374**(16): p. 1552-63.

185. Fonseca, K., et al., *First case of Zika virus infection in a returning Canadian traveler.* Am J Trop Med Hyg, 2014. **91**(5): p. 1035-8.

186. Gyurech, D., et al., *False positive dengue NS1 antigen test in a traveller with an acute Zika virus infection imported into Switzerland.* Swiss Med Wkly, 2016. **146**: p. w14296.

187. Chen, L.H., *Zika Virus Infection in a Massachusetts Resident After Travel to Costa Rica: A Case Report.* Ann Intern Med, 2016. **164**(8): p. 574-6.

188. Zammarchi, L., et al., *Zika virus infections imported to Italy: clinical, immunological and virological findings, and public health implications.* J Clin Virol, 2015. **63**: p. 32-5.

189. Zammarchi, L., et al., *Zika virus infection in a traveller returning to Europe from Brazil, March 2015.* Euro Surveill, 2015. **20**(23).

190. Tappe, D., et al., *Acute Zika virus infection after travel to Malaysian Borneo, September 2014.* Emerg Infect Dis, 2015. **21**(5): p. 911-3.

191. Summers, D.J., R.W. Acosta, and A.M. Acosta, *Zika Virus in an American Recreational Traveler.* J Travel Med, 2015. **22**(5): p. 338-40.

192. Maria, A.T., et al., *Zika virus infections in three travellers returning from South America and the Caribbean respectively, to Montpellier, France, December 2015 to January 2016.* Euro Surveill, 2016. **21**(6).

193. Sarmiento-Ospina, A., et al., *Zika virus associated deaths in Colombia.* Lancet Infect Dis, 2016.

194. Arzuza-Ortega, L., et al., *Fatal Sickle Cell Disease and Zika Virus Infection in Girl from Colombia.* Emerg Infect Dis, 2016. **22**(5): p. 925-7.

195. Araujo, A.Q., M.T. Silva, and A.P. Araujo, *Zika virus-associated neurological disorders: a review.* Brain, 2016. **139**(Pt 8): p. 2122-30.

196. Araujo, L.M., M.L. Ferreira, and O.J. Nascimento, *Guillain-Barre syndrome associated with the Zika virus outbreak in Brazil.* Arq Neuropsiquiatr, 2016. **74**(3): p. 253-5.

197. Alshekhlee, A., et al., *Guillain-Barre syndrome: incidence and mortality rates in US hospitals.* Neurology, 2008. **70**(18): p. 1608-13.

198. Mecharles, S., et al., *Acute myelitis due to Zika virus infection.* Lancet, 2016. **387**(10026): p. 1481.

199. MICROCEFALIAS, C.D.O.D.E.E.S.P.S., *INFORME EPIDEMIOLÓGICO Nº 25 – SEMANA EPIDEMIOLÓGICA (SE) 18/2016 (01/05 A 07/05/2016)*

MONITORAMENTO DOS CASOS DE MICROCEFALIA NO BRASIL. Minesterio de Salud, Brasil, 2016.

200. Rasmussen, S.A., et al., *Zika Virus and Birth Defects--Reviewing the Evidence for Causality.* N Engl J Med, 2016. **374**(20): p. 1981-7.

201. Adibi, J.J., et al., *Teratogenic effects of the Zika virus and the role of the placenta.* Lancet, 2016. **387**(10027): p. 1587-90.

202. Adibi, J.J., et al., *Placental Mechanics in the Zika-Microcephaly Relationship.* Cell Host Microbe, 2016. **20**(1): p. 9-11.

203. Nishiura, H., et al., *A theoretical estimate of the risk of microcephaly during pregnancy with Zika virus infection.* Epidemics, 2016. **15**: p. 66-70.

204. Brasil, P., et al., *Zika Virus Outbreak in Rio de Janeiro, Brazil: Clinical Characterization, Epidemiological and Virological Aspects.* Plos Neglected Tropical Diseases, 2016. **10**(4).

205. Brasil, P., et al., *Zika Virus Infection in Pregnant Women in Rio de JaneiroPreliminary Report.* Obstetrical & Gynecological Survey, 2016. **71**(6): p. 331-333.

206. Franca, G.V., et al., *Congenital Zika virus syndrome in Brazil: a case series of the first 1501 livebirths with complete investigation.* Lancet, 2016.

207. Miner, J.J., et al., *Zika Virus Infection during Pregnancy in Mice Causes Placental Damage and Fetal Demise.* Cell, 2016. **165**(5): p. 1081-91.

208. Quicke, K.M., et al., *Zika Virus Infects Human Placental Macrophages.* Cell Host Microbe, 2016. **20**(1): p. 83-90.

209. Tabata, T., et al., *Zika Virus Targets Different Primary Human Placental Cells, Suggesting Two Routes for Vertical Transmission.* Cell Host Microbe, 2016. **20**(2): p. 155-66.

210. Reed, L.C., et al., *Evaluating maternal hyperglycemic exposure and fetal placental arterial dysfunction in a dual cotyledon, dual perfusion model.* Placenta, 2018. **69**: p. 109-116.

APPENDIX A

CLINICAL ANALYSIS TO DETERMINE CNS PATHOLOGY

Introduction

Clinical scoring for neurological models is predominantly utilized to monitor overall condition of the mouse for the purpose of 1) tracking progression of disease, 2) description of disease severity and 3) determining end-point euthanasia criteria for humanitarian purposes. Most clinical scoring systems are based in early descriptive studies following rabies vaccination studies from the 1930s [145], which informed current scoring methods developed for EAE models [113-116, 151]. Scoring for the WNV model used for this body of work was also based on an EAE scoring model [152], which is predominantly focused on paresis and paralysis of the hind-limbs (Table A1). Other models for EAE clinical scoring describe limp tails, tilting of the head or body, axial rotation, and fore-limb involvement and associate that to disease outcome. To date, no consistent clinical scoring model exists for neurological diseases, nor does one exist that correlates clinical scores with disease progression and outcome [115]. Using WNV as a model for neurological disease, we utilized the differences in neurological symptoms as well as disease progression and outcome between WT and STING$^{-/-}$ mice to develop a novel scoring system. The purpose of this is to track 1) the progression of disease, 2) correlate it to histopathology, 3) use this information to develop a predictive model for disease and pathological development/outcome. Further, establishing a consistent scoring system allows for distinction between neurological phenotypes and progression of disease between strains of mice, viruses and also be broadly applicable to a variety of mouse models of neurologic diseases.

There are two scoring systems that were developed over the course of this study to describe the clinical progression of WNV disease. The first is a comprised of two parts; a descriptive and severity portion to describe the daily clinical condition of each animal, or a 'Quick-Code' (Table A2; Figure A1). This is related to the current IACUC protocol (Table A1), however is further refined to give a daily description of the phenotype associated with a given clinical score. This is a powerful tool to distinguish between multiple clinical factors that may result in the same overall score, and include symptoms that are currently not scored. For example, in the Bebo based model, factors such as balance, GI distress and tremors are not considered at all [152]. In the modified model used for this study, eye disease is limited to 'conjunctivitis', and is an automatic clinical score (CS) = 3, but because multiple factors could result in a CS = 3 no data is recorded to identify what symptom(s) resulted in the score. Similarly, multiple factors can give a mouse a CS = 1, however general weakness is not currently scored, and as the scoring progresses it is lost if the mouse maintains grooming or behavioral phenotypes. The 'Quick-Code' is a way to track symptoms daily, while the actual clinical score gives the severity score. Together these increase resolution of the clinical scoring model and describe disease progression and outcome in a way that can be correlated to disease pathology.

The second clinical scoring model is the 'Extended scoring system' which expands on the 'Quick-Code' and provides further refinement of determining histopathologic lesions with clinical symptom and disease outcome. This system groups clinical manifestations into four categories, including 1) grooming, 2) behavioral, 3) physical and 4) neurological disease. The overarching purpose of this is to be able to associate clinical symptoms to anatomical location of neuropathologic lesions and disease. The initial portion of this study is to design and develop a neurological scoring system, followed by independent analysis and prediction of the anatomical

disease each mouse would display and then confirmed by pathological review. Once the scoring model is validated, computational analysis will be able to incorporate additional data including morbidity, mortality (outcome), histopathologic and other data types including molecular, immunological and virologic to assess the relation between different clinical phenotypes and disease outcomes.

Study Design and Methodology

To develop the 'Quick Code' and 'Extended Code' scoring systems, mice were monitored in accordance with the IACUC protocols and then further monitored daily for a 'Quick Code' and every three days for the 'Extended Code'. Per IACUC approved protocols, clinical score (CS) and bodyweight (BW) were assessed daily until a CS of 3; subsequently all mice within the cage of any mouse with a CS = 3 or more will be monitored daily. The average of these two CS was used to generate a single daily score. A CS of 6 or BW loss of <20% original weight are criteria for euthanasia. Mice that meet euthanasia criteria were identified as terminal (T), and mice that did not meet euthanasia criteria until study end were considered survivors (S) as previously described. Each day, mice were monitored per the 'Quick Code' and given an alpha-numeric score for the most common symptoms associated with IACUC assigned clinical score and severity (Table A2; Figure A1). Additionally, on the day of infection and every third day after until study end, an extended neurological clinical analysis will be performed (Table A3). Both score systems will utilize binary analysis, where 0 = symptom not present and 1 = symptom present. In the case of increasing symptoms such as paresis severity, binary scores will be weighted in downstream analysis. These symptoms will be used in R-based modeling predictions for onset, location and severity of CNS pathogenesis, to be validated by pathological analysis. Additional downstream analysis will be performed to examine clinical differences

between T and S groups. From this, we can determine if earlier or increased clinical scores and loss of bodyweight are associated with both increased morbidity (T and S populations) and mortality (T population only), or if the differences occur only in the surviving population, which would indicate that there may be different mechanisms of action leading to increased mortality vs. morbidity associated with STING $^{-/-}$ mice. Similar analysis will be performed using clinical and neurological symptoms associated with T vs. S populations in both WT and STING $^{-/-}$ mice.

Quick Code

In the current IACUC scoring protocol, the resolution of clinical scores is poor due to mixing qualitative descriptive and quantitative severity scores (Table A1). The current IACUC protocol follows the Bebo 1998 EAE model [152], scoring severity based predominantly on hind-limb function, with modifications to include behavioral and grooming for initial symptoms and eye conjunctivitis as additional symptoms that relegate disease severity. In order to increase the accuracy in tracking clinical progression of disease, a revised proposed clinical score methodology is proposed that is comprised of 1) severity scoring including GI, eye disease and other common symptoms, and 2) a descriptive clinical 'Quick Code' that can be transferred to excel and analyzed by R using the code in (Table A2). This allows for much finer resolution of daily symptoms, progression of disease and severity to include non-paralytic symptoms. The results of the 'Quick Code' also can suggest potential localization of histopathology, particularly in the CNS or GI.

Table A1: Current IACUC Scoring Protocol

IACUC Scoring Criteria		
1	Ruffled Fur/Lethargic/Hunched/General weakness	Slight decrease in ability to grip in addition to decreased strength
2	Very mild to mild paresis	Mild impact to grip strength; still able to grip bars completely and hold on by toes but releases more easily.
3	Frank paresis involving at least 1 hind limb and/or conjunctivitis or mild paresis in 2 hind limbs	Clear reduction in ability to grip bars; still capable of gripping but when testing feet slip hold.
4	Severe paresis, still retains feeling and possibly limbic	Inability to grip and hold on but still attempts to grip; has some level of control over limb(s); grip continually slips with mild to moderate pressure from tail lift.
5	True paralysis	No control of limb(s); drags while mouse is moving. No ability to grip or hold rack bars.
6	Moribund	**Physical:** Complete loss of limb function/lack or refusal to move. **NOTE:** May or may not be associated with paralytic symptoms. Typically characterized by refusal to move even up on stimulation (transfer to rack, gentle nudge with pen). Eyes closed or partially closed, "O" shaped hunched, shallow respiratory (or) severely increased respiratory rate, concave (dehydration) or convex (GI distress) shape to abdomen.

Table A2: Proposed revised Scoring Protocol (Severity Score)

Proposed Daily IACUC Scoring			
Score	**Paresis/Paralysis**	**Other symptoms**	
1	General weakness	Ruffled Fur/Lethargic/Hunched/Tremors (mild)	Any of the symptoms listed here result in a CS = 1. Annotate using Quick Code.
2	Very mild to mild paresis	GI distress (very mild); loss of balance/wide-based stance	Mild impact to grip strength; still able to grip bars completely and hold on by toes but releases more easily.
3	Frank paresis involving at least 1 hind limb or mild paresis in 2 hind limbs	GI distress (mild); eye disease	Clear reduction in ability to grip bars; still capable of gripping but when testing feet slip hold.
4	Severe paresis, still retains feeling and possibly limbic	GI distress (moderate); severe eye disease; Parkinsons-like tremors; hair clumping	Inability to grip and hold on but still attempts to grip; has some level of control over limb(s); grip continually slips with mild to moderate pressure from tail lift.
5	True paralysis	GI distress (severe); blindness; hair loss	No control of limb(s); drags while mouse is moving. No ability to grip or hold rack bars.
6	Moribund: inability or refusal to move; grip or respond (ambulatory) to stimuli	Extreme GI distress; resulting in moribund behavior, slow to no movement; compaction (no stool movement); bloat >3x normal width	**Physical:** Complete loss of limb function/lack or refusal to move. **NOTE:** May or may not be associated with paralytic symptoms. Typically characterized by refusal to move even up on stimulation (transfer to rack, gentle nudge with pen). Eyes closed or partially closed, "O" shaped hunched, shallow respiratory (or) severely increased respiratory rate, concave (dehydration) or convex (GI distress) shape to abdomin. Excessive respiratory, compacted or hardened GI tract or severe GI distension to the point where movement is severely restricted are grounds for automatic euthanasia criteria.

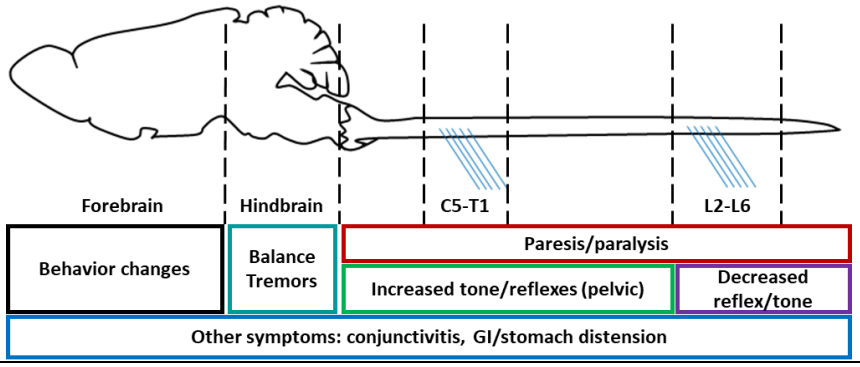

Clinical Scoring: Quick Code		
Code	**Clinical Symptom**	**Description**
L	Lethargic	For the 'quick code' system, lethargy covers both "lethargy" and "reduced movement" definitions of the extended scale. Lethargy is behavioral without aparent physical limitations. Reduced movement is behavioral due to clear physical limitations and/or discomfort. Lethargy is often observed early in infection and may appear as reduced or slow movement but with the physical ability to move. Observe both in cage and out of cage. Look to see if mice are acting 'sleepy' and moving slowly as a behavior rather than physical limitation. If gently nudged with a pen, mouse will not respnde with increased movement.
R	Ruffled/oily	Puffed up/extended fur (looks like a porcupine), not smoothed down due to lack of grooming, dull or dirty. Ruffling and lack of grooming may be with or without increased sheen (oily). Can also be very dull and fur look lifeless. Ruffled: mild loss of grooming/hair lifted and not smoothed. Extreme lack of grooming: excessive lack of grooming but not hair clumping/matting.
H	Hunched	Mice will typically hunch into a C shape if generally not feeling well, but as they become more symptomatic can ball up into a completely rounded "O"-often a sign preceeding moribund status."O" shape is possibly due to being cold (look for hunching with cagemates and ruffling fur); GI distress (look for abdominal distension) or morbundity (non-respnsive to stimuli; eyes partially closed, paresis/paralysis of limbs). In some cases, possibly associated with extreme paresis/paralysis or morbundity an inverted "V" shape in the spine occurs. Observe while moving and stationary; look at spine for rounding. A "C" or in more extreme cases "O" or "V" shape are positive results).
P	Paresis/paralysis	For the following tests, place mouse on rack tail toward tester. Hold tail (approx 1/3 away from tip) and ensure mouse is stable on rack with access to bars. Lift by tail smoothly until hind quarters are extended-mouse should be gripping bars strongly; additional force shifts grip from full foot to toes and eventually release of hind-quarters. Continue to lift tail to test front-quarters in the same manner (less force required). Score as no impact (0) or very mild (1) to moribund (6) as per IACUC protocol (see IACUC Scoring Criteria).
G	GI/abdominal distension	Using the tail lift, examine abdomine in context of rib-cage and pelvic bones. Look for abdominal distension wider than pelvic bones (width) or ribcage (depth). Securly grasping the mouse, holding head securly palpate abdomen to assess for hardness in the GI, tension on cavity or look for any protrusions (often ceacum or small intestine). Should also be able to massage a stool release to assess function. NOTE: in some cases where the mouse just ate they may also be slightly distended; re-examine later that day if there is question and/or don't do the checks after they tend to eat.
T	Tremors	Observe for visable tremors on the rack or in cage. Touch center of spine and suspend by tail. Typically a mouse will be jerking to get away from restraint but tremors are different in that they are constant and uncontrolled parkinson-like tremors/shivers.
F	Floppy tail (drags)	draging behind the mouse. If the tail is raised by running a pen under it, the tail drops once pen is removed. Often the tail will drag behind the mouse over the food once placed on rack.
S	Stiff tail (doesn't relax)	In the cage, observe position of mouse tail. Increased tone is observed as the tail being upright without curvature or relaxing. If the tail is lowered, running a pen under it immediately brings it straight.
Q	Intermediate tail phenotype	Typically a mouse is using it's tail for balance and during normal movement the tail will have an S curvature to it or being actively used to balance movement. If the tail is in between an S and F phenotype, or is otherwise not being normally engaged, score as Q.
E	Eye disease (opaque/blind/infected/etc.)	Conjunctivitis, infection, blindness, opaque, bulging eyes. Indicate type of disease. Multiple eye diseases can occur for a variety of reasons; infection may be increased in immune deficient models, whereas eye bulging may occur where there is increased encephalitis/swelling of the CNS.
B	Balance	Place mouse on rack and allow to move toward and onto food. Watch as they move over food for ability to maintain balance. Then using a pen gently press against the side and quickly release; see if mouse is able to quickly regain balance. Repeat if unclear. If balance is lost over food and/or with pen test annotate.

Figure A1: Quick Code anatomical map and scoring methodology

Code to analyze ‘Quick Code’

```
---
title: "Nuertz_dataConversion"
author: "Courtney Wilkins"
output: pdf_document
---

## Convert phenotype spreadsheet into form that can be searched for given phenotypes

```{r}
## Load libraries
require(xlsx, quietly = TRUE) # For reading excel files
require(plyr, quietly = TRUE) # For merging data frames
require(ggplot2, quietly = TRUE) # For pretty plotting
```

Read and analyze data
```{r}
## Read in data
filename <- "../raw_data/KW 2.40 STING Survival 3.Bioinformatics File.KW2.xlsx"

# Find where rows to start and end data frame around extra information
header <- read.xlsx2(filename, sheetIndex = 1, as.data.frame = TRUE,
                     header = FALSE, stringsAsFactors = FALSE,
                     colIndex = c(1:2))
start <- which(header[, 1] == "Mouse#" & header[, 2] == "Experiment")
end <- which(header[, 1] == "Date/time checked:")

# Read in actual data
data <- read.xlsx2(filename, header = FALSE, as.data.frame = TRUE,
                   sheetIndex = 1, startRow = start + 1,
                   endRow = end - 1, stringsAsFactors = FALSE)

# Label data columns from custom file
colnames(data) <- read.table("../codebook/column_names.txt", header = FALSE)[, 1]


## Identify each of the pathologies found at each day post-infection
# List each of the potential pathologies exhibited per mouse
pathologies <- c("L", "R", "H", "P", "B", "T", "S", "G", "E", "F")
titles <- c("Lethargic (L)", "Ruffled/Grooming (R)",
            "Hunched (H)", "Paresis/Paralysis (P)",
            "Balance (B)", "Tremors (T)",
            "Stiff/Increased Innervation (S)",
            "GI/Stomach Distension (G)",
            "Eye Conjunctivitis (E)",
            "Floppy/Decreased Innervation (F)")
filenames <- c("Lethargic.png", "Ruffled.png", "Hunched.png",
               "Paresis.png", "Balance.png", "Tremors.png",
               "Stiff.png", "GI.png", "EyeConj.png", "Floppy.png")
for (i in pathologies) {
  # Loop through pathologies
  for (j in 0:18) {
    # Loop through days post-infection

    # Identify the column containing pathology data for day "j"
    path_day <- paste("Path_D", j, sep = "")
    placing <- which(colnames(data) == path_day) # Column index

    # Find each mouse with pathology "i" listed that day
    hits <- rep(NA, dim(data)[1]) # create empty vector to hold data
    for (k in 1:length(hits)) {
      # loop through mice in study
      if (data[k, placing] == "") {
        hits[k] <- NA
      } else if (grepl(i, data[k, placing])) {
        # if mouse has any path scores listed and one is pathology "i",
        # give the new column a score of 1 (otherwise will be zero)
        hits[k] <- 1
      } else {
        hits[k] <- 0
      }
    }

    # Name the new column based on the day of infection + pathology
    if ((j == 18) && (placing == dim(data)[2])) {
      data <- cbind(data[, 1:placing, drop = FALSE], hits)
    } else if ((j == 18) && (placing == (dim(data)[2] - 1))) {
      data <- cbind(data[, 1:placing, drop = FALSE], hits,
                    data[, placing + 1, drop = FALSE])
    } else {
      data <- cbind(data[, 1:placing], hits,
                    data[, (placing + 1):(dim(data)[2]), drop = FALSE])
    }

    # Add the pathology column in directly following the existing column
```
```

```
    colnames(data)[which(colnames(data) == "hits")] <- paste(path_day, i, sep = "_")
  }
}
```

Create figures
```{r}
## Figures for pathology by genotype by time
# Remove spaces in strain, infection columns (computers don't like spaces!!)
data$Strain <- gsub(pattern = "(\\w*) (\\w*)",
                    replacement = "\\U\\1",
                    x = data$Strain,
                    perl = TRUE, ignore.case = TRUE)
data$Infection <- gsub(pattern = "(WNV 100PFU)",
                    replacement = "WNV",
                    x = data$Infection,
                    perl = TRUE, ignore.case = TRUE)
# Pull out only data from WT or STING KO mice
figure_data <- data[which(data$Strain == "WT" |
                          data$Strain == "STING"), ]
row.names(figure_data) <- figure_data[, 1]

# For each pathology, aggregate data by line by day and plot
for (i in pathologies) {
  # Loop once again through pathologies

  # Create unique identifier for each treatment
  sample_days <- figure_data[, c(3, 7)]
  sample_days$Treatment <- paste(sample_days[, 1],
                                 sample_days[, 2],
                                 sep = "_")
  sample_days <- sample_days[, 3, drop = FALSE]

  # Extract data from each day for that pathology
  for (j in 0:18) {
    sample_col <- paste("Path_D", j, "_", i, sep = "")
    sample_days <- cbind(sample_days, figure_data[sample_col])
  }

  # Aggregate samples by strain and by infection
  agg_data <- aggregate(sample_days[, -1],
                        by = list(sample_days$Treatment),
                        FUN = function(x)
                          {(sum(x, na.rm = TRUE) / sum(!is.na(x))) * 100})

  ## Reshape data for ggplot2
  combined_data <- data.frame("Sample" = rep(agg_data[, 1], 19),
                              "Day" = NA,
                              "Percent" = NA)
  for (j in 0:18) {
    combined_data[((j * 4) + 1):((j * 4) + 4),
                  "Day"] <- rep(j, 4)
    combined_data[((j * 4) + 1):((j * 4) + 4),
                  "Percent"] <- agg_data[, (j + 2)]
  }

  # Set factor levels of Sample for correct ordering
  combined_data$Sample <- factor(combined_data$Sample,
                                 levels = c("WT_Mock", "WT_WNV",
                                            "STING_Mock", "STING_WNV"))

  # Create a title for each plot
  title_index <- which(pathologies == i)
  title <- titles[title_index]

  # Set up plotting parameters in ggplot2
  p <- ggplot(combined_data, aes(x = Day, y = Percent,
                                 group = Sample, color = Sample)) +
    scale_color_manual("combined_data",
                       values = c("WT_Mock" = "gray",
                                  "WT_WNV" = "black",
                                  "STING_Mock" = "lightblue3",
                                  "STING_WNV" = "blue")) +
    geom_point() +
    geom_line(size = 1) +
    ggtitle(title) +
    ylim(0, 100) +
    theme_bw() +
    theme(panel.grid.major.x = element_blank(),
          panel.grid.major.y = element_blank(),
          legend.title = element_blank())

  # Print plot to png
  fileName <- paste("../figures/", filenames[title_index], sep = "")
  png(fileName)
```

```
  print(p)
  dev.off()
}
```

Extended Code

Although the proposed changes to the existing IACUC protocol will significantly increase the resolution to track clinical illness, it still does not reflect many symptoms described in other clinical models or observed during infection with WNV, including hair loss, excessive loss of grooming or oily hair, front vs. hind-limb paresis and paralysis (and their respective severity) and many neurological or CNS-related phenotypes. Further, by analyzing these factors it may be possible to attribute these phenotypes in a very specific way to different anatomical regions (Figure A2). For example, increased paresis can occur in the fore-limbs simultaneously with a corresponding increase in muscle tone/reflexes in both fore and hind-limbs and would predict damage within the upper spinal cord. Damage lower in the spine would predict increased reflexes in the pelvic muscles (hind-limbs) with normal to decreased thoracic muscle reflex and tone. A clinical scoring method of this detail does not currently exist in the literature, so using WT and STING$^{-/-}$ mice infected with WNV as a model we followed their clinical outcomes to develop a scoring system to analyze the clinical progression of neurological disease.

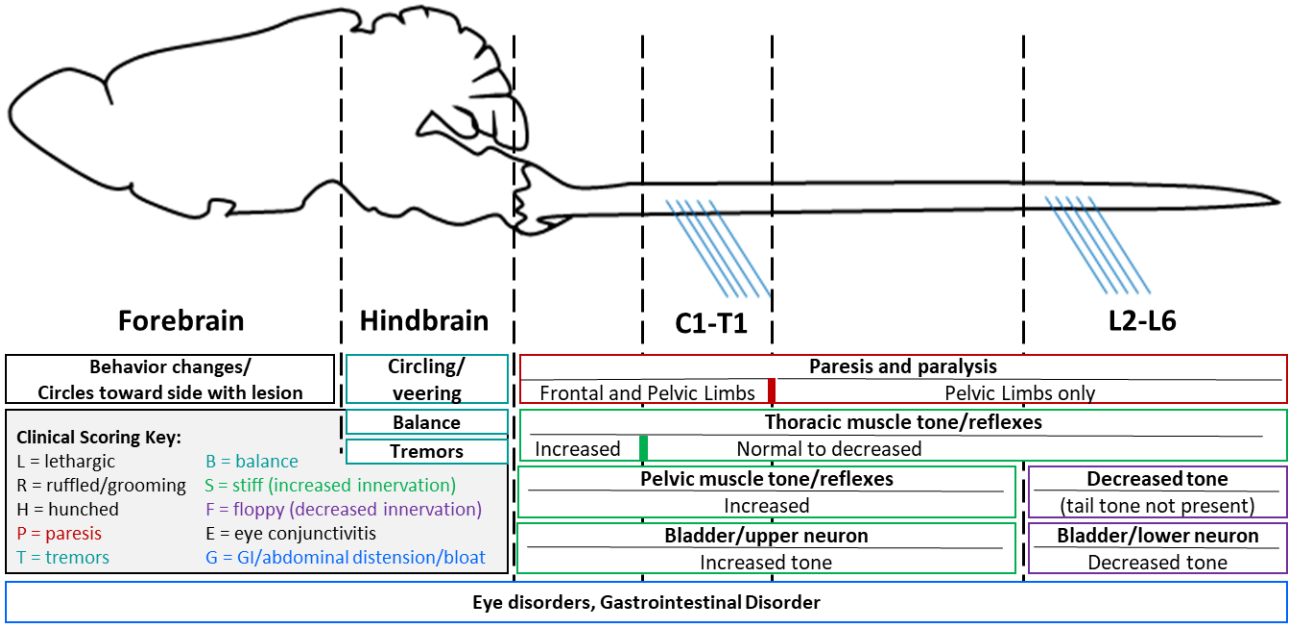

Figure A2: Predicted lesions in CNS based on clinical symptoms

Table A3 (1 of 4): Extended clinical scores: Methodology

Weighted Score	Test Category	Method/ Equipment	Cage/Rack	Score (normal = 0)	Score (abnormal = 1)	How to test
NOTE: All clinical tests should be done at a consistant time of day, preferably after noon but before lights-out. If scored in the morning, mice are sleepy and display symptoms similar to the ones described below as a						
	Behavior	For all behavioral tests, first examine visually only in the cage, then transfer all mice to rack and continue to observe. The purpose is to see how they interact in a familiar environment, and then in a new environment after stimuli (handling). It is important to observe in this order to gain consistent and accurate information.				
1	Not exploring environment	Visual/Pen	Cage/Rack	Exploring = 0	Not exploring = 1	Typically mice are curious and are continually exploring their environment. In the cage, they often will examine the perimiter of their cage, the water bottle, bedding etc. Once placed on the rack, they are very inquisitive, exploring the new environment. Note: that some mice are 'shy' upon initial introduction to a new environment. Gently nudge with a pen to see if they explore; if so (0) if not (1).
1	Reduced movement	Visual	Cage/Rack	Normal movement = 0	Reduced movement = 1	Reduced movement may be caused by paresis/paralysis, inflammation and general discomfort and/or GI distress/abdominal bloat. It is common to have decreased movement early during infection (likely general malaise) and then later during infection when GI/P complications increase. Observe to see if mice are moving around cage and rack with comparable velocity and distance to WT Mock. Looking for physical limitations to movement.
1	Not playing with cagemates	Visual	Cage	Playing with cagemates = 0	Not playing with cagemates = 1	Mice are social creatures and lack of engagement with cagemates is a strong indicator of distress. If paralytic and/or acutely symptomatic, mice typically huddle in a hunched position and tremble (0). More commonly, GI and/or abdominal distension leads to decreased interaction, as do factors leading to morbundity (excessive inflammatory responses; general maliase) (1). Observe in the cage to see if the mice engage with each other; nose-to-nose, nose-tail, etc. Yes (0); No (1).
1	Hunched	Visual	Cage/Rack	Back flat and mouse elongated = 0	Mouse hunched, rounded or spine has an inverted V shape = 1	Mice will typically hunch into a C shape if generally not feeling well, but as they become more symptomatic can ball up into a completely rounded "O"-often a sign preceeding moribund status. "O" shape is possibly due to being cold (look for hunching with cagemates and ruffling fur); GI distress (look for abdominal distension) or morbundity (non-respnsive to stimuli; eyes partially closed, paresis/paralysis of limbs). In some cases, possibly associated with extreme paresis/paralysis or morbundity an inverted "V" shape in the spine occurs. Observe while moving and stationary; look at spine for rounding. A "C" or in more extreme cases "O" or "V" shape are positive results).
1	Lethargic	Visual	Cage/Rack	Normal energy, interest and alertness = 0	Sleepy, decreased energy, intrest and alertness = 1	There are key differences between "lethargy" and "reduced movement" even though they have similar characteristics. Lethargy is behavioral without aparent physical limitations. Reduced movement is behavioral due to clear physical limitations and/or discomfort. Lethargy is often observed early in infection and may appear as reduced or slow movement but with the physical ability to move. Observe both in cage and out of cage. Look to see if mice are acting 'sleepy' and moving slowly as a behavior rather than physical limitation. If gently nudged with a pen, mouse will not respnde with increased movement even though they are physically able to do so.
	Grooming					
1	Oily	Visual	Rack	Dry coat = 0	Oily coat = 1	Look for sheen, also associated with matting and/or separation of fur. NOTE: Hair is often both oily and ruffled.
1	Ruffled	Visual	Rack	Smooth, well groomed coat = 0	Mildly ruffled/lack of grooming = 1	Same symptoms, weighted due to severity. Puffed up/extended fur (looks like a porcupine), not smoothed down due to lack of grooming, dull or dirty. Ruffling and lack of grooming may be with or without increased sheen (oily). Can also be very dull and fur look lifeless. Ruffled: mild loss of grooming/hair lifted and not smoothed. Extreme lack of grooming: excessive lack of grooming but not hair clumping/matting.
2	Extreme lack of grooming	Visual	Rack	Smooth, well groomed coat = 0	Excessive lack of grooming = 1	
2	Hair clumping	Visual	Rack	Smooth, well groomed coat = 0	Severe lack of grooming = 1	Lack of grooming to the point where hair is matting and clumping. Possible to find food or bedding in coat.

Table A3 (2 of 4): Extended clinical scores: Methodology

		Damp gloved/ handle mouse				With damp glove, handle mouse (stroke or hold). Set mouse down and look at glove; see if hair is stuck to the glove. Can range from mild shedding to hair falling out in chunks. When handling mice it is common for a few hairs to come off, but not many. If when handling the mice hair is severely shedding or falling out in clumps it may be indicitave of a skin condition (allergic/neurological)
3	Hair loss	Rack	No hair loss = 0	Hair loss = 1		
		For the following tests, place mouse on rack tail toward tester. Hold tail (approx 1/3 away from tip) and ensure mouse is stable on rack with access to bars. Lift by tail smoothly until hind quarters are extended-mouse should be gripping bars strongly; additional force shifts grip from full foot to toes and eventually release of hind-quarters. Continue to lift tail to test front-quarters in the same manner (less force required). For each FT/HQ choose # limbs impacted and average degree of impact (1-6)				
Paresis/physical score						
1	General weakness/loss of strength	Tail test	Rack	No weakness, paresis or paralysis	Weak but no impact to grip = 1	Grip is fully functional, but muscular activation is decreased.
1	Paresis in front quarter (1ft) R/L	Tail test	Rack	No weakness or paralysis	Grip deficiencies noted in 1 foot	Inhibition of grip strength in only 1 foot
2	Paresis in front quarter 2 ft	Tail test	Rack		Grip deficiencies noted in 2 feet	Inhibition of grip strength in both feet
1	Front: very mild paresis (lack of strength)	Tail test	Rack		Slight to mild grip deficit = 1	Slight decrease in ability to grip in addition to decreased strength
2	Front: mild paresis (weak grip)	Tail test	Rack		Mild to moderate grip deficit = 1	Mild impact to grip strength; still able to grip bars completely and hold on by toes but releases more easily.
3	Front: Frank paresis	Tail test	Rack	No weakness, paresis or paralysis	Clearly reduced ability to sustain grip = 1	Clear reduction in ability to grip bars; still capable of gripping but when testing feet slip hold.
4	Front: severe paresis	Tail test	Rack		Lost ability to sustain grip but not paralytic = 1	Inability to grip and hold on but still attempts to grip; has some level of control over limb(s); grip continually slips with mild to moderate pressure from tail lift.
5	Front: paralysis	Tail test	Rack		Paralytic limb = 1	No control of limb(s); drags while mouse is moving. No ability to grip or hold rack bars.
6	Front: moribund	Tail test	Rack		No attempt to move = 1	Physical: Complete loss of limb function/lack or refusal to move. NOTE: May or may not be associated with paralytic symptoms. Typically characterized by refusal to move even up on stimulation (transfer to rack, gentle nudge with pen). Eyes closed or partially closed, "O" shaped hunched, shallow respiratory (or) severely increased respiratory rate, concave (dehydration) or convex (GI distress) shape to abdomin. Excessive respiratory, compacted or hardened GI tract or severe GI distension to the point where movement is severely restricted are grounds for automatic euthanasia criteria.
1	Paresis in hind quarter (1hq) R/L	Tail test	Rack	No weakness, paresis or paralysis	Grip deficiencies noted in 1 foot	Inhibition of grip strength in only 1 foot
2	Paresis in hind quarter 2 hq	Tail test	Rack		Grip deficiencies noted in 2 feet	Inhibition of grip strength in both feet
1	Hind: very mild paresis (lack of strength)	Tail test	Rack		Slight to mild grip deficit = 1	Slight decrease in ability to grip in addition to decreased strength
2	(weak grip)	Tail test	Rack		deficit = 1	Mild impact to grip strength; still able to grip bars completely and hold on by toes but releases more easily.
3	Hind: Frank paresis	Tail test	Rack		Clearly reduced ability to	Clear reduction in ability to grip bars; still capable of gripping but when testing feet slip hold.
4	Hind: severe paresis	Tail test	Rack		Lost ability to sustain grip but not paralytic = 1	Inability to grip and hold on but still attempts to grip; has some level of control over limb(s); grip continually slips with mild to moderate pressure from tail lift.
5	Hind: paralysis	Tail test	Rack		Paralytic limb = 1	No control of limb(s); drags while mouse is moving. No ability to grip or hold rack bars.

Table A3 (3 of 4): Extended clinical scores: Methodology

6	Hind: moribund	Tail test	Rack		No attempt to move = 1		Physical: Complete loss of limb function/lack or refusal to move. NOTE: May or may not be associated with paralytic symptoms. Typically characterized by refusal to move even up on stimulation (transfer to rack, gentle nudge with pen). Eyes closed or partially closed, "O" shaped hunched, shallow respiratory (or) severely increased respiratory rate, concave (dehydration) or convex (GI distress) shape to abdomin. Excessive respiratory, compacted or hardened GI tract or severe GI distension to the point where movement is severely restricted are grounds for automatic euthanasia criteria.
	Neurological Symptoms						
1	Eye disease	Visual	Rack	Eyes are normal sized, no build-up, clear shiny and able to see = 0	Eyes bulging or sinking in, build-up, infection, opaque, etc . = 1		Conjunctivitis, infection, blindness, opaque, bulging eyes. Indicate type of disease. Multiple eye diseases can occur for a variety of reasons; infection may be increased in immune deficient models, whereas eye bulging may occur where there is increased encephalitis/swelling of the CNS.
1	Feet falling through cage	Visual	Rack	without slipping between bars = 0	Not able to place feet without slipping = 1		Observe movement across rack. Monitor for inability to grip bars as they walk, leading to feet slipping between cage bars (may occur in both hind and fore-limbs)
1	Tilting head (R/L)	Visual	Rack	Head is aligned with spine = 0	Head is angled to the left or right compared to spine = 1		While walking away from tester, observe alignment of head with spine. If head is continually tilted to the L/R in relation to the spine annotate.
1	Decreased response to stimuli	Visual/Pen	Rack	Whiskers twitch; mouse moves promptly to nudge =	Whiskers don't move; mouse isn't aware of/respond to nudge = 1		On rack, use pen to tickle whiskers; look for reactive flicker of whiskers. In cage or on rack, use pen to gently nudge the mouse. If the mouse and/or their whiskers do not move following stimuli, annotate.
1	Decreased facial response	Visual/Pen	Rack	Face twitches and eyes blink to stimuli = 0	Face does not move; eyes don't blink = 1		Use pen to tickle whiskers and look for blinking eyes and contraction of the facial muscles (normal response). If face does not move or eyes don't close, annotate.
1	Loss of balance	Visual/Pen/Food	Rack	Mouse does not loose balance or quickly regains = 0	Mouse looses balance and is unable to regain balance easily = 1		Place mouse on rack and allow to move toward and onto food. Watch as they move over food for ability to maintain balance. Then using a pen gently press against the side and quickly release; see if mouse is able to quickly regain balance. Repeat if unclear. If balance is lost over food and/or with pen test annotate.
1	Circling/veering/ tilting	Visual	Rack	Mouse walks in a straight line toward a target = 0	Mouse does not walk straight; altered direction = 1		Observe movement in cage and on rack. Look for circling (continual movement in one direction), veering (while moving forward continually drifting L/R) and tilting (full-body tilt to the left or right). Annotate and also note direction.
1	Wide based stance	Visual/Food	Rack	Hind feed square under pelvic bones.	Hind feet are extended past pelvic bones, often		While moving across food and cage, look if feet are directly under abdomen and parallel with spine, or if feet are angled outward and/or feet are placed to the left and right of abdomin).
1	Decreased placement (hq)	Visual/Food	Rack	While walking, mouse moves with surity over food and novel objects (rack)	Mouse is looking continually for placement and is not assured.		While walking across rack and food, watch for tentative placement (repeatedly setting down/lifting foot before settling in place), or when stepping placing foot unawaredly out of position (too wide, to the side/behind mouse, not on bar or slipping through due to being unaware-not inability), reduced ability or awareness to correct.
1	Stomach bloat/tension	Visual/Tail/Palpation-Ab	Rack	No distension, normal palpation and no gross phenotype; stool expressed normally.	Abdomen distended; visual protrusion (GI) from abdomen, respiratory complications, etc = 1		Using the tail lift, examine abdomine in context of rib-cage and pelvic bones. Look for abdominal distension wider than pelvic bones (width) or ribcage (depth). Securly grasping the mouse, holding head securly palpate abdomen to assess for hardness in the GI, tension on cavity or look for any protrusions (often ceacum or small intestine). Should also be able to massage a stool release to assess function. NOTE: in some cases where the mouse just ate they may also be slightly distended; re-examine later that day if there is question and/or don't do the checks after they tend to eat.
1	Urine leakage/express	Visual/Palpation-Ab	Rack	No leakage = 0	Leakage found either while handling or palpating abdomen = 1		While checking for abdominal/GI distension, look also for urine expression-any urine release should be noted if associated with palpation or holding the mouse.
1	Tremors	Visual/Tail	Rack	go away when mouse isn't handled	Continual to severe tremors = 1		mouse will be jerking to get away from restraint but tremors are different in that they are constant and uncontrolled parkinson-like tremors/shivers.
1	Increased muscle tone	Visual/Tail lift	Rack		Increased tone = 1		When lifting mouse off of rack in the same way as the paresis/paralysis test, increased tone is observed when mice have an excessive grip on the bars; they can't release the bars. Similarly, they respond to any stimuli by contracting muscles but can't relax after.

Table A3 (4 of 4): Extended clinical scores: Methodology

1	Increased tail tone/response	Visual/Pen	Cage/Rack	Normal tone/reflex = 0	Increased tone in tail; continually stiff = 1	In the cage, observe position of mouse tail. Increased tone is observed as the tail being upright without curvature or relaxing. If the tail is lowered, running a pen under it immediately brings it straight.
1	Increased reflexes (hq toe pinch)	Toe test	Rack		Increased reflex = 1	Align mice parallel with bars; allow to grip bars with front feet and holding by the tail stretch mouse out to extend hind feet to the edge of rack/cage. Hold tail with dominant hand and use index and thumb of non-dominant hand to pinch toes. Steady, quick withdrawl following firm pinch is normal. Immediate or spasmastic jerking back, or with light touch instead of firm pinch is an increased response.
1	Loss of muscle tone	Visual/Tail	Cage/Rack		Decreased tone = 1	Holding the mouse by the tail, look at hind legs above the knee; loss of muscle tone will result in thinning of muscle in 'theighs', in correspondence to a geneneral weakness in response. Note that this is a muscular, not functional or neurological test-so this is specifically due to loss of musculature not neurological function.
1	Loss of tail tone/response	Visual/Pen	Cage/Rack		Decreased tone, continually stiff = 1	In the cage, observe position of mouse tail. Decreased tone is observed when the tail is hung low or draging behind the mouse. If the tail is raised by running a pen under it, the tail drops once pen is removed. Often the tail will drag behind the mouse over the food once placed on rack.
1	Loss of reflexes (hq toe pinch)	Toe test	Rack	Normal tone/reflex = 0	Decreased reflex = 1	Align mice parallel with bars; allow to grip bars with front feet and holding by the tail stretch mouse out to extend hind feet to the edge of rack/cage. Hold tail with dominant hand and use index and thumb of non-dominant hand to pinch toes. Steady, quick withdrawl following firm pinch is normal. Lack of response, slow removal of foot from pinch, not noticing pinch are all signs of loss of reflexes.
1	Shuffling gait/dragging limbs	Visual/Food	Cage/Rack	Normal gait = 0	Altered gait = 1	While moving in cage and/or on rack, abnormal stride pattern and/or dragging limbs; often will shuffle instead of taking full strides or if paralytic or have a 'floppy response' will drag feet as they move instead of placing precisely (spacial instead of paralytic assessment)
1	HQ: splayed	Visual/Tail	Rack	Feet aligned with body = 0	Feet spread away from body = 1	Using tail lift determine if mouse responds by tucking hind quarters and feet in alignment with body, that is normal. If mouse responds by going spread-eagle, particularly by extending hind-quarters away from body, that is splayed
1	HQ: curled to body	Visual/Tail	Rack	Feet aligned with body = 0	Feet tightly curled to body = 1	Using tail lift determine if mouse responds by tucking hind quarters and feet in alignment with body, that is normal. If mouse responds by bringing feet all the way to the body, tightly curled that is abnormal.

Symptoms typically grouped into one of four categories, including 1) grooming, 2) behavioral, 3) physical (weakness, paresis and paralysis) and 4) neurological. Throughout the infection, it was common that symptoms in each of these categories could be found at multiple points of infection. For example, mice could demonstrate behavioral and physical deficiencies, or a mix of grooming and behavioral phenotypes. Mice could score in one or a combination of any of the four categories throughout the experiment. This system also differentiated mice that may have each scored the same severity score but reflect different phenotypes. This scoring system also revealed slight phenotypes that were previously lost, such as in the $STING^{-/-}$ Mock mice. As the experiment progressed, the $STING^{-/-}$ Mock mice began displaying mild neurological phenotypes, unlike their WT counterparts. This is critical to understand if there is a background phenotype that may contribute or confound results while analyzing the impact of infection or other neurological disease in knockouts.

To record the data, mice were scored as either having the symptom (1) or not having the symptom (0). While scoring, this can be annotated as easily as checking all applicable symptoms on a score-sheet and then later when transferring the data transferring checks/x as a (1) in the spreadsheet and blank wells as (0). Data from all mice at each timepoint analyzed and the average (median or mean?) for each strain and timepoint built into heat-maps. The total score for each category was analyzed, and as described previously indicated that $STING^{-/-}$ were more severely impacted than WT. If desired, statistics internal to each day between groups can be analyzed if there are 3 or more mice representing each well.

Figure A2 (1 of 2): Results of Extended clinical score
Top panel: Behavioral; Middle panel: Grooming; Bottom panel: Physical (paresis, paralysis). Columns are the mean score for each strain per day, for each individual test performed (rows). Final row of each panel is the sum of all individual scores for that section. n = 3-12 per timepoint.

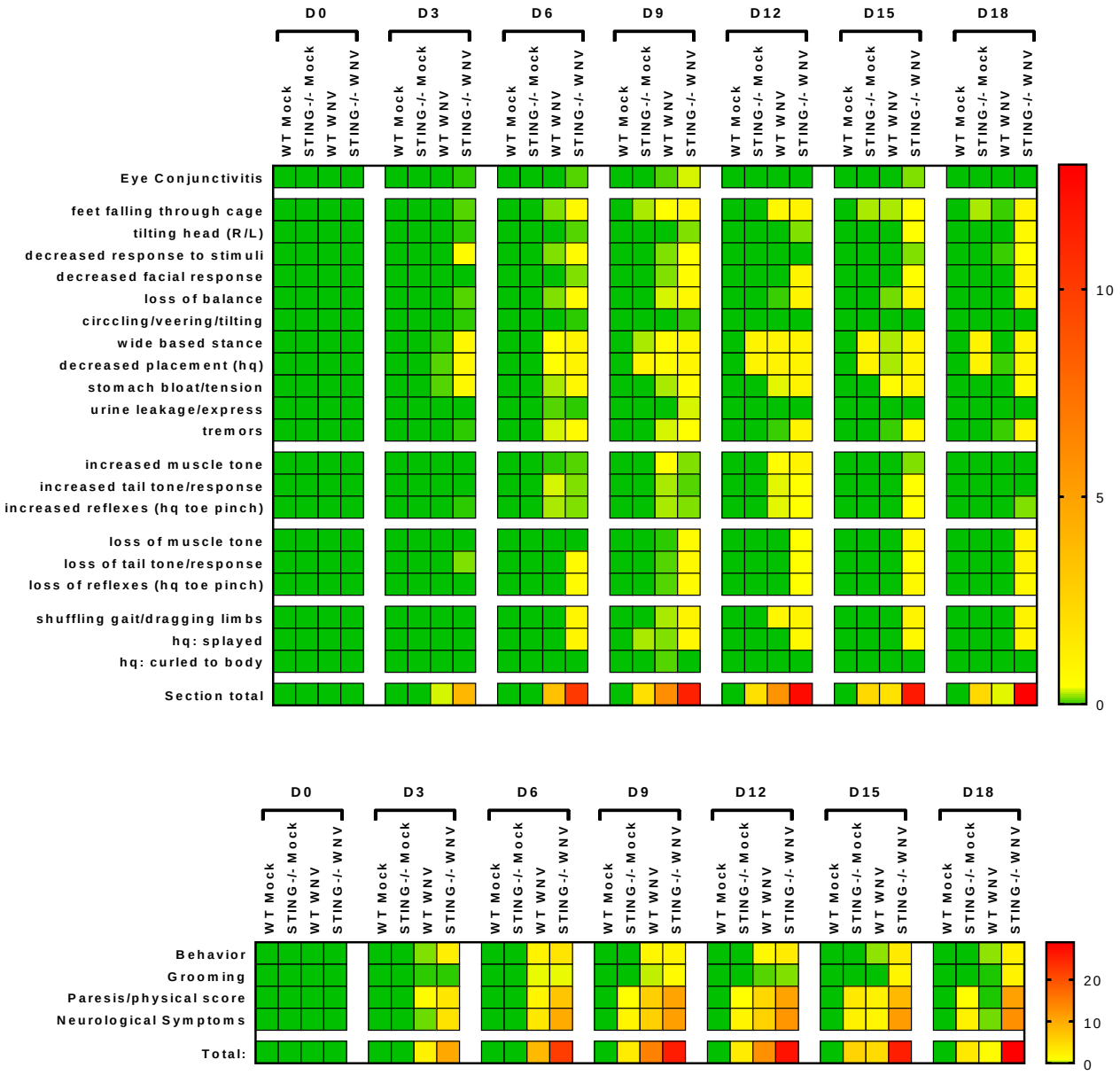

Figure A2 (2 of 2): Results of Extended clinical score
Top panel: Neurological; Bottom panel: Summary of total scores. Columns are the mean score for each strain per day, for each individual test performed (rows). Final row of each panel is the sum of all individual scores for that section. n = 3-12 per timepoint.

Next, each scores in each category was analyzed. In the behavioral scoring, the first thing that was noted is that there is a mild difference between WT and STING$^{-/-}$ mice, but not as severe as in the physical or neurological categories. In a similar way, both WT and STING$^{-/-}$ displayed initial loss of grooming, then improved and worsened again. This may be due to initial febrile illness and malaise caused by an innate inflammatory response initially, followed by reduced inflammatory responses. Symptoms may then worsen when paresis and paralysis limit their ability to groom.

Analyzing the physical response in the mice revealed increased paresis and paralysis in STING$^{-/-}$ as well as earlier onset of symptoms. Intriguingly, we also saw a mild increase in symptoms in STING$^{-/-}$ Mock mice, particularly in spatial neurological symptoms (Figure A2). STING$^{-/-}$ also displayed increased and earlier onset of paresis in the fore-limbs, suggesting broader spinal pathology than experienced by WT mice.

Results and Discussion

Further analysis is ongoing with these data, because each individual mouse can be analyzed in context with its known outcome and downstream data collection including histopathology, and IHC for WNV and cellular markers. Also ongoing is validation of the model by having a neuropathologist analyze the scores of each mouse blinded followed by comparison to previously determined pathology. The end outcome will determine whether anatomical localization of histopathology can be predicted from clinical scores.

APPENDIX B

ZIKA PERFUSION OF HUMAN PLACENTAL COTYLEDONS USING AN *EX-VIVO* DUAL COTYLEDON, DUAL PERFUSION MODEL

Introduction

Zika virus (ZIKV) emerged in 2015 as a significant global public health threat, after epidemiologic studies associated ZIKV infection with the surge of microcephaly cases in Brazil [153-156]. ZIKV was first identified in 1947, but it was unclear whether infection caused clinical disease in humans. Early studies in mice however, indicated that ZIKV infection may cause neuropathic effects [157-159]. The first pathogenic human infections were confirmed in 1953, with generally mild symptoms including fever and rash [157, 158, 160]. In the decades following, ZIKV was detected through serological detection [161-166] and isolation of the virus from mosquitoes [167-172], humans [160, 163, 173-175]and non-human primates [176]. Of these infections however, few clinical cases were reported until 2007, where the first significant ZIKV outbreak occurred on Yap Island, in the Federated State of Micronesia [160, 163, 166, 175, 177]. During the outbreak, approximately 73% of the island's residents were infected with ZIKV, but the symptoms were generally mild and short in duration [177]. In 2011, the first case of human-to-human transmission of ZIKV was documented, separating ZIKV from other flaviviruses where humans are predominantly accidental hosts, such as West Nile Virus [178]. The next significant outbreak occurred in 2013, where 66% of the general population in French Polynesia was infected [179, 180]. During this outbreak, ZIKV infections were correlated with a dramatic increase in reported cases of Guillain-Barre syndrome (GBS), for the first time

indicating neurological pathology of ZIKV infection in humans [179, 180]. In late 2014, the first recorded case in the Americas was reported in northeastern Brazil [155]. From there, ZIKV infections swiftly spread across Brazil, with affected regions reporting subsequent increases in cases of microcephaly and GBS [154, 181]. Since the first case was reported in Brazil, ZIKV has spread throughout South and Central America, and the Caribbean, leading to the World Health Organization declaring a Public Health Emergency of International Concern on February 1, 2016 [153, 182]. As of August 2016, over 47 countries in the Americas have reported locally circulating ZIKV, with the ultimate global impact and spread undetermined [183]. The widespread emergence of ZIKV, coupled with the increase in symptom severity and transmission demonstrate the essential need to understand the host and viral factors leading to the increased pathology, in order to generate therapeutics and preventative mechanisms.

Clinical symptoms in adults infected with ZIKV are typically nonspecific and mild, characterized by rash, fever, arthritis, conjunctivitis, headache, retro-orbital pain and vomiting [177, 184]. Case reports suggest that symptoms resolve typically within 1-2 weeks of onset [178, 185-192]. Cases resolving in death are extremely rare, and typically occur in immunocompromised individuals or patients with a pre-existing co-morbidity [193, 194]. Subsequent to ZIKV infection, individuals have an increased risk for sever neurologic sequelae [195, 196]. Most notably, the risk for GBS increases from an annual rate in the USA of 1.8 per 100k individuals, to 24 per 100k in ZIKV infected persons [179, 180, 197]. Additional neurologic sequelae are correlated with ZIKV infection in adults, including meningoencephalitis and acute myelitis though causation has yet to be confirmed [121, 198]. Currently, strain specific differences in pathology, transmission, viremea and immunologic impact of ZIKV infection are relatively unknown.

Since the outbreak in Brazil, ZIKV infections have correlated with a significant increase in the number of microcephaly cases, leading to studies seeking to determine if ZIKV infection during or prior to pregnancy can cause microcephaly. Prior to the outbreak, Brazil reported less than 200 cases of fetal microcephaly per year, in contrast to over 1,326 confirmed and 4,005 additional cases undergoing investigation, reported as of May 7th, 2016 [190, 199]. In April 2016, the CDC confirmed a causal association between ZIKV infection and microcephaly through multiple epidemiologic studies, as well as detection of ZIKV in fetal brain tissue and amniotic fluids [200]. Currently, the estimated prediction of ZIKV infected pregnancies resulting in microcephaly is 10-40% [201-205]. While the perceived risk is highest if ZIKV infection occurs early during pregnancy, recent work indicates that infections occurring later in pregnancy can still pose a threat to the developing fetus [206]. Significant work has gone into developing murine and NHP models of infection to assess the ability of ZIKV to impact the developing fetus through maternal-fetal transmission models. In mice, ZIKV infection during pregnancy with mice results in infection of the placenta and fetal brain, causing placental damage and fetal demise [207]. Further supporting the ability of ZIKV to infect placental cells leading to maternal-fetal transmission during pregnancy, studies have demonstrated that ZIKV can infect human placental macrophages [208], in addition to other primary cell types and explants of human placenta, suggesting placental and paraplacental routes of virus transmission [209]. Studies in our lab have demonstrated maternal-fetal ZIKV transmission using a non-human primate model [citation]. Currently however, the viral and immunologic effect to the placenta in a human model are unknown.

Methods and Results

These experiments utilized a dual-cotyledon, dual perfusion model to study ZIKA in a human placental model. There are multiple benefits to this model: 1) the cotyledons retain a functional fetal vasculature and maternal interface. 2) The intervillous space (maternal side) and fetal vasculature can be perfused to simulate physiological conditions. 3) Perfused cotyledons are purely fetal in origin, allowing us to examine infection in the absence of maternal factor. 4) Importantly, from a single donor, paired control and experimental cotyledons are perfused in parallel, eliminating genetic variability from multiple donors [210]. This allows for data normalization downstream during host-gene analysis.

Experimental model

This study utilized placentas from term, unlabored C-sections from non-complicated pregnancies. Isolating both cotyledons and initiating the perfusions must be completed under 30 minutes post-delivery, to avoid clotting and necrosis that will compromise tissue viability and function. All placental collections were done in accordance with IRB approved protocols including informed consent and patient deidentification. Placentas were moved whole from the delivery location to a BSL2+ approved lab space. Two cotyledons were removed from the placenta, blocked between gasketed plates to seal the vasculature system and transferred into a BSC as previously described [210]. From the remaining tissue, pre-perfused samples were collected prior to perfusion. For each cotyledon, the fetal main fetal artery and vein were cannulated and perfused. Maternal perfusion was simulated by two butterfly needles that perfuse the intervillous space. Maternal arteries were perfused and the fetal artery single perfused. For each experiment one cotyledon is randomly selected to receive the vehicle (Hank's Balanced Salt Solution (HBSS) media) or ZIKV (experimental) through the maternal side. At the same time as the perfusion was

set up, pressures were monitored within the fetal arteries and continually monitored throughout the duration of the experiment. Following an initial acclimatization phase, the control sample was continually be perfused with HBSS while the experimental cotyledon was perfused for a set length of time with the experimental condition, be it virus, cytokine, drug or other condition [210].

After four hours of ZIKV (experimental) perfusion, the line was switched again to normal media which is continued until the end of the experimental procedure; an additional 24 hours. At any point during the procedure, if the pressure indicated vasospasm, a sign of viability loss in this assay, the experiment was terminated. At the pre-determined end-point, fetal effluent was collected, and the perfusion terminated followed by and tissue samples collected (see sample collection; Table B2).

Sample Collection

Clinical data from each de-identified placental donor was collected and stored for use in bioinformatics analysis to look for any associations, bias or confounding with experimental outcome (Table B1). Tissue viability was determined through the analysis of pressure (mmHg) throughout the experiment and iSTAT data was collected at termination of experimental from the venous effluent. The iSTAT analyzes metabolic factors including pH, pCO2, pO2, sO2%, Lactate and HCO_3, additional indicators of viability and hypoxia. After confirming tissue viability during and throughout the experimental procedure, samples were collected for downstream analysis (Table B2). Fetal venous effluent will be collected from the collection butterfly tubing at the termination of the experiment. To collect tissue samples, tissue were cut from the intervillous tissue directly under the chorionic plate. RNA samples were collected in triplicate to increase statistical power and ability to reduce noise in downstream bioinformatics analysis. Additional

samples were and preserved either by flash-freezing or formalin fixation for protein, protein, histological and IHC analysis.

Table B1: Clinical Data collected for placental model

Clinical Data
Race: White=1 Black =2 Asian/Pac Islander=3 Other=4
Ethnicity: Hispanic=1
Prenatal Medication
Tobacco/Alcohol: none=0 Alcohol=1 Tobacco=2
Drugs
Previous prenatal admissions: Yes=1 No=0
BP >140/90 mmHg: No=0 CHTN no meds=1 CHTN meds=2 G-HTN, no meds=3 G-HTN, meds=4 PEC w/out SF=5 PEC with SF=6
Diabetic: No=0 Yes=specify
Diabetic medication
Antibiotics before incision: none=0 Ancef=1 Other (list) Unknown=3
Beta Strep status: Positive=1 Negative=2 Unknown=3
Anenatal Steroids: Yes=1 No=0 If Yes, weeks GA
Magnesium Sulfate: Yes=1 No=0
Anasthesia: Spinal / Epidural = 0 Narcotics = 1 General = 3 Other/none
Cervical Ripening: Yes=1 No=0
Labor: Yes=1 No=0
Delivery Mode: C-section, primary no labor=1 C-section, repeat no labor=2 C-section, primary labor=3 C-section,repeat, with labor=4
Abnormal 1hr: Yes=1 No=2
1hr glucose test value
3hr results
Birth weight (grams)
Baby Sex: Female=F Male=M
BMI (at delivery)

Table B2: Sample Collection

Sample collection	Timepoint	Collection	Utilization
Tissue samples			
Pre-perfused	Prior to perfusion	RNA/Protein/Histology	
Control perfused	End-point	RNA/Protein/Histology	
Experimentally perfused	End-point	RNA/Protein/Histology	
Sample types			
RNA	End-point	Fix in RNALater; store tissue at -80oC	qRT-PCR; RNAseq; Nanostring; etc.
Protein	End-point	Flash-freeze; store at -80oC	WB; Mass spectrometry
Histology-frozen	End-point	Flash-freeze; store at -80oC	IHC
Histology-formalin fixed	End-point	Fix in formalin; store at RT	H&E; IHC
Fetal effluent	End-point	From fetal vein tubing	ELISA; vRNA isolation; ZIKV ELISA or PFU

Proof-of concept: IFNL Perfusion

Placental cotyledon models have been used to monitor the effect of different treatments or compounds on placental tissues, however none have been utilized to access the immunological, virologic, and pathologic phenotype following viral infection. Further, most perfusion models are accessing short-term (<6h) experimental conditions after acclimation of the tissue. This is restrictive during a viral infection, where longer experimental times are required to

access the impact of viral replication. Further, while some studies have accessed immunological outcomes following experimental treatment, no study has perfused these tissues with cytokines or chemokines and accessed downstream immunological responses.

As a proof-of-concept to confirm that changes in immunological response can be detected within these tissues, we perfused tissues with IFNL and accessed downstream ISG responses by RT-pPCR. For this study, we acclimatized the tissues for 30 min followed by 6 hours of perfusion with IFNL (Figure B1). At the end of the 6hr IFNL treatment, tissues were collected for RNA analysis by transferring to RNALater, fixed for (24h) and stored at -80^{o}C until RNA was isolated. RNA was isolated using TRIZOL:Chloroform extraction followed by QIAGEN RNeasy extraction kit. Bioanalyzer analysis of the RNA confirmed quality, demonstrating that the experimental protocol and collection techniques were sufficient to harvest viable samples (Figure B2). RT-pQCR was performed on the RNA from control (vehicle) and experimentally (IFNL) perfused samples, looking at ISG induction. For both ISGs examined (IFITM1) and (IFIT1), tissue perfused with IFNL demonstrated increased signal, indicating that these tissues are responsive to innate immune stimuli and a viable model to interrogate the role of cytokines and chemokines in inducing innate immune stimuli in the placenta (Figure B3). It also provided a proof-of-concept for the model, allowing for us to proceed to analyze the impact of ZIKA in tissues.

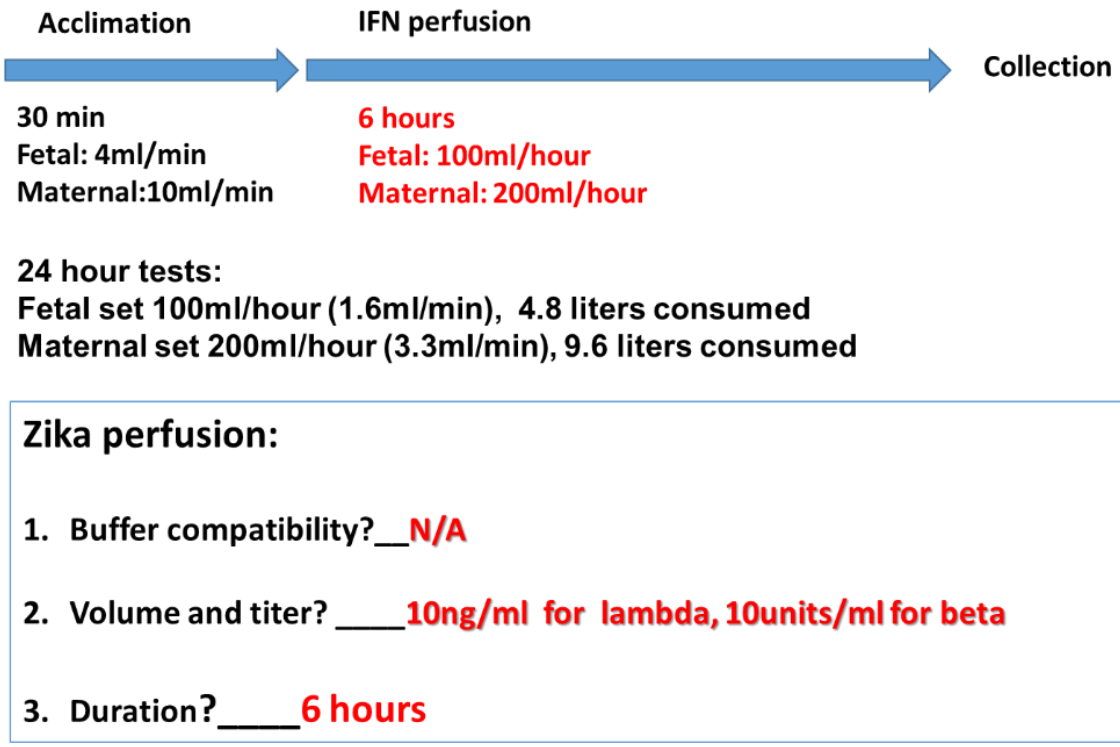

Figure B1: Preliminary model-IFNL perfusion

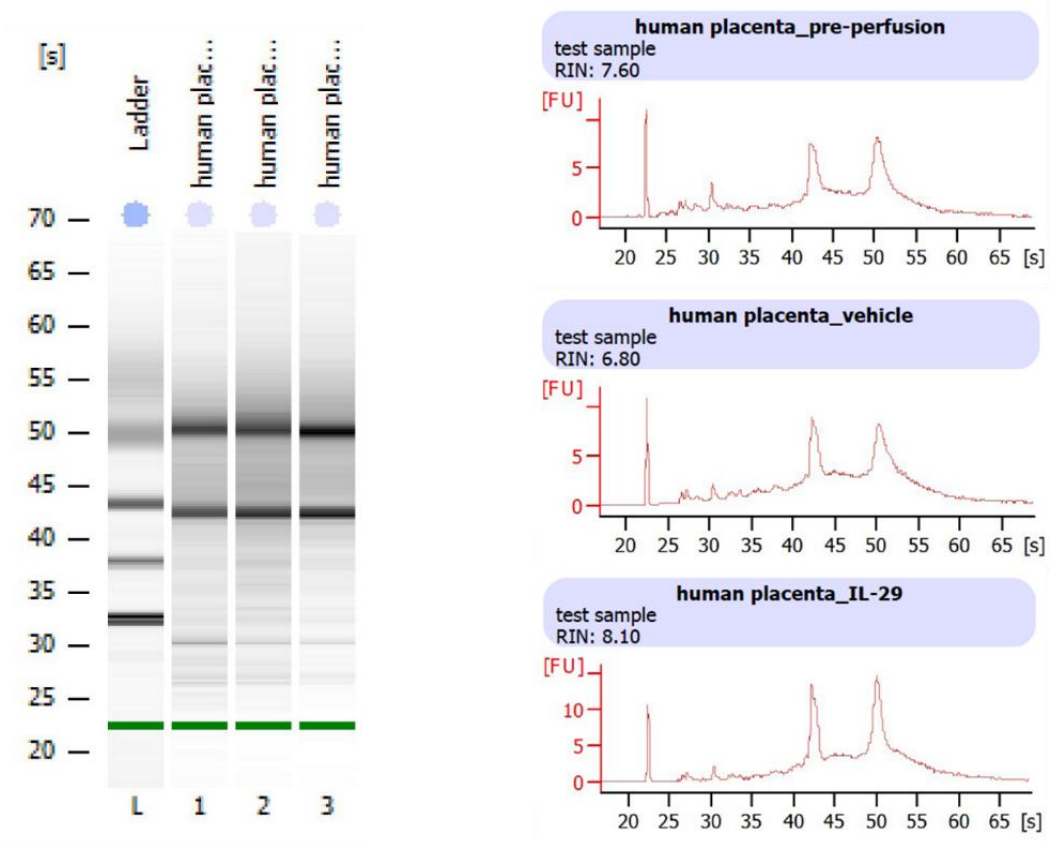

Figure B2: RNA extraction and QC

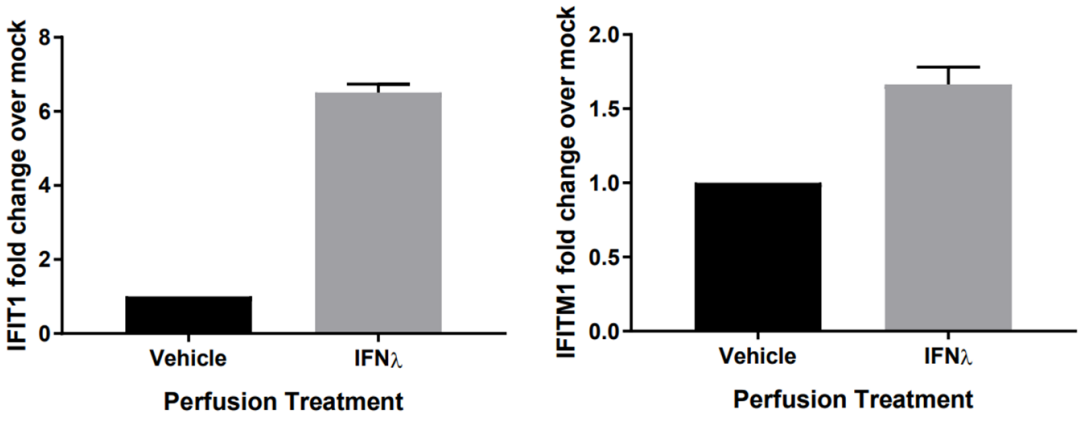

Figure B3: ISG detection post perfusion

ZIKA Viral Perfusion Model

The first challenge to perfusing with ZIKA virus was to establish conditions that would increase the lifespan of the cotyledons. After optimization of the buffered conditions, tissues were able to be kept viable for >24 hours, allowing for an infection period that allowed for viral replication. For ZIKV studies, tissues were acclimatized for 30 minutes, followed by a 4 hr ZIKA perfusion which delivered a total of 1E5 PFU/cotyledon (Figure B4). The infected cotyledon was continuously perfused for an additional 24 hours. At the end of this time, samples were collected as described above.

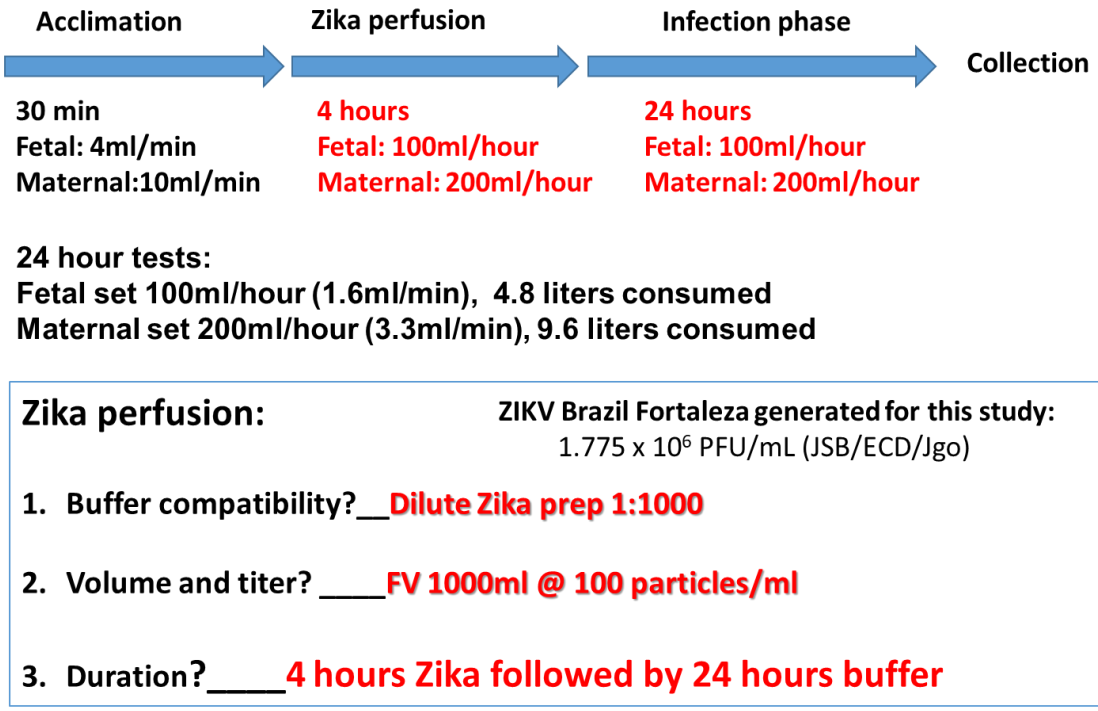

Figure B4: ZIKV perfusion experimental design

RNA was isolated from these initial experiments, and quality was assessed using the Bioanalyzer. Unlike the previous experiment with IFNL perfusion however, RNA quality in the control and ZIKV perfused sample was very poor (Figure B5). The RNA quality in the pre-perfused sample was good, indicating that something in the experimental process resulted in degraded RNA. Histological

examination of the tissues showed bacterial growth, suggesting contamination in the lines or equipment used to perfuse which histology confirmed. All equipment, tubing and containers used for the perfusion were autoclaved or replaced and the experiment was repeated. This time no bacterial contamination was found, RNA quality was good and samples were of sufficient quality to perform downstream analysis.

We then wanted to determine what was the best protocol to isolate RNA from the tissues. In the lab, two RNA isolation protocols are regularly utilized. TRIZOL/Chloroform extraction is used typically for NHP specimens, where the RiboPure extraction protocol is used for mouse tissues (Figure B6). To determine if the method of RNA extraction made a difference, we extracted RNA from the same samples utilizing both protocols and found that they extracted the RNA relatively equally, with both giving acceptable RNA quality. After running subsequent RT-qPCR on RNA from both isolations however, the TRIZOL/Chloroform gave superior detection of target genes. For the remainder of the study, TRIZOL/Chloroform isolation was utilized. In addition to the protocol to isolate RNA, we sought to determine if analyzing un-diluted or diluted cDNA gave the most sensitive results. We ran undiluted and diluted cDNA for detection of ZIKV and found that cDNA diluted 1:5 gave the most sensitive results. Even still, low levels of ZIKV required us to run samples for 45 cycles, instead of the standard 40 cycles (Figure B7).

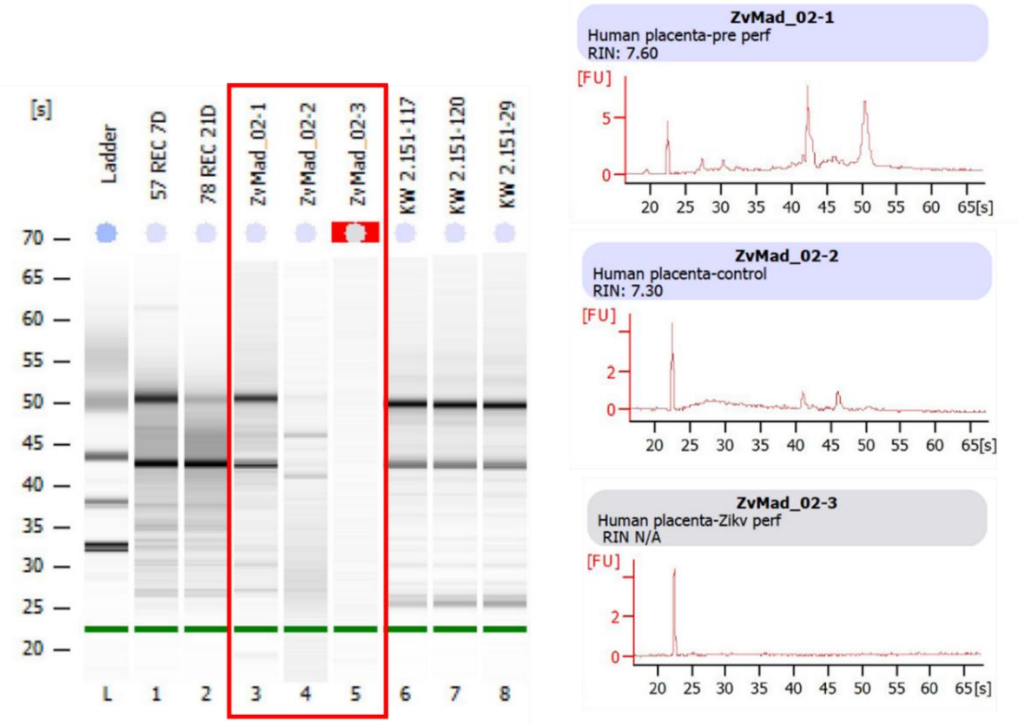

Figure B5: RIN of initial experiments

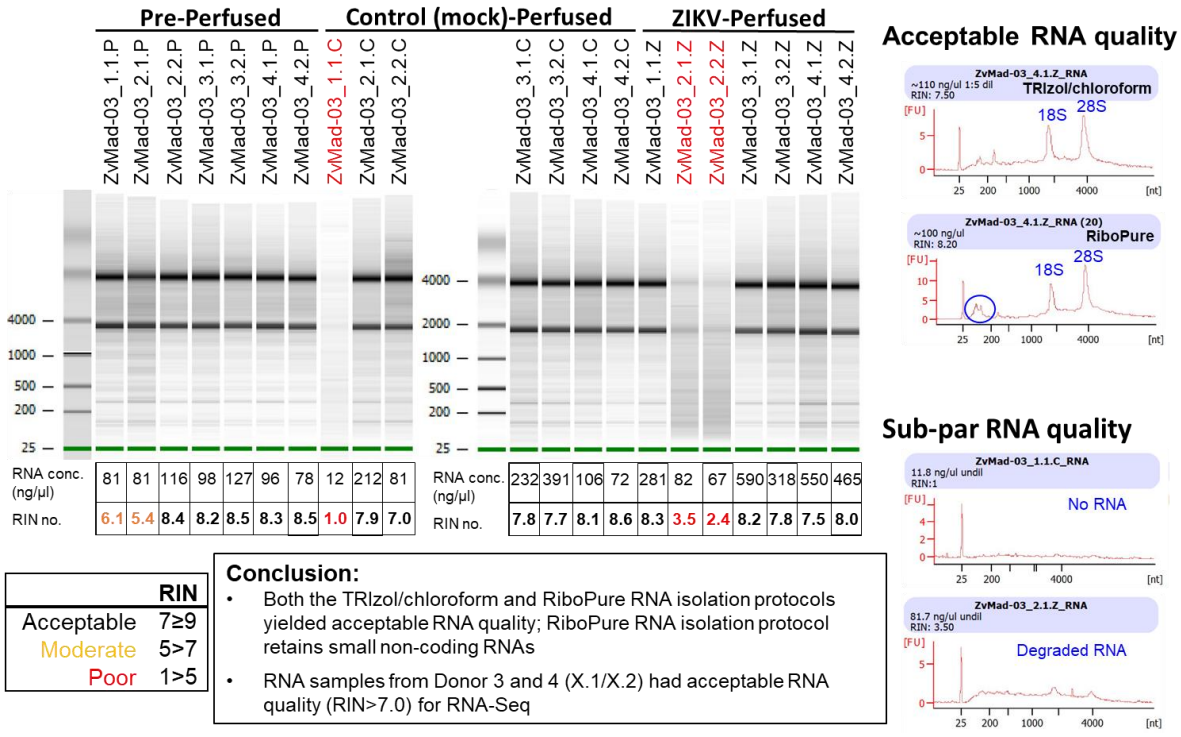

Figure B6: Comparison of RNA quality between different extraction methodologies

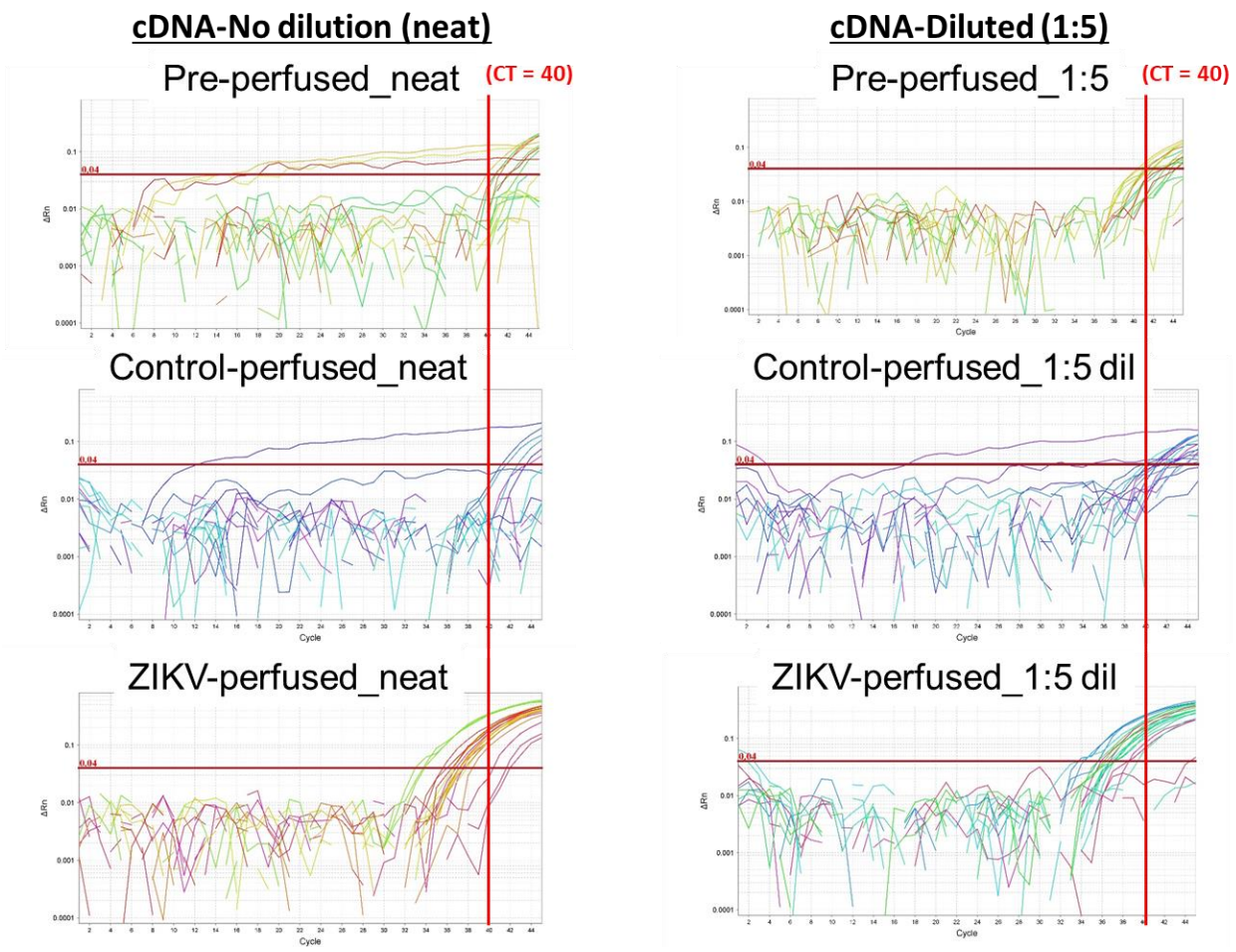

Figure B7: Detection of viral cDNA

Quantification of ZIKV in each of the first 4 donors confirmed detection in ZIKA perfused tissues, even in samples that were compromised due to bacterial contamination (Donor 1 and Donor 2) (Figure B8). No signal was observed in either the pre-perfused or control-perfused samples. We then went on to perform initial host gene analysis, looking at IFNb, IFNL and ISGs including IFIT1 and Mx1. Donors 1 and 2 were the samples compromised by bacterial contamination, and Donors 2 and 3 did not have clear trends in results. Further host gene analysis will need to be performed to determine if perfusion with ZIKV initiates changes in innate immune signaling in placental tissues (Figure B9-10).

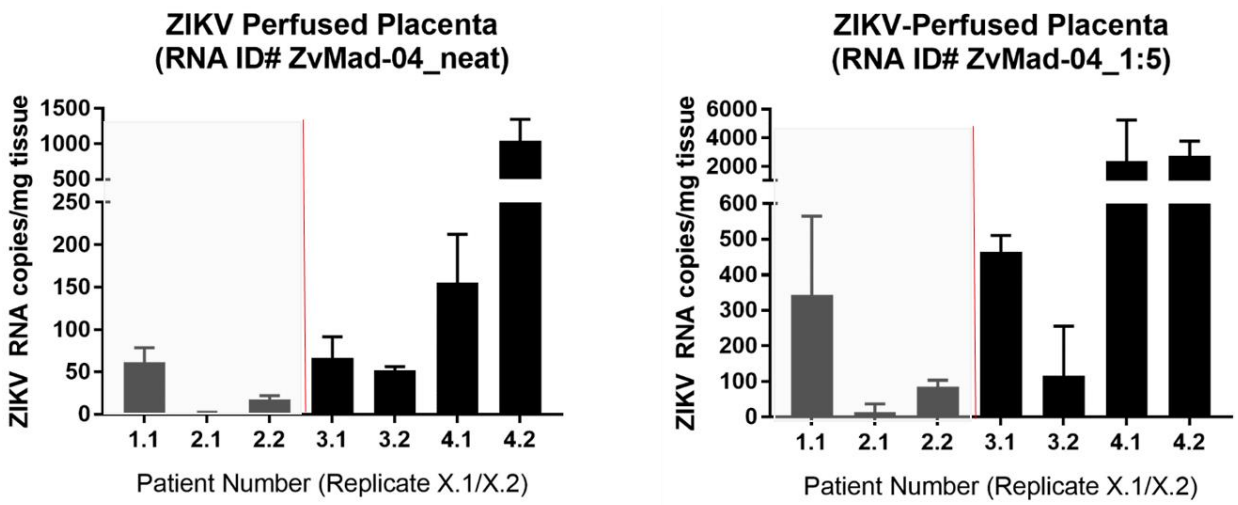

Figure B8: ZIKV is detectable in perfused tissues

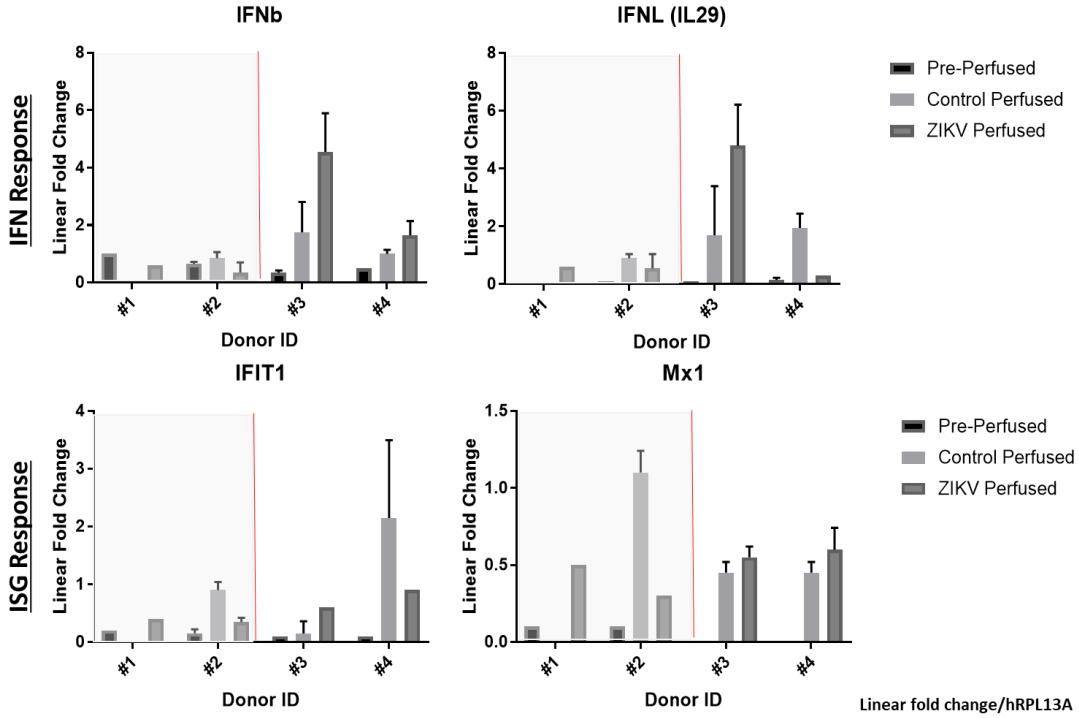

Figure B9: Detection of innate immune genes in mock and ZIKV perfused tissues

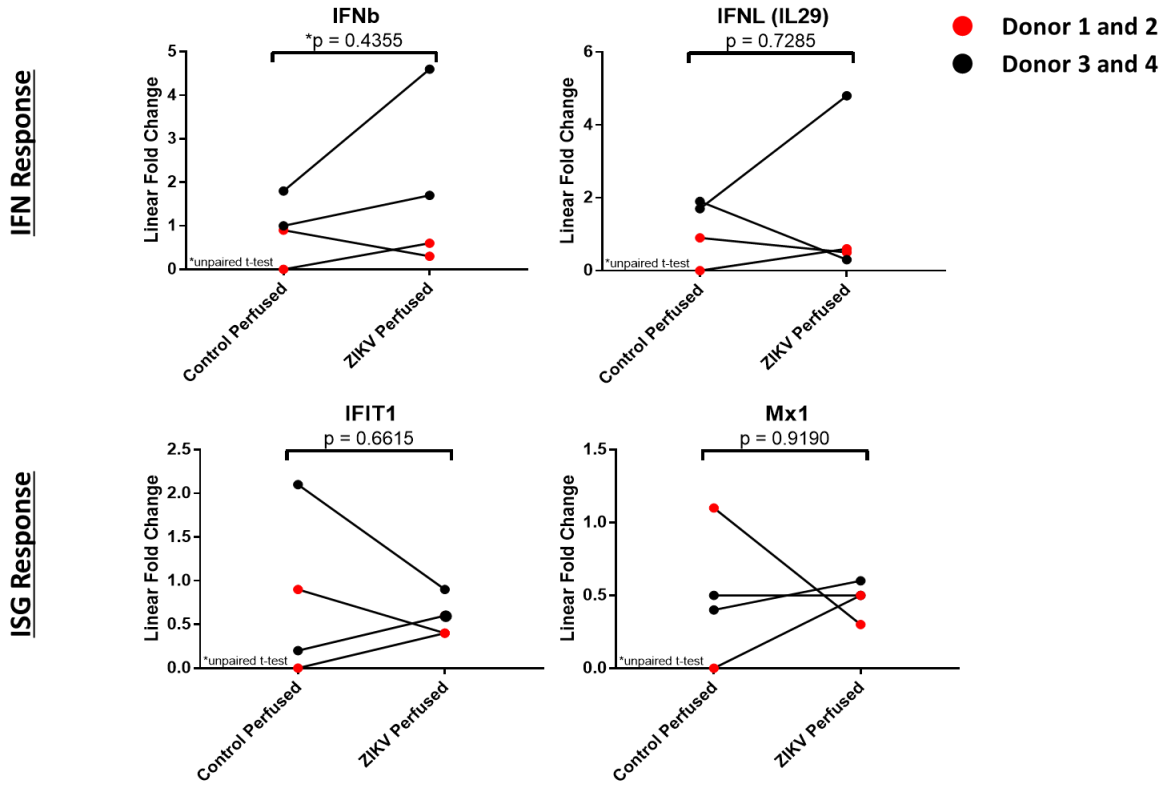

Figure B10: Relative comparison of innate immune genes in mock and ZIKV perfused tissues

Ongoing studies

After we determined that the model was technically valid, the goal was to collect sufficient samples to perform RNAseq analysis to access the host gene profile in tissues with and without ZIKV perfusion. To that end, an n = 10 donors have been successfully collected, RNA isolated in triplicate and are pending RNAseq analysis. From each donor, triplicate technical replicates were harvested and isolated for RNA, for both the control and ZIKV perfused samples. From each donor, at least one of the technical triplicates tested positive for ZIKV, but there were also technical replicates that were negative for ZIKV. This may have been because of proximity to vasculature and the further from the maternal arteries the less likely virus would be detected. It also gives an interesting opportunity to analyze the localized host response in replicates that tested positive for ZIKA against those that did not, from the same cotyledon.

In addition to RNA samples, H&E and IHC analysis of these samples are ongoing and have revealed pathological differences in ZIKA perfused tissues such as membrane sluffing, changes in cellular architecture and death. ZIKV has also been detected by IHC and ongoing work is being done to characterize infected cell types and the cellular response to ZIKV infection. To determine if changes observed in the ZIKV perfused sample were due to viral replication, an n = 5 donors were perfused with UV-inactivated ZIKV. Histology and RNA analysis will be performed in the same way as the live ZIKV perfused samples. Downstream analysis will utilize bioinformatics to analyze the differences in host gene response with and without viral replication.

Summary and conclusion

Previous to this study, ex-vivo placental cotyledons have not been reported to be viable for >24 hours, nor have they been used in an infectious maternal-fetal health model. This model is unique and powerful in that it allows for experimental examination of the placental response to pathological insult in human placental tissues. For infectious models such as ZIKV, this will allow for studies to examine the impact of both viral and host immune factors on the placenta, as well as transfer of these factors from the maternal to fetal tissues in the absence of maternal factors. Additionally, very little is known about the placental responses to different immune signaling factors. This model will enable further study to examine the impact of cytokines, chemokines, viruses, bacteria or other experimental factors to expand on the current knowledge of basic placental biology, immunology and pathobiology.

VITA

CPT Kathryn McGuckin Wuertz has served for the last 8 years in the U.S. Army as a military microbiologist. Currently, she is stationed in Seattle, WA at the University of Washington, completing a PhD fellowship in Pathobiology studying innate immune factors involved in controlling neuropathic flaviviruses. After completion of her PhD, Kathryn will perform her follow-on assignment continuing her research in flaviviruses, at the Walter Reed Army Institute of Research, in Washington D.C. Kathryn graduated with her BS and MS in Microbiology/Molecular Biology and Biochemistry from the University of Idaho, studying the host-pathogen responses to picornaviruses and coronaviruses. Upon completion of her Master's she was commissioned into the U.S. Army and stationed at Landstuhl Regional Medical Center, in Landstuhl, Germany. There she was Deputy Chief, Infectious Diseases, overseeing the clinical testing of patient samples from Europe, the Middle East and Africa. During this time, Kathryn volunteered and was selected for a historic program known as Cultural Support Teams, where women deployed in support of Special Operations units in Afghanistan, to facilitate culturally sensitive engagements with women and children in combat affected areas. It was here that she gained a passion for the unique health concerns that afflict countries torn by war. Of most interest to Kathryn are the impact of emerging and re-emerging viruses in the world and addressing the intersect between security and Global Health.